Transient Hydrodynamics and Heat Transfer Behaviour along with Heat Recovery in a Pressurized Circulating Fluidized Bed Unit

A Thesis

Submitted in Partial Fulfillment of the Requirements for the Award of the Degree of

DOCTOR OF PHILOSOPHY

By

Rituraj Saikia

(11610335)

Department of Mechanical Engineering
Indian Institute of Technology Guwahati
September 2019

This thesis is dedicated to my parents

Late Khagendra Nath Saikia and Late Nirala Saikia

Declaration

I hereby certify that the information presented in this thesis is entirely my own account of my research and contains as its main content work except where otherwise stated, which has not previously been submitted for a degree or diploma at this institute or any other tertiary educational institution.

Rituraj Saikia
Regn. No. 11610335
Department of Mechanical Engineering
Indian Institute of Technology Guwahati
Guwahati – 781039, India
May 2019

Certificate

It is certified that the work contained in the thesis entitled **Transient Hydrodynamics and Heat Transfer Behaviour along with Heat Recovery in a Pressurized Circulating Fluidized Bed Unit** by **Rituraj Saikia (Roll No 11610335)**, a student in the Department of Mechanical Engineering, Indian Institute of Technology Guwahati, India, for the award of the degree of **Doctor of Philosophy** has been carried out under my supervision and this work has not been submitted elsewhere for a degree.

Dr. Pinakeswar Mahanta
Professor
Department of Mechanical Engineering
Indian Institute of Technology Guwahati
Guwahati – 718039
India

Acknowledgement

I express my deepest sense of gratitude to my supervisor, Prof. Pinakeswar Mahanta for his invaluable guidance, inspiration and encouragement throughout my research on this thesis. His thoughtful ideas and suggestions were vital in shaping up my research. It was a privilege for me to work for my Ph.D under his care and supervision all through the years.

I would like to thank my doctoral committee members, Prof. Manmohan Pandey, Dr. Vinayak Kulkarni and Dr. Subrata K. Majumder for their continued support and suggestions on critical points during my research.

I would also like to thank Prof. Santosha K. Dwivedy, Head, Department of Mechanical Engineering Department, IIT Guwahati for his encouragement and support. I also thank Prof. Anoop K. Dass, Prof. P. S. Robi, Prof. K.S.R.K Murthy, Prof Ujjwal K. Saha and Prof. D. Chakrabarty of the same department for their continued support during various issues like material procurement and others for my research.

My special thanks to Dr. Pankaj Kalita, my senior in research, for his support during the initial stage of my work.

I offer my gratitude to Mr. Dilip Chetri, Mr. Mrinal Sarma, Mr. D. Khaklary, Mr Chandan Banikya and Mr J. K. Saikia of Central Workshop, and Mr Jiten Basumatary, ME Department, IIT Guwahati for their immense contribution towards the fabrication of my experimental set up.

Project Staff members of Centre for energy, Mr Bhaskar Bharadwaj, Mr Biren Barman, Mr Dipankar Das, Mr Jon Kalita and others also deserve my sincere thanks.

I am also thankful to my co research scholars, Mr Debarshi Mallick, Mr. Hirakh J. Das, Mr. Abhinash Mahapatro, Mr Plaban Tamuly and others for their help.

My sincere thanks to my colleagues, Mr. Sanjib Sarma, Mr. Nip Borah, Mr. Pranjol Paul, Mr. M. Dowarah, Mr. S. Ahmed, Dr. D. J. Bordoloi and Mr J. K. Kakaty for their support and encouragement during my hectic days.

Grateful thanks to my wife Mrs Rajshri Deka, daughters Ms Nandika Saikia, Ms Jaishnavi Saikia and brother Mr Rishiraj Saikia for their immense sacrifice, unwavering love, encouragement, understanding and moral support without which this work would not have become a reality.

ABSTRACT

The consumption of energy has always been on the rising trend. In the year 2017, the world consumed 153,595 terawatt-hours (TWh) of primary energy which is above 2500 % more than in the year 1800. Majority of our current power systems are dominated by the three basic sources of fossil fuel viz. coal, oil and gas. The combustion of these fuels produces carbon dioxide (CO_2) and other greenhouse gases responsible for global climate change. Biomass-based energy has several distinct advantages such as wide availability and uniform distribution that puts it ahead among the renewable and clean energy options for India. The estimated potential of power generation through renewable sources in India is 85 GW with biomass power contributing approximately 20 GW. Circulating fluidized bed technology is one such technology that can be utilised to harness the vast resources of biomass that is abundantly available in our country with a very amiable impact on the environment. Pressurized circulating fluidized bed (PCFB) which is an extension of ACFB technology is another such technology that can be utilized even further due to its fuel flexibility, compact furnace size, low emission of pollutant, high combustion efficiency and adaptability to load change. However due to its vast diversity in designs and the complex hydrodynamics and heat transfer phenomenon involved coupled with different bed geometry and fuels, extensive research is needed for proper and optimized design of PCFB. Furthermore, PCFBs are mostly subjected to load variations or transients during startup and shutdown and also due to variations in load demands when used as a combined heat and power generation unit. This makes understanding the complexities of its hydrodynamics and heat transfer behavior even more challenging. Therefore, investigation of these complex transient hydrodynamics and heat transfer phenomenon of a PCFB is very crucial for the better understanding of this system.

Additionally, an enormous amount of heat energy is available in the cyclone and downcomer of a CFB. Very few investigations have reported regarding the utilization of this heat in these components. Hence there is a scope for investigating on prospects of recovering heat from the downcomer.

In the present work, the transient hydrodynamics and heat transfer characteristics are investigated in a PCFB unit with a riser of 2.0 mm height and 54 mm inner diameter. The unit is used alternatively for studying the transient heat transfer in the upper splash region and the whole riser. During the studies on the upper splash region, the heat is supplied to the wall surface of this section through a heater coil, while for the studies on the riser; heat is supplied directly to the bed by heating the air before entering the bed with a tubular furnace fitted below the distributor plate. The heat recovery experiments are performed on the PCFB under the steady state as well as transient conditions. Bed voidage with fluctuations as high as 48% are observed during the transient periods. Heat transfer coefficient is observed to fluctuate by 5 to 50 % for various transient conditions. Heat recovered is around 290 W which is observed to fluctuate by 50% at various transient conditions.

Contents

NOMENCLATURE

A_b	=	Cross sectional area of the bed in m^2
A_d	=	cross sectional area of downcomer in m^2
A_{htp}	=	Surface area of heat transfer probe in m^2
G_s	=	Solid circulation rate in $kgm^{-2}s^{-1}$
h	=	Heat transfer coefficient in W/m^2K
ΔH	=	Difference of height in manometric fluid measured in cm of water column
ΔT	=	Difference in temperature between inlet and outlet of water in heat exchanger
I	=	Supply current to the heater coil
V	=	Supply voltage to the heater coil
L_a	=	Solid accumulation height in m
L_m	=	Distance between two consecutive pressure tappings in m
q	=	Heat flux in W/m^2
t	=	Time taken by solid to accumulate upto a particular height in the downcomer after closing the ball valve
T_{bi}	=	Bed temperature in K
T_{bs}	=	Bulk surface temperature in K
U_{sup}	=	Superficial velocity in m/s
ε	=	Bed voidage
ε_{mf}	=	Bed voidage at minimum fluidization
ρ_g	=	Gas density in kg/m^3
ρ_s	=	Soild density in kg/m^3
ρ_{sus}	=	Suspension density in kg/m^3

W = Weight of bed inventory in g

Q = Power input in kW

ABBREVIATIONS

ACFB	Atmospheric Circulating Fluidized Bed
B & W	Babcock and Wilcox
BET	Biomass Energy Technologies
BFB	Bubbling Fluidized Bed
BHEL	Bharat Heavy Electricals Limited
CFB	Circulating Fluidized Bed
CFBC	Circulating Fluidized Bed Combustion
DP	Distributor Plate
DSU	Dense Suspension Upflow
FBAC	Fluidized Bed Ash Cooler
HTC	Heat Transfer Coefficient
ID	Internal Diameter
IGCC	Integrated Coal Gasification Combined Cycle
MNRE	Ministry Of New And Renewable Energy
MTOE	Million Tonnes Of Oil Equivalent
ORC	Organic Rankine Cycle
PBFB	Pressurized Bubbling Fluidized Bed
PCFB	Pressurized Circulating Fluidized Bed
PCM	Phase Change Material
RAC	Rolling Cylinder Ash Cooler
TEG	Thermo Electric Generator
THA	Turbine Heat Acceptance

LIST OF FIGURES

LIST OF TABLES

Chapter - 1

INTRODUCTION

1.1 MOTIVATION

Utilization of energy for development of infrastructure, industries, commerce and agriculture is the key for economic growth, human welfare and overall growth of a developing nation like India. Providing sufficient access of energy to everyone is an ongoing and pressing challenge for any nation. Recently there has been a noticeable change in the pattern of supply and demand of energy. The share of commercial fuels in the total energy supply in India has risen from 41% in the year 1970–1971 to approximately 70% in 2003–2004, despite the dominance of the traditional fuels in the energy sector in India. The total domestic primary commercial energy supply in India has risen from 147.05 MTOE (Million Tonnes of Oil Equivalent) in 1970–1971 to 248 MTOE in 2003.

However, most of the power generation systems also have undeniable negative impacts on the environment. Majority of our current systems are dominated by the three basic sources of fossil fuel viz. coal, oil and gas. The combustion of these fuels produces carbon dioxide (CO_2) and other greenhouse gases responsible for global climate change. Hence to meet the global climate standard and avoid further climate change, the world needs a significant and concerted transition in its energy sources.

The consumption of energy has always been on the rising trend. In the year 2017, the world consumed 153,595 terawatt-hours (TWh) of primary energy which is more than 25 times more than in the year 1800. The source of energy generation is posing alarming threat to the ecosystem of the earth. To mitigate the environmental pollution and secure sustainability in energy use, researchers have started showing interest in harnessing renewable sources of energy instead of fossil fuel for the last few decades. However, technology development to harness renewable energy such as solar, wind and biomass is not matured enough. Energy utilization from solar is developed but cost of device for this system is not affordable for all sections of people. Similarly, wind energy is site specific. Development of process and equipment is not in a position to utilize energy from biomass in a large scale. Hence dependence still lies with utilization of coal. The maximum power generation units in our country are dependent on coal fuel whereas biomass

usage is only 2.6% (Fig. 1.1). The world has a long way to go before a meaningful transition from the fossil fuel dominated energy generation systems to a renewable energy dominated one takes place.

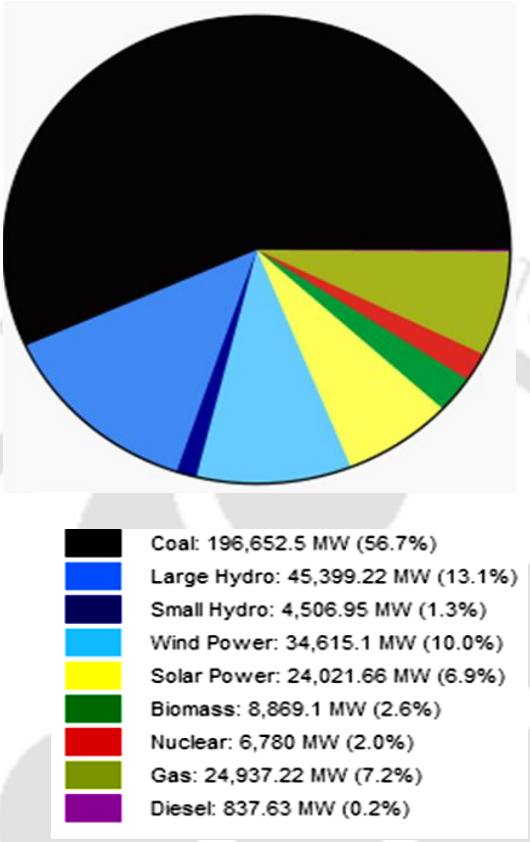

Fig. 1.1 Total Installed power generation capacity in India till Nov 2018. [Executive summary of Power sector (2018)]

There exists a potential for generating about 1500 MW of power from the urban and municipal wastes and about 1000 MW from industrial wastes in India. [Indian power scenario analysis (2012 edition)]. The potential for expanding the use of biomass energy technologies (BETs) for energy generation is vast in India and awaits further exploitation. Biomass-based energy has several distinct advantages such as wide availability and uniform distribution that puts it ahead among the renewable energy options for India. The estimated potential of power generation through renewable sources in India is 85 GW with biomass power contributing approximately 20 GW. Especially, in the remote areas and hilly terrains of India, biomass gasification-based power generation offers a highly viable solution for meeting energy demands of small villages and

hamlets, which would not only make them independent but will also reduce burden on state electricity boards. Circulating fluidized bed (CFB) or atmospheric circulating fluidized bed (ACFB) technology is one such technology that can be utilised to harness the vast resources of biomass that is abundantly available in our country. This can be used for both combustion and gasification purpose. Above all this technology also has a very amiable impact on the environment. Pressurized circulating fluidized bed (PCFB) which is an extension of ACFB technology is another such technology that can be utilized even further due to its fuel flexibility, compact furnace size, low emission of pollutant, high combustion efficiency and adaptability to load change. It has therefore become a subject of interest as a new technique alternative to pulverized coal fired steam generator and combined power cycle. PCFBs are mostly subjected to load variations due to fluctuating load demands when used as a combined heat and power generation unit. Therefore, investigation of transient heat transfer and hydrodynamics in PCFB is a very critical. Transient heating and cooling also occur in PCFB during the startup and shutdown process. However, the behavior of PCFB during these transient periods is not fully understood in spite of its high significance.

1.2 ATMOSPHERIC CIRCULATING FLUIDIZED BED

ACFB technology utilizes the fluidized bed principle in which crushed fuel and limestones are injected into the furnace or combustor. The particles are suspended in a stream of upwardly flowing air (60-70% of the total air) which enters the bottom of the furnace through air distribution nozzles. The balance of combustion air is admitted above the bottom of the furnace as secondary air. While combustion takes place at 840-900 °C under ambient pressure, the fine particles of less than 450 micron size are elutriated out of the furnace with flue gas velocity of 4-6 m/s. The particles are then collected by the solids separators and circulated back into the furnace. This combustion process is called atmospheric circulating fluidized bed (ACFB) combustion. The particles' circulation provides efficient heat transfer to the furnace walls and longer residence time for carbon and limestone utilization. The controlling parameters in the ACFB combustion process are temperature, residence time and air velocity. The major components of a typical ACFB furnace are shown in Fig. 1.2

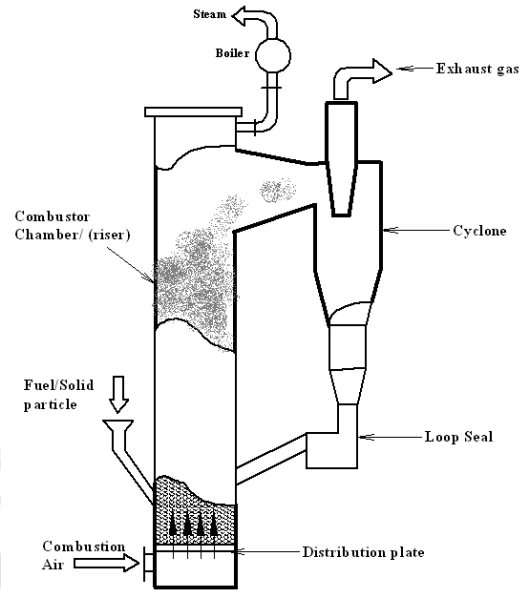

Fig. 1.2 Schematic of atmospheric circulating fluidized bed boiler

The ACFB furnace consists of a combustion chamber (riser), a cyclone, and a loop seal. Silica sand, the fluidizing medium, is blown upward by the combustion air from the bottom of the riser to the top. The gas velocity inside the riser is as high as 4-6 m/sec and the air is in a turbulent state. In the riser, sludge and screen residue are dried and burned rapidly, turning into fine ash except the incombustibles. The combustion ash is sent to the cyclone together with the silica sand. The sand and the ash are separated by the difference in specific gravity and particle size, and the ash is sent to the flue-gas-treating unit downstream with the exhaust gas. The sand falls into the loop seal, and is returned to the furnace. Filtration residue and the incombustibles in the sand remain and accumulate in the furnace, and are drawn out from the ash classifier.

1.3 PRESSURIZED CIRCULATING FLUIDIZED BED TECHNOLOGY

The pressurized circulating bed is a more recent development from the atmospheric circulation fluidized bed technology. This technology was developed in the late eighties to further improve the efficiency levels in coal-fired power plants. The PCFB Combustion Systems employ a combination of Rankine Cycle and Brayton Cycle with the objective of achieving high cycle efficiency and lower emission. The process employs a pressurized fluidized boiler which operates at a temperature of around 860 ^{o}C, pressure of around 16-18 bars and generates the flue

gases at high pressure. The pressurized flue gases are cleaned off all the suspended particulate by means of high efficiency cyclones and are expanded into a gas turbine. This expansion of flue gases in the gas turbine generates power. The figure below shows a schematic of PCFB process

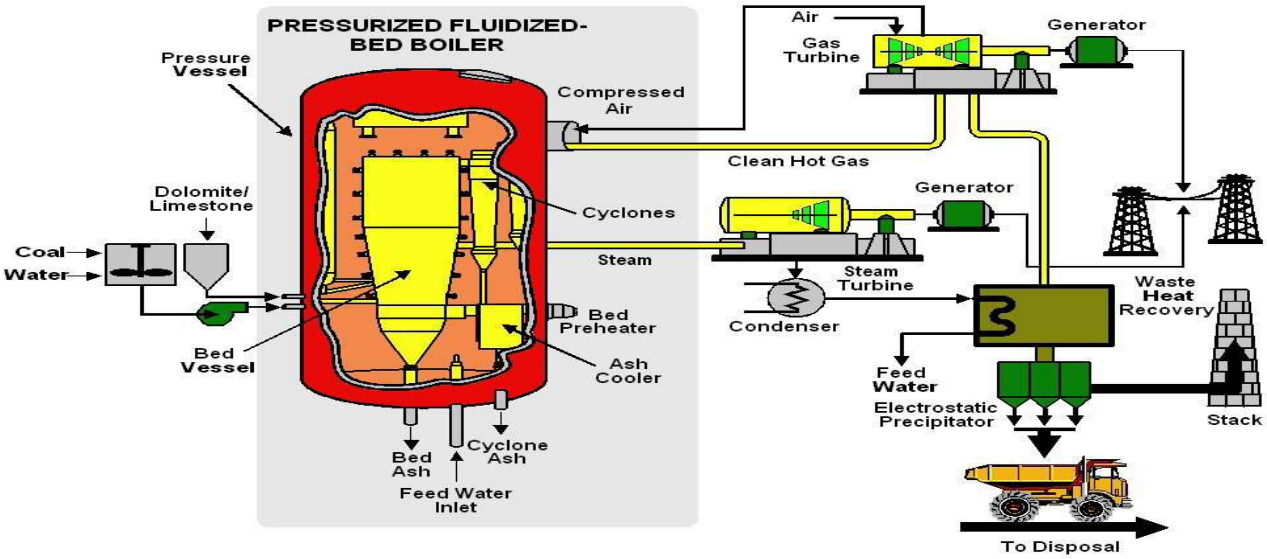

Fig. 1.3 PCFB process diagram (TIDD USA) [www.emt-india.net]

On the steam cycle side, the fluidized boiler, the heat transfer surfaces are embedded in the fluidized bed and steam generated is passed through the conventional steam cycle operating on Rankine Cycle. Thus a combination of Rankine Cycle & Brayton Cycle results in higher cycle efficiencies which are projected to be higher than conventional steam plants by 4-5%.

1.4 ADVANTAGES OF PRESSURIZED CIRCULATING FLUIDIZED BED TECHNOLOGY

- **Improved cycle efficiency:** The major advantage of PFBC process is that plant efficiency can be significantly improved by combining Rankine Cycle & Brayton Cycle
- **Reduced emission and improved combustion:** The increased pressure and corresponding air/gas density allow much lower fluidizing velocities (around 1m/sec) which reduce the risk of erosion for immersed heat transfer tubes. At elevated pressures

the heat released within the combustors increases and deeper beds are needed to accommodate the required heat transfer surface. The use of compressors for combustion air takes care of the higher pressure drop across these deep beds. Full load bed depths range from 3.5-4.5 m depending upon pressure. The combined effect of lower velocity and deeper beds results in greater in-bed residence time which reduces emissions of SOx and thus improves combustion efficiency.

- **Reduction in boiler size:** Since air mass flow m= VA, the high air/gas density results in much lower required bed plan area.
- **Standardization of boiler:** Since the gas turbine compressor capability sets the requirement of the boiler and major components, PCFB lends itself to a high degree of standardization. The range of PFBC design sizes is set by the compatible gas turbine sizes

1.5 DISADVANTAGES OF PRESSURISED CIRCULATING FLUIDIZED BED TECHNOLOGY

- Erosion of the reactor walls, pipes and vessels from abrasion by particles.
- For catalytic reaction, continuous movement of porous catalyst particles contributes to back mixing of gaseous reactant-thus reducing the performance.
- Hydrodynamic character is very complex and not easy to comprehend.
- Significant power consumption due to use of compressor.

1.6 STATUS OF ACFB

Over the past sixty years, the development of power plant technology has been governed by various objectives, the trends being influenced by factors relating to the energy, economy and ecology. The shift towards oil and gas as fuels began in the sixties and was followed by the energy crisis in the seventies, during which period the problem of dwindling fuel resources became a primary concern. As a result, combustion methods are developed in which poor quality fuels were utilized with reduced pollutants. By operating at below ash melting temperature and

adding appropriate substances to the fuel it is possible to bond the pollutants as they are formed, a process which eventually resulted in the development of Fluidized bed combustion. There are various attractions to generate power from biomass derived fuels such as coal, biomass etc. through Fluid Bed Technologies.

1.6.1 HISTORY OF ACFB

In 1922 the first industrial application of fluidization in a reactor for a coal gasification process was made by a German chemist Fritz Winkler for which he was awarded a patent. Fluid bed processes came into wide use in the petroleum industry in the 1940's. These processes are also used extensively in the chemical and metallurgical fields. In 1942, the first atmospheric circulating fluidized bed was built for catalytic cracking of mineral oils, with fluidization technology applied to metallurgical processing (roasting arsenopyrite) in the late 1940s. During this time theoretical and experimental research improved the design of the fluidized bed. In the 1960s VAW-Lippewerk in Lünen, Germany implemented the first industrial bed for the combustion of coal and later for the calcination of aluminium hydroxide. Some of the milestones in the development of ACFB technology are given below [website of Outotec]

1959 First laboratory ACFB plant at Metallgesellschaft, Germany, 0.5 tpd

1961 First pilot plant for alumina calcination, VAW Lünen, Germany, 24 tpd

1968 First industrial alumina calciner, VAW Lünen, Germany, 500 tpd

1973 First laboratory tests for iron ore reduction using ACFB technology, R&D Center, Germany

1979 Significant capacity increase of alumina calciners, Interalumina, Venezuela, 3 x 1,400 tpd

1982 First coal combustion plant, VAW Lünen, Germany, 84 MW

1985 Duisburg CHP Plant, Germany, 100 MWe

1987 First gold ore roasting plant, KCGM, Australia, 575 tpd

1990 First alumina calciner with hydrate bypass, Worsley Alumina, Australia, 1,850 tpd

1991 Circodust demonstration plant, Thyssen, Germany, 120 tpd

1992 Largest roaster for gold ore, Newmont, USA, 2 x 3,800 tpd

1993 Largest ACFB (11.5 x 14.7 m) based power plant, Soprolif, France, 650 MW

1996 Circored direct reduction plant, CAL, Trinidad, 1,500 tpd

1999 World's largest ACFB boiler installed in Åagisza plant, Southern Polland, 660MWe

2001 Oxidizing ilmenite roaster, Iscor, South Africa, 1,000 tpd

2002 Ore preheater, HIsmelt Corporation, Australia, 4,000 tpd

2003 Significant capacity increase of alumina calciners, Alunorte, Brazil, 2 x 3,300 tpd

2005 Reducing ilmenite roaster, Kenmare Resources plc, Mozambique, 1,200 tpd

2005 First preassembled module supply of alumina calciners, Alcan Gove, Australia, 2 x 3,500 tpd

2009 Lagiza, Polland, 460 MWe SC.

2013 Baima, China, 600 MWe SC

1.6.2 CURRENT STATUS OF ACFB TECHNOLOGY

Fluidized bed combustion technology is being rapidly utilized all over the world in thermal and power industries. Rapid diffusion of ACFB technology also started in North America where the largest part of cumulative capacity is installed. However the expansion of ACFB technology in western Europe has been comparatively stable since the early 1990s due to the economic restructuring of the coal industries in Germany. The ACFB capacity, which is added in Germany since, consists of mainly small biomass fired plants of below 20 MWe capacity and small bituminous coal fired plants of below 50 MWe capacity. Scandinavia and Asia started the diffusion with steady growth of capacity in the mid-1980s and Scandinavia continued that growth. However, ACFB technology diffused rapidly in Asia from the beginning of 1990s. In the

same period Eastern Europe, especially Poland and the Czech Republic, emerged. There, new coal-fired plants were built and old installations were retrofitted with CFB technology.

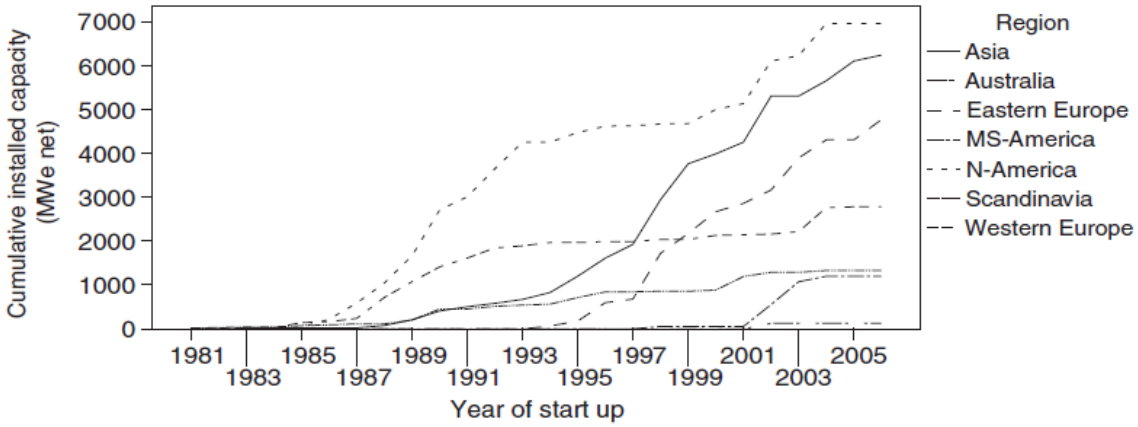

Fig. 1.4 Diffusion of ACFB for different regions of the world [Koornneef *et al*. (2007)]

Both the ACFB and bubbling fluidized bed (BFB) have gain equal importance depending on the application. Currently a major expansion in the ACFB capacity is happening in the Asian region specially and more rapidly in China. Hundreds of major ACFB boiler plants for coal are being installed which may double the global FBC capacity within just 5 years. In Europe emphasis are made to design boilers in such a way as to burn several fuels simultaneously. Besides coal, wood, biomasses and various waste derived fuels such as bagasse, rice husk, saw dust etc have become important fuels in various recent FBC projects. The first ACFB power plant of 110 MW at Nuclu. Colorado, USA is operating since 1990. Several such CFBC power plants are operating in Germany, UK, Canada and Japan using various kinds of coal and bio-mass fuels. The largest ACFB power plant is the 250 MW unit in Gardane, France, commissioned in 1996.

Table 1.1 Overview of installed technology, capacity and market entry for the selected manufacturers [Koornneef *et al*. (2007)]

Manufacturer	Technology	Installed capacity in Mwe			# of boilers	# of installations	Start up year
		Minimum	Maximum	Total			
Alstom	BFB	17	142	355	12	7	1988–99
	CFB	2	520	8229	75	51	1986–2005
Babcock and Wilcox	CFB	3	76	580	25	22	1982–2002
Babcock Borsig	BFB	0	35	88	7	5	1982–2000
	CFB	9	120	408	13	10	1989–99
Bharat Heavy Electricals	BFB	5	50	392	28	18	1987–98
EPI	BFB	10	45	185	10	9	1981–93
Foster Wheeler	BFB	0	117	1229	57	51	1976–2002
	CFB	0	460	10648	199	161	1981–2006
Kvaerner Pulping	BFB	6	117	1762	59	56	1985–2005
	CFB	0	240	1375	41	32	1984–2002
Lurgi-Lentjes	CFB	9	225	2182	43	35	1982–2004
Totals for selected manufacturers	BFB	0	142	4011	173	146	1976–2005
	CFB	0	520	23422	396	311	1981–2006

1.6.3 STATUS OF ACFB IN INDIA

Pilot and experimental AFBC boilers were in operation as early as 1977 in India at Bharat heavy electricals limited, Trichy; Central forest research institute, Dhanbad etc. In India, Hirakud Power uses environmentally friendly atmospheric circulating fluidized bed (ACFB) combustion technology to produce electricity for one of the world's oldest aluminum-smelting operations. Currently Foster Wheeler is directly executing two new orders from Rain Calcining, Vizag (25 MW, petroleum coke) and Mysore Paper Mills, Bhadravati (20 MW, multifuel). Babcock & Wilcox (B&W) has also supplied few bubbling bed FBC boilers in India since 1992. The most important of these is the Kanoria Chemicals, Renukoot 81 MW captive power plant based on the most advanced Internal-particle recirculation FBC. Recently, B&W has formed a joint venture with Thermax Ltd. to supply B&W boilers of all types in India as Thermax Babcock & Wicox Ltd. This company has supplied the FBC boilers to Kanoria Chemicals, Renukoot and Central Pulp Mills, Surat. Currently most Indian oil refineries are planning to set up refinery residue fired captive power plants. Foster Wheeler is the only experienced pet-coke fired CFBC supplier in India, currently. However with pet-coke, IGCC is also techno economically competitive with FBC. [www.emt-india.net]. Some of the largest CFBC units in operation in India are listed in the Table 1.2 below

Table 1.2 Large CFB SG units in India [Tata engineering service (2014)]

Sl no	Location	Unit Capacity (MW)	Year of commissioning/Fuel
1	Indian Aluminium Hirakud, India	60	1992 / coal
2	Tata Chemicals Ltd., Mithapur, India	16.5 (Co-gen)	1995 / coal
3	Kanoria Chemicals & Industries Ltd., Renukoot, India	25	1996 / coal
4	Gujarat Industries Power Co. Ltd., India ,Surat Lignite Power Plant (SLPP)-Phase -I	2 ×125	1999/2000 / Lignite
5	Gujarat Industries Power Co. Ltd., India ,Surat Lignite Power Plant (SLPP)-Phase -II	2 ×125	2010 / Lignite
6	RRUVNL, Giral Thermal Power Station,Rajasthan,India	2 × 125	2009 / Lignite
7	RRUVNL, Giral Thermal Power Station,Rajasthan,India	2 × 125	Under execution / Lignite
8	Neyveli Lignite Corporation, TPS –II Expansion at Neyveli,Tamilnadu	2 × 250	Under advanced stage of execution / Lignite
9	Bhavnagar Energy Company Limited,	2 × 250	Under advanced stage of execution / Lignite

1.7 OBJECTIVE OF THE PRESENT WORK

The aim of the present work is to investigate the transient hydrodynamics, heat transfer behavior and heat recovery in a PCFB unit. The following objectives are included in the scope of the present work.

- Investigation of the transient hydrodynamics along the height of the riser under varied operating conditions in a PCFB with sand and coal blends as bed inventory
- Investigation of the transient bed temperature profile, surface temperature profile and transient heat transfer along the riser during stepped changes in operating pressure,

superficial velocity, exhaust flow rates and power input in a PCFB with sand and coal blends as bed inventory

- Development of a heat recovery system to recover heat from the down comer in a PCFB and investigation of the transient heat recovery during stepped and ramped changes in superficial velocity and power input from the same

1.8 OUTLINE OF THE THESIS

The thesis has seven chapters. Chapter 2 reports the detailed review of literature on the various experiments on CFB hydrodynamics, heat transfer, transient studies, heat recovery along with a summary and scope for future works. Chapter 3 discusses the experimental set up and procedure for transient studies on a PCFB. Chapter 4 includes the detailed studies on hydrodynamics with various input parameters. Chapter 5 presents the transient heat transfer studies on the PCFB. Chapter 6 includes parametric study on heat recovery along the down comer of a PCFB. Chapter 7 presents the conclusion and scope for future work.

Chapter - 2

LITERATURE REVIEW

2.1 INTRODUCTION

A detail literature review regarding the hydrodynamic and heat transfer in fluidized bed boiler is presented in the following sections. The literature review is divided into four major sections. Section 2.2 and 2.3 discusses the literatures available on ACFB and PCFB, respectively. Few literatures on transient studies in ACFB are discussed in section 2.4. A literature review regarding waste heat recovery from thermal systems also follows in section 2.5.

2.2 LITERATURE REVIEW ON STUDIES ON ACFB

ACFBs are used as a technical process which has the ability to promote high levels of contact between gases and solids. In a fluidized bed a characteristic set of basic properties that are indispensable to modern process and technology are utilized, these properties include: extremely high surface area contact between fluid and solid per unit bed volume, High relative velocities between the fluid and the dispersed solid phase, High levels of intermixing of the particulate phase, frequent particle-particle and particle-wall collisions. The two major phenomena that occur in an ACFB are its hydrodynamic behaviour and the heat transfer between the bed and wall. The following sections present a detailed literature review on these two aspects of an ACFB.

2.2.1 BED HYDRODYNAMICS IN ACFB

In order to model heat transfer in a physically realistic manner, it is important to achieve a reasonable understanding of the local and overall hydrodynamics in ACFB. Glicksman (1993) stated that the important hydrodynamic factors in a ACFB are the fraction of wall covered by particles and gas, i.e. voidage phenomena and average contact time of particles at the wall. Weinstein *et al.* (1983) have confirmed the existence of core annulus structure of the dense phase of fast fluidized bed. In simple terms, there exists relatively dilute up flow core in which solid

particles are entrained upward by a high velocity gas stream and a much denser annulus layer near the column wall in which solid particles congregate and fall as dense structures similar to waves of strands or streamers. As heat transfer surfaces are commonly located at the column wall for most ACFB applications, the influence of down flowing wall layer on heat transfer is significant. The velocity of descent of strands in the wall layer, the duration of their stay at the wall and time fraction of wall coverage are all important hydrodynamic parameters that affect the heat transfer between the gas solids suspension and the wall.

Numerous attempts through various approaches have been made to devise methods to predict the aspects of fluidization and their transposition from one mode to another. [Kunni and Levenspiel (2005)]. However Geldart (1973) devised the criterion in a different way. His approach is significant because it is simple and has great generalizing power. According to his criteria, particles can be classified in four main groups based on their density, fluidization properties and mean size. This classification is depicted in the figure 2.1 below for any solid of known density ρ_s and mean particle size d_p

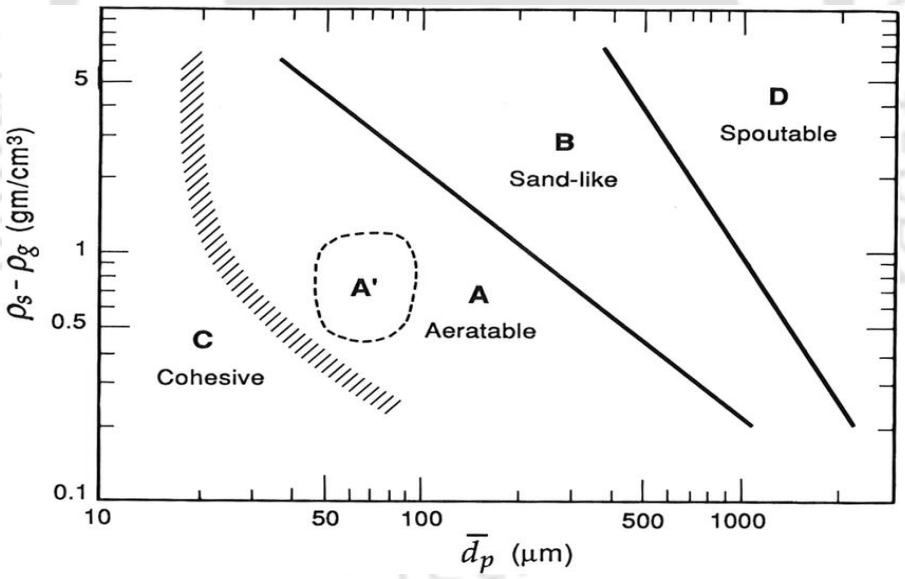

Fig. 2.1 The Geldart classification of particles for air at ambient condition. [Kunii and Levenspiel (1991)]

However, this information about particle sizes applies only for the particles used in the atmospheric fluidized beds and no significant information is available regarding the aspects of fluidization in pressurized fluidized beds. Further, for proper prediction of the behaviour of the gas solid in an ACFB, various flow regimes have been identified and mapped by various

investigators [Grace (1986), Zenz and Othmer (1960), Li and Kwuak (1980)]. The different regimes of fluidization are depicted in Fig.1.2 and are explained below

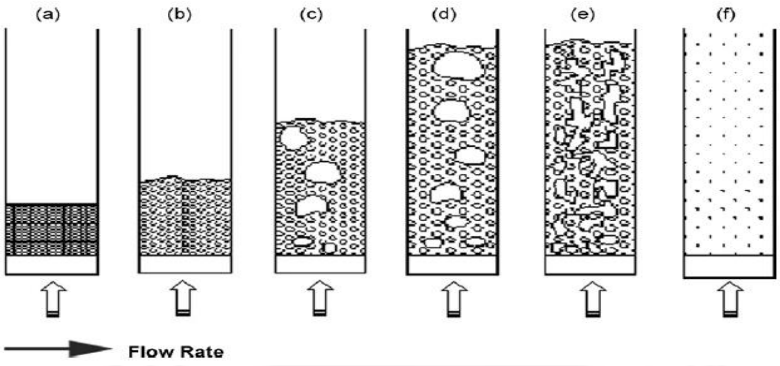

Fig.2.2 Fluidized bed regimes: (a) fixed bed regime, (b) minimum fluidization, (c) bubbling bed regime, (d) slugging bed regime, (e) turbulent bed regime, and (f) pneumatic bed regime. [Barletta (2009)]

(a) At a low flow rate the fluid passing upward through a bed of fine particles simply percolates through the voids. This is "fixed flow bed". With increasing flow rates, particles move apart with a few vibrating and even entering restricted regions. This is *expanded bed*.

(b) At still higher velocity, the particles get suspended by upward-flowing gas or liquid. At this stage of fluidization the frictional force counter balances the weight of particles. The pressure drop through any section of bed equals the weight of fluids and particles in that section. This stage of fluidization is called *incipient* or *minimum* fluidization.

(c) Increase in flow rate beyond minimum fluidization results in large instabilities with bubbling and gas channeling. At high flow rate, vigorous agitation of particles is seen. Such a bed is called *aggregative* or *heterogeneous* or *bubbling* fluidized bed. Such a behavior is seen in case solid – liquid systems as well, when the densities of particles and the fluidizing medium differ greatly.

(d) In gas-solid system, gas bubbles coalesce and grow. In deep and narrow beds they may grow and spread across vessel. The fine particles smoothly flow down by the wall around rising void of gas. This is slugging bed regime. Particles rain down from the slug, which finally disintegrates. At about the same location, another slug forms and the phenomenon continue.

(e) At this stage the clearly defined upper surface of the bed no longer exists; turbulent motion of solid clusters and gas voids of various size and shape appears. This is turbulent bed regime.

(f) Further rise in velocity results in this phase where the bed after becoming turbulent results in carrying away of particles out of the bed. This is called disperse or dilute or lean phase fluidized bed or pneumatic bed regime.

A thorough understanding of these regimes and the bed hydrodynamics are very critical as these would finally affect the heat transfer and performance of an ACFB and thus has a significance impact on their designs.

The variation of axial bed voidage is a typical S-shaped profile as shown in the Fig 2.3 below. There is a variation of the solid fraction in the bottom of the riser and then it decreases along the height almost in a constant trend. The lower portion is the dense region and the upper region is the lean region which is generally the fast fluidization mode. Gupta and Nag (2002) observed that the bed voidages increases in the bottom and decrease at the top with an increase in superficial velocity,.

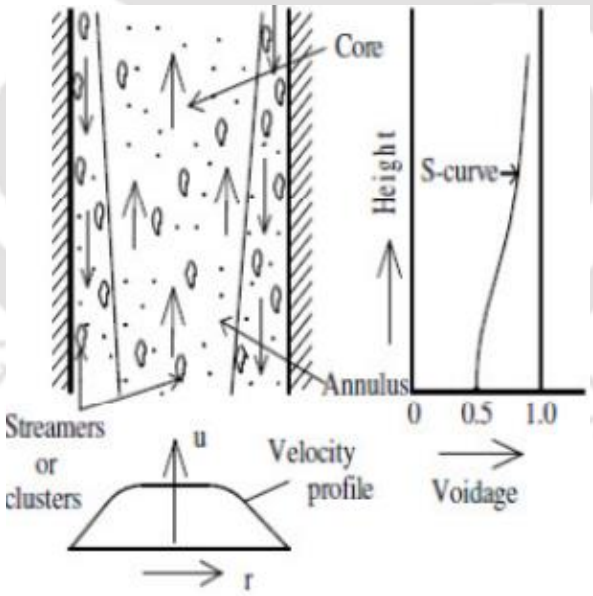

Fig. 2.3 S shaped voidage profile along the axial direction [Nag 2001]

Many researchers have investigated the effect of solid circulation on the flow pattern and performance of ACFBs. An experiment on a bench scale ICFB performed by Milne *et al.* (1993) to study the hydrodynamics at temperature as high as 800°C showed that the solid circulation rate varied linearly with the auxiliary gas flow rate but were effected less by riser gas flow rate. Solid circulation rate also increased with increase in bed temperature. Solid flow rate was correlated with by a simple equation for gas-solids orifice flow. Later Grace *et al.* (2000) has shown that with an increasing solid circulation rate above 300 kg/m^2 at a fixed high gas velocity 6-10 m/s, a new regime called the dense suspension up flow (DSU) regime transpires. DSU offers a greater uniformity in radial solid distribution compared to the fast fluidization regime and an absence of net solid downward flow near the walls. Matsuda (2008) developed a novel method that uses a optical mouse to monitor the moving velocity of solid particles in a circulating fluidized bed. His results using this method show practical agreement with those obtained using visual observation and reveal that the descending movements in the downcomer of the ACFB have various patterns. However velocities less than 0.3 m/s can only be monitored by this method.

The radial profile of particle mass fluxes and particle size distribution along the radial direction in an ACFB shows that dilute flow and a dense flow regime with each exhibiting specific flow profiles exists along with Internal recirculation in the riser along the walls for dense flow as observed by Bodelin *et al,* (1993). Zheng *et al.* (1993) experimentally studied the performance of three different types of bed exits of a CFB boiler and investigated their effects and the effect of exit area on flow regimes, density profile and resident time of fine circulating particle. They observed that the geometric structures of bed exits significantly influence the hydrodynamics. The exit structure influences the flow regime in bed. The bulk density increases with decreasing exit area.

Sobrino *et al.* (2009) investigated the effects of distributor plate on the hydrodynamic characteristics of turbulent fluidized beds by obtaining measurements of pressure and radial voidage profiles in a column diameter of 0.29 m with Group A particles using bubble-cap or perforated plate distributors. Differential and gauge pressure transducers located at different axial positions along the bed was used. The radial voidage profile in the bed was also measured using

optical fiber probes. They observed that the distributor plate has a significant effect on the bed hydrodynamics. Earlier onset of the transition to the turbulent fluidization flow regime was observed with the perforated plate distributor due to the jetting. Moreover, increased carry over for the perforated plate compared with the bubble caps was observed. A lower U_c velocity and a higher decrease of the dense bed height with increasing superficial gas velocity were observed with the use of perforated plate. Solids density near the bottom region was observed to be higher for the bubble-cap distributors; while a more homogeneous radial structure in terms of voidage was found. A dilute core and a denser annulus structure were also observed in the bottom region of the bed for the two distributors studied. However the effect of percentage openings of distributor plate was not studied. Seo *et al*. (2014) determined the transition velocities such as minimum fluidization velocity, turbulent fluidization velocity and transport velocity in a dual circulating fluidized bed reactor for different particle sizes as a function of temperature. The minimum fluidization velocity determined by measuring bed pressure drop with increasing gas velocity was found to be decreasing with increasing temperature due to increase in viscosity of gas.

2.2.2 HEAT TRANSFER IN ACFB

Circulating fluidized bed are operated at superficial gas velocity much higher than the minimum fluidizing velocity, where bubbles are absent and particle flow is dilute. As already discussed ACFB has great fuel flexibility. In addition to coal, other solid materials such as biomass, municipal waste, bagasse, sawdust and wood chips can also be used as the primary fuel to produce high pressure and temperature in an ACFB [Sundaresan and Kolar (2002)]. Heat transfers in an ACFB take place between particles and gas, between particles and other particles and also between the gas–solid suspension and heat transfer surfaces [Rusheljuk (2006)]. Researches have established that there are two major flow patterns in an ACFB riser a dilute core region where particles are transported upward by flowing gases, and a denser wall layer region where particles reverse their flow directions and descend along the wall [Eriksson and Golriz (2005)]. A major feature of the overall flow structure in most ACFB units is a core-annulus flow pattern as indicated by Fig. 2.4 below.

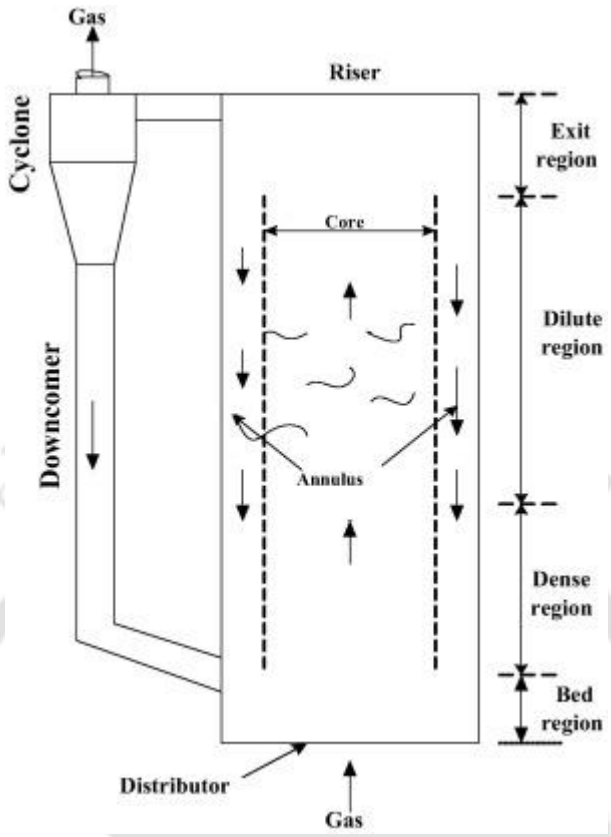

Fig 2.4 Core annulus structure of a atmospheric circulating fluidized bed combustor. [Abdelmotlib *et al.* (2016)]

Particles, after staying in the wall layer for an average residence length, are re-entrained into the core and replaced by fresh particles that have the same temperature as the bulk. Another notable feature of ACFB reactors is the temperature uniformity in the core region [Rusheljuk (2006)].

It has been established by many researchers that the heat transfer in an ACFB increases from the bottom along the height of the riser. [Grace (1986), Basu and Nag (1987), Basu (2006)]. Heat transfer is also dependent on many operating parameters like operating pressure, superficial velocity, input heat flux, suspension density and bed voidage, particle size, soild inventory and particle distribution. [Basu (2006), Werther (2009), Anthony (1995), Gupta and Nag (2002)]. Numerous investigations have also been made on methods to enhance heat transfer in ACFBs. Many literatures are available on various aspects of heat transfer in ACFBs. Shen *et al*. (1991) investigated the bed-to-wall heat transfer in a ACFB at high pressures. Wirth (1994,1995) and Molerus (1993) made some investigations in a PCFB and the results were presented in terms of

dimensionless numbers. Investigation on installations of fins in ACFB were also carried out by Basu *et al*. (1990) and Nag and Ali (1993). It is established from their research that fins can enhance the heat transfer in an ACFB. The effectiveness of the fin surfaces was around 90%. However, the optimum parameters to limit the erosion of fins and the deposition on fins if gasification is done can be an important investigation which the authors have not reported. Another notable investigation was regarding local lateral heat flow by Anderson and Leckner (1993) who experimentally investigated the variation of local lateral heat flow with different location in the combustion chamber and with various operating parameters. Their results yielded that the average heat flow was found to be higher at the crest and lowest at the side of the tube. The lateral variation of heat transfer is slightly smaller at higher gas velocity than at lower velocity. Radiative heat transfer is more at the upper part of the combustion chamber but as boundary layer develops, other modes of heat transfer occur. However, their investigations did not cover the cyclone separator and downcomer. Further in another investigation, a correlation was developed by Mahalingan and Kolar (1993) where the heat transfer coefficient was found to be related to suspension density, superficial gas velocity, solid circulation flux and particle size.They also found that the local heat transfer coefficient varies all throughout the riser column length. Another literature on modelling work by Eriksson and Golriz (2005) proposed a model for predicting radiation heat transfer in circulating fluidized bed combustor by assuming two phase structure, the flow at the wall dominated by streamers of clusters travelling mostly downward, interspersed with periods of upward flow of dilute suspension and also assuming the intensity distribution to be semi-isotropic in the forward and backward direction. Stefanova *et al*. (2011) measured the heat transfer coefficient in two fluidizing columns of different diameter of 0.29 m and 1.5 6m using alumina particles as bed material. The maximum heat transfer coefficient was found to be unaffected by column diameter and it was found to reach in the range of superficial gas velocities where the turbulent region became more dominant. Sundaresan and Kolar (2013) conducted experiments to determine the total tube to suspension surface average heat transfer coefficient for several vertical tubes placed in the core of a square ACFB riser. The influence of axial location of the tubes and its axial length on heat transfer was studied suing sand as bed material. They observed that the heat transfer coefficient decreased with increasing tube length and increasing axial location from the distributor plate. Izquierdo-Barrientos *et al*.

(2015) used granular form of a phase change material (PCM) in a fixed and fluidized bed to study the heat transfer. They found that the heat transfer coefficient for fluidized bed with PCM was 3 (three) times higher than those for fixed beds at the same gas flow rate. They also found that the heat transfer coefficient with granular PCM is notable increased because of the latent heat stored by the PCM when the bed is at a temperature below the transition temperature.

2.2.3 WASTE HEAT RECOVERY IN ACFB

The downcomer is a vital component in an ACFB which facilitates the pneumatic circulation system for the solid particles. The downcomer section can be a major source of waste heat recovery. The excellent heat transfer characteristics of powder beds moreover facilitate the integration of encapsulated phase change materials as temporary heat storage medium [zhao *et al*. (2013), Zhang *et al*. (2014)]. Investigations on waste heat recovery from ACFB are almost nil though a few literatures are available on recovery of heat from waste gases [Salam and Grabbs (1987)] remains of combustion process [Rodriguez *et al.* (2002)] and bottom ash [Zeng *et al.* (2010)] in ACFB. These are discussed. Salam and Grabbs (1987) developed a multiple fluidized-bed heat recovery system which utilizes solids transfer between adjacent fluidized beds by means of jet jumps for recovering and/or storing waste heat and obtained an improvement of overall efficiency by heat recovery from waste gases, the recovered heat being utilised for raising steam, preheating air, etc. The fluidized bed heat exchanger effectiveness approached 80% of a perfect parallel flow heat exchanger. Still another research analysed the energy recovery from solid particles leaving a combustion process [Rodriguez *et al*, (2002)] by studying a heat exchanger with a shallow gas-solid fluidized bed. Effects of vertical baffles in the fluidized bed with immersed horizontal water filled tubes were also studied for two different particle sizes and flow rates with counter flow arrangement. They observed that the heat transfer increased by 55% and higher values of heat exchanger effectiveness were obtained for experiments with presence of baffles. The suspension wall heat transfer co efficient in a shallow fluidized bed increased with the increase in solid flow rate and particle diameter. Another investigation by Zeng *et al.* (2010) analysed the influence of two different bottom ash heat recovery modes, fluidized bed ash cooler and rolling cylinder ash cooler, on thermal economy of three ACFB power plants in

THA(Turbine heat acceptance) condition. Both modes improved the thermal economy of units. FBAC mode had higher plant thermal efficiency lower plant heat rate and less standard coal consumption (b_s) than the RAC mode. The FBAC mode could save more b_s, approximately 2 g/(kW h). While fundamental and applied research has been carried out [Zhu *et al*, (1995)], few results have been reported on heat recovery in downcomers of ACFB, even though it is an important element which carries solid particle at a comparatively high temperature.

2.2.4 STUDIES ALONG THE DOWN COMER OF ACFB

One of the investigations related to the down comer or return leg of the ACFB is regarding the entrainment of gas flow rate in the downcomer [Li (1994)] where in the existence of gas flow entrained by the solids recycle the rate of which depends on the solids circulation rate was observed. It was also observed that the direction of the net gas flow in the downcomer was changed with solids circulation rate. Fine particles and high solids flow rates would result in a co-current downward net gas flow, leading to a reduced drag coefficient. Another study on the downcomer investigated the heat transfer between an electrically heated vertical finned tube bundle and cracking catalyst, fluidized with air in the downcomer of an ACFB system. [Ouyang *et al*. (1996)] where a 40% increase in the heat transfer coefficient at low fluidizing velocity in the downcomer with the external recirculation of solids was obtained. Later Zhang and Zhu (2000) measured the radial distribution of local particle velocities along the downcomer column, 9.3m high and 0.10 m ID of a gas-solid fuidized bed to study the hydrodynamics. They used a fiber optic particle velocity probe for their measurements. Local solids fluxes were also calculated from the local particle velocities and solids hold-ups. They observed that the particle velocity profile in the downer have a relatively flat core and an annulus where the particle velocity drops towards the wall. Uniformity in radial distribution of particle velocity both in the development and the fully developed zones was more in downers than risers. The radial profiles of solid flux were observed to be rather flat for gas velocities lower than 7m/s. One investigation on the downcomer carried out by Chen and Li (2004) studied the hydrodynamics of a down comer operating at high soild concentration and high solid flux in a specially designed atmospheric circulating fluidized bed system. They also studied the characters of the transient solids fraction, the radial solids concentration distribution and axial profiles of pressure gradient

under the condition of high solids concentration. They observed that the dilute phase is more dominant in the low-density downer, while the dense phase is more dominant in the high-density downer. The heavier/better fluidity particle could achieve the higher solids flux and the smaller/lighter particle were better for the higher solids holdup. The radial non uniform core/annulus structure still exists in the high-density downer, but radial solids distribution gradually becomes more uniform with downward distance and with the increase of solids flux. There were also investigations regarding the flow of solids and friction in a downcomer of an ACFB. Qi *et al*. (2008) investigated the occurrence of friction between co-current downflow gas–solid flow and column wall by measuring apparent and actual solids concentrations in an ACFB downer. A new model to predict pressure drops due to friction between the gas–solid suspension in the fully developed zone and the downer wall was developed. Their study showed that the friction between the gas–solid suspension and the downer wall causes a significant deviation of the apparent solids concentrations from the actual ones, especially for those operating conditions with higher superficial gas velocities and solids circulation rates. Particle diameters have different influences on the frictional pressure drops under different superficial gas velocity

2.3 LITERATURE REVIEW ON STUDIES ON PCFB

The following section elaborately discusses the available literatures dealing on the various aspects of a PCFB.

2.3.1 BED HYDRODYNAMICS IN PCFB

Most of the literatures available have reported the various aspects of fluid flow and bed hydrodynamics on ACFB which have been discussed in detail in the section 2.2.1 earlier in this chapter. For a proper understanding of the flow patterns inside a PCFB, the mixing quality, solid particle attrition behavior and mas and heat transfer, a thorough understanding of the bed hydrodynamics is very essential. The state of the solid flows is vastly different in various components of a PCFB. Generally the solids are in a turbulent fluidized state in the lower furnace regime, fast fluidized in the upper splash region, swirling flow state in the cyclone and

moving bed in the downcomer region. The bed hydrodynamics in a PCFB also differ greatly from that of an ACFB. Numerous publications deal with the experimental determination of the transition velocities between bubbling and turbulent fluidization, and between turbulent and fast fluidization [Schnitzlein and Weinstein (1988), Perales *et al*,(1991), Brereton and Grace (1992)]. Very few published literatures are available on hydrodynamics in a PCFB. Plasynski *et al*. (1996) studied the variation of the pressure gradient in a 26 mm diameter tube with glass beads and coal as the bed material and nitrogen as the fluidizing gas for different operating pressures. Reddy and Knowlton (1994) also investigated the effect of operating pressure on CFB riser hydrodynamics in a 300 mm diameter tube and obtained results exactly contradictory to those obtained by Plasynski *et al*. (1996). The difference between the results obtained by them is due to higher gas pressure drop in the smaller tube compared to that in the larger diameter tube. In a major research by Yates (1996) on experimental and theoretical studies of gas solid fluidization at elevated temperatures and pressures, it was observed that the minimum fluidization velocity, the bubbling velocity and the terminal velocity decreases with increase of operating pressure. Later the influence of pressure, fluidization velocity, particle size and tube bank geometry on hydrodynamics and local tube erosion was studied by Wiman and Almstedt (1997) where it was observed that an increased pressure causes a transition towards dispersedly bubbling, or turbulent, bed behavior. This subsequently indicated a strong coupling between the erosion and the bubble rise velocity, and between the heat transfer and the local bubble frequency. Studies on loop seal in PCFB are also plenty where in one study, Chang and Basu (1999) showed that solids flow rate increases with aeration rate as well as the system pressure. The influence of the solid/gas density ratio on the flow pattern in a riser reactor of a PCFB was investigated by Richtberg *et al*. (2005) who observed more uniform axial and radial solids distribution with increasing absolute pressure or decreasing density ratios ρ_S / ρ_F, indicating flow conditions which are different to a well-known core-annulus flow structure. Parametric studies on a PCFB were carried out by Kalita *et al*. (2013c) for both the hydrodynamics and heat transfer in a PCFB for various particle sizes, solid inventories, operating pressure and superficial velocities. They also studied the performance of various percentages blending of sawdust with sand. They observed an S-shaped voidage profile along the height. They observed decrease in suspension density and heat transfer co efficient with increase in particle size. Increasing operating pressure

causes increase in suspension density, axial heat transfer coefficient and solid circulation rate. Increasing superficial velocity also increases axial heat transfer coefficient. Radial heat transfer coefficient always decreases from wall towards the core. Uniformity in heat transfer coefficient and more homogeneous fluidization occurs for higher operating pressure. Moreover, they concluded that 7.5 – 15% sawdust blend causes highest local heat transfer coefficient.

2.3.2 HEAT TRANSFER IN A PCFB

At present, not much information is reported on PCFB riser flow characteristics and heat transfer behaviour. The heat transfer coefficient in a PCFB unit is influenced by a number of factors, including superficial velocity, solid circulation rate, solid inventory, and particle size distribution. The effect of these operating parameters was studied by various researchers and can be summarized in Table 2.1 below

Table 2.1 Heat transfer coefficient in PCFB

Reference	**FBC size (m)**	**Bed material and size (µm)**	**Operating parameters**	**Local h (W/m^2K)**
Kalita *et al*. (2013a)	0.054	Sand, 300	Pressure, biomass blending	95-390
Basu and Cheng (1996)	0.052	Sand, 232, 507	Pressure, Suspension density, particle size	60-200
Kalita et al. (2013b)	0.054	Sand, 309	Pressure, Suspension density, superficial velocity	102-145
Kim and Kim (2013)	0.20 ×0.26×0.58	Sand, 500	Pressure, Superficial velocity	390-550

Among some of the literatures involving investigations on PCFB were those by Gupta and Nag (2002) who experimentally investigated the effects of pressure and other relevant parameters on bed hydro dynamics and bed to wall heat transfer in a PCFB riser column of 37.5 mm inner diameter and 1940 mm height with and without bed material to consider the frictional pressure

drop due to gas density at elevated pressures. They observed that the axial bed voidage is less in the bottom zone of the riser and increases along the height of the bed. The bed voidage increases in the bottom zone and decreases in the top zone with the increase in system pressure. The heat transfer co efficient increases with system pressure as well as with gas superficial velocity and average suspension density. All these observations were in agreement with published literatures. In another research on a PCFB, Winaya and Basu (2001) investigated the phenomenon of bed to wall heat transfer in an electrically heated pressurized bed with a diameter of 52.5 mm and height of 2020 mm. by studying the radial temperature distribution in the wall. Carbon di-oxide content of the fluidizing gas was changed by either adding varying amounts of carbon dioxide to the air or burning coal and coke with and without addition of adding limestone. Their observations were similar to other investigators who concluded that heat transfer coefficient increase with both system pressure and bed temperature due to increased contribution of gas convection and radiation. Heat transfer coefficient also increase with carbon dioxide concentration due to increased non-luminous radiation from carbon dioxide. Further Reddy and Basu (2002) studied the effect of CO_2 concentration and system pressure on radiation heat transfer in a pressurized circulating □ fluidized combustor and presented the basic heat transfer mechanism in a pressurized circulating fluidized bed combustor. They observed that for a given CO_2 concentration in a pressurized circulating fluidized bed combustor, radiation heat transfer increases slightly with system pressure due to increased gas partial pressure and gas emissivity. Their results demonstrate that for the given CO_2 concentration, the effect of system pressure on radiation heat transfer is minimal in a PCFB combustor. The effect of variation in CO_2 concentration levels on bed to wall radiation heat transfer during combustion in a PCFB combustor is not significant for a narrow combustor. The heat transfer processes in PCFB unit were also studied by Basu and Leming (1996). They investigated the heat transfer phenomenon in PCFB by modifying the cluster renewal model atmospheric circulating fluidized bed [Basu. (1990)] to account for the effect of pressure on heat transfer. They measured bed-to-wall heat transfer coefficients at different operating pressures. The effects of system pressure, bed suspension density, particle size and superficial gas velocity were investigated in the tests. In addition to the modified model, a semi-empirical equation based on the test data is proposed for the prediction of heat transfer coefficients. Their major observations were: The bed-to-wall

convective heat transfer coefficient increases with increasing system pressures and bed suspension density, but not with particle size for a short heat transfer surface. The effect of superficial gas velocity on the heat transfer coefficient is negligible. The effect of system pressure on the heat transfer coefficient can be explained by its effect on the gas density and cluster thermal conductivity. No major effect of the additional hydrodynamic changes was observed within the limited range of the present experiments. The modified cluster renewal model predicts the heat transfer coefficient with a reasonable accuracy. They finally proposed an empirical relation is proposed to predict the heat transfer coefficient at room temperature. Further, investigations by Reddy and Basu (2001) could adequately predict the heat transfer behavior of a PCFB through a model based on the cluster renewal process. They also observed that the heat transfer coefficient increases with operating pressure. In the investigations by Kalita *et al*. (2013a) mentioned in the Table 2.1 above, they also studied the effect of biomass blend in sand and superficial velocity on bed hydrodynamics and heat transfer. They found that the axial heat transfer coefficient increased from bottom to top with increase in operating pressure. The radial variation of heat transfer coefficient decreased from wall to the core. Heat transfer was found to be high in 7.5 to 155 biomass blends. Further Kalita *et al*. (2013b) performed experiments on a PCFB at 3 (three) different heat inputs and 3 (three) different operating pressures. They also studied the effect of twisted tape inserts on heat transfer coefficient at the upper splash region. The heat transfer coefficient was found to increase at the upper splash region with increase in operating pressure and with the use of twisted tapes having twist ratio of 4. Average increase in heat transfer coefficient was found to be 2 to 2.9 times more under the mentioned operating conditions. Among the latest researches on gasification in PCFB, mention may be made on the work of Kilmanek and Bigda (2018) who developed two CFB models of CO_2 enhanced coal gasification in a PCFB rector by which they could predict the syngas composition at the outlet of the reactor where insight into the process was also obtained. Later Shi *et al*. (2019) established a pressurized oxy coal combustion system with CFB. They also observed that elevated operating pressure leads to an increase in efficiency of the system.

2.4. TRANSIENT BEHAVIOR IN ACFB

Although much work has been on the investigations of various parameters of an ACFB during the steady state, no specific experimental investigations has been done to understand the transient hydrodynamics and heat transfer in ACFB. Rietema *et al*. (1977) studied the transient phenomenon in a fluidized bed when switching the fluidizing agent from one gas to another with different gases and observed that the intensity of the phenomenon depends on the viscosities and the molecular weights of the gases used. Jiang *et al*. (1993) studied the transient behavior of solid flow in a fast flow circulating fluidized bed by concurrently measuring the voidages and visual observations at various locations. They proposed a physical model of the transient flow pattern based on the analysis of instantaneous voidage. They found that instantaneous voidages were strongly related to solid flow structure. High degree of fluctuation of voidages causes bursting of clusters. Park and Basu (1997) developed a dynamic mathematical model to predict the transient temperature response of ACFB combustors as well as the corresponding transient carbon and oxygen concentrations in the bed. The model includes mass balances of oxygen and carbon, energy balances, as well as sub-models for the gas-solid flow structure, combustion, and heat transfer from the bed to both the refractory walls and to a waterwall located in the fast bed section. The model was validated against data collected in the 0.23 m x 0.23 m CFB combustor. Good agreement between predicted and measured values of different parameters in both time and space domains were observed. Tuzla *et al.* (1998) studied the instantaneous solid concentrations ϵ_s in a 15 cm diameter down-flow fast-fluidized bed at room temperature and near atmospheric pressure with 125 μm glass beads and superficial gas velocities ranging from 0 to 6 m/s. using a needle capacitance probe in a small sampling volume of approximately 0.1 cm^3 where they found that solid concentrations were smaller for downflow than for equivalent up flow fluidization. They also identified particle clusters in the downflow. Huang *et al*. (2006) developed two models to describe the dynamic response of the riser in an ACFB. 1) The riser as a set of well-mixed tanks connected in series and 2) as a 1-D axisymetric cluster flow. The tank-in-series model predicted the phase shift of pressure drops at different locations in the riser reasonably well. They could also predict the pressure drops along the height of the riser reasonably well using 1-D axisymetric cluster model. However the dynamic response for pressure drop at the bottom of the riser was poor despite good steady state predictions. Liu *et al*.

(2008) analyzed the instantaneous data of inner wall temperatures at certain axial positions for different heated tubes or at various axial positions for the same heated tube in a tube-bank fluidized bed evaporator with a vapor–liquid–solid external natural circulation flow employing linear and nonlinear time series analysis methods. They observed that nonlinear characteristics of the wall temperature time series vary with spatial position in the evaporator at given operation conditions. The same for given axial position but different heated tubes in the evaporator shows more nonlinear evolution behavior, and those measured in the same heated tube but at different axial heights in the evaporator undergo more distinct nonlinear dynamic behavior. These transient aspects of inner wall temperatures vary with average holdup of solid particles and motion of vapor bubbles in vapor–liquid–solid flow. Riyadh *et al*. (2012) made an unsteady investigation of experimental and theoretical study for effect of particle size, fluidized bed velocity and heat flux on the thermal behavior for gas-solid flow. He observed that increase of heat flux cause increase in the temperature profile for different particle and fluidized bed velocity. Temperature distribution along the fluidization column increases with fluid velocity. The temperature profile increases as the mean solid particle diameter decreases. Baskakov *et al*. (2013) attempted to describe transients using the automatic closed loop control analysis methods. The parameters calculated from an analysis of unsteady heat balance equations are compared with the experimental data obtained in a 12 MW boiler. The equations were observed to describe the transient modes of operation with good accuracy. Dependences for calculating the time constants of unsteady processes were also obtained. Brown and Lattimer (2013) studied the gas to particle heat transfer characteristics in a pseudo 2-dimensional bed under fixed, fluidized and spouted regimes. They successfully captured full field view of transient particle temperature distribution using infra red tomography measurement technique. The highest rates of energy resulting from intra particle temporal change was found in the annular zone from the downward entrainment of particulates surrounding the spout channel

2.5 WASTE HEAT RECOVERY

The primary waste heat recovery methods consist of capturing and transferring the waste heat from a system through a fluid medium back to the system as an extra energy source [Reddy *et al*. (2013)]. This additional or extra energy source can be used to create an additional heat or to

generate electrical and mechanical power [Naik *et al*. (2012)]. A thorough investigation is required regarding the amount and grade of heat recoverable from a system which may depend on the type and source of waste heat and also in order to justify which waste heat recovery system can be used. Among the many different heat recovery technologies available for capturing and recovering the waste heat most of them mainly consist of energy recovery heat exchangers in the form of a waste heat recovery unit. These waste heat recovery systems mainly comprise of the common heat exchanger systems such as air preheaters including recuperators, regenerators, rotary regenerators, heat wheels and run around coil, regenerative and recuperative burners, heat pipe heat exchangers, plate heat exchangers, economisers, waste heat boilers and direct electrical conversion devices. The principles behind all these units are the same- to capture, recover and exchange heat with potential energy content in a process. Waste heat recovery is a very popular and major area of research investigation, and literatures dealing with this aspect are available in plenty where in the investigators have devised novel methods to recover waste heat from various thermal systems, engines and other machineries. Roy *et al*. (2010) analysed an organic Rankine cycle using refrigerant as working fluid such as R-12, R-123 and R-134a and their abilities to convert low-grade heat source to power. Their investigation showed that R-123 has the maximum work output and efficiencies Investigations on waste heat from organic wastes in industries [Zhongyi *et al*. (2015)], reusability of the energy of the exhaust gas from the calciner for production of carbon [Liang-Chen *et al*. (2014)], analytical study on the waste heat recovery Combined Ejector and Vapour Compression Refrigeration System [Maurya (2014)] have been carried out. Researches on the performance improvement of a boiler through waste heat recovery from an air conditioning unit [Jain *et al*, 2013], waste heat recovery steam generator in sponge iron plant. [Loganathan *et al*. (2013)], efficient way to generate captive power through Waste Heat Recovery (WHR) to meet the needs of Iron and Steel Industries [Umamaheswari *et al*. (2013)], power generation from waste clinkers in cement industries [Saidawat (2015)] have been reported. In a major research involving feasibility analysis of a thermos economic waste heat recovery system, Soylemez (2008) presented a simple algebraic optimization formula for estimating the optimum length of a finned pipe that is used for waste heat recovery wherein it was deduced that there exists a local maximum net life cycle energy savings value for heat recovery applications. Literatures on waste heat recovery through shell

and finned tube heat exchangers from exhaust gas [Pandiyarajan *et al*. (2011)], single-effect ammonia-water heat pump from industrial processes [Srinivas (2012)], thermoelectric generator to recover heat from automobiles [Demir *et al*. (2017)], application of ORC and Kalina cycle for heat recovery from air cooler [Varga and Palotai (2017)] are also available. Fu *et al*. (2012) proposed an open steam power cycle used for IC engine exhaust gas energy recovery where they took an I C engine where three cylinders were taken as ignition cylinder and the last one used for steam expansion cylinder. The exhaust pipe was coupled with a Rankine steam cycle system which used the high temperature exhaust gas to generate steam; then, the steam was injected into steam expansion cylinder. An optimal single-loop organic Rankine cycle (ORC) system proposed by Negash *et al*. (2018) was capable of improving the net power output by efficiently utilizing the available waste heat sources of excavator engines. Many researchers also investigated various unconventional and novel methods of heat recovery. Dai *et al*. (2011) investigated both the technical concept and basic features of a novel liquid metal based thermo electric generator (TEG) for waste heat recovery where a calculated efficiency of 2% in the whole TEG system was obtained. Another innovative technology based on shape memory was studied by Langan and O'Toole (2017) where one such alloy nitinol utilized heat in the form of hot water or water-glycol mixture and was designed into an innovative system to convert heat into linear motion thus inventing a new engine cycle that runs on hot water. Systematic methodologies for extracting waste heat from industrial zones [Stijepovic *et al*. (2011)], exergy balance and exergy analysis on I C engines for recovering waste heat through combined Rankine and kalina cycle [He *et al*. (2011)], and analysis of the performance of different bottoming Rankine cycles with water-steam and/or ORC configurations in classical and innovative setups such as a waste heat recovery system in a Heavy Duty Diesel (HDD) Engine [Dolz *et al*. (2012)] are some of the investigations that have made some remarkable contributions towards the field of waste heat recovery studies.

Thus it is seen that fundamental and applied research towards waste heat recoveries from various thermal systems has been carried out, but few results have been reported on heat recovery in downcomers even though it is an important element in their design and application. One literature mentioned about the wall-to-suspension heat transfer coefficient (HTC) in the downcomer [Zhang *et al*. (2015)]. This particular investigation found that the HTC increases

linearly with the solids flux until a certain fixed value. However, waste heat recovery from the downcomer of a PCFB is yet to be investigated.

2.6 SUMMARY OF THE LITERATURE REVIEW

A large number of literatures are available on investigation of heat transfer and hydrodynamic of circulating fluidized bed. The major components which found interest in the literatures were the riser section and cyclone. Most of the literatures dealt with the steady state behavior of the circulating fluidized beds. However very less literature is available for investigation of transient hydrodynamics and heat transfer behavior. This is a very important area of research necessary to fully understand the behavior of the bed during load variations and enhance the performance of an ACFB unit during the transient period and also during start up and shut down of the unit. Moreover the phenomenon of heat transfer in the upper splash region is important because this is the region where most of the super heater tubes, recuperators are installed. Hence a thorough understanding of heat transfer in this region is specifically required. Further it is has been observed that various literatures are available on waste heat recovery systems and their optimization. Organic Rankine cycle has been mostly used for low grade waste heat recovery. Different types of heat exchangers and thermo electric generators were also used by investigators for waste heat recovery. However, it is seen that very limited literatures are available on the experimental works related to the recovery of waste heat from the down comer part of an ACFB or PCFB. Hence it is observed that literatures on steady state hydrodynamic studies and heat transfer on mostly ACFBs are available. Waste heat recovery from various thermal systems under steady state conditions are also plenty. Transient studies on PCFB are limited to investigations of the hydrodynamics during switching of fluidizing gas, transient behavior of solid flow by concurrent visual observation and voidage measurement and instantaneous measurements of solid concentrations whereas extensive experimental investigations on transient heat transfer and hydrodynamics in a PCFB is lacking. Also no research has been done on the waste heat recovery from the downcomer of a PCFB though a few research on the waste heat recovery from waste gas and ash of ACFB are available.

2.7 SCOPE OF THE PRESENT WORK

In the view of above closure of literature reviews, the following aspects are considered in the present thesis work

- Investigation of the transient hydrodynamics along the height of the riser under varied operating conditions in a PCFB with sand and coal blends as bed inventory.
- Investigation of the transient bed temperature profile, surface temperature profile and transient heat transfer along the riser during sudden changes in operating pressure, superficial velocity, exhaust flow rates and power input in a PCFB with sand and coal blends as bed inventory
- Development of a heat recovery system to recover heat from the down comer in a PCFB and investigation of the transient heat recovery during stepped and ramped changes in superficial velocity and power input from the same

2.8 SUMMARY

In this chapter, an elaborate discussion on the literatures available on the various aspects of ACFB and PCFB were discussed along with a discussion on the investigations on waste heat recovery from various thermal systems including ACFBs. Based on the outcome of this literature review, the scope of present work was presented. The following chapter addresses the details of the experimental set ups and the procedures for the present investigation.

Chapter – 3

EXPERIMENTAL SETUP AND PROCEDURE

3.1 INTRODUCTION

In this chapter, description of the pressurized circulating fluidized bed (PCFB) setup and experimental procedure has been discussed. Experiments are conducted in a PCFB unit with sand and coal as inventory. Experimental conditions and procedure followed for the experiments are elaborated. Experimental set up on the heat recovery and procedure followed are described.

3.2 THE PCFB EXPERIMENTAL SETUP

A PCFB unit comprising of a riser, a downcomer, and a cyclone separator used in order to investigate the heat transfer and hydrodynamics at varied condition. Two sets of experiments are performed, one at the upper splash region and the other all along the riser. Figure 3.1 presents the detail of the component of the PCFB unit. The height of the riser fabricated from stainless steel (SS) considered in the present study is 2000 mm with an inner diameter of 54mm. The wall thickness is 3 mm. The cyclone separator of the PCFB unit is constructed out of mild steel with a barrel diameter of 80 mm and height 160 mm. A dust filter and fine wire mesh is attached to the top of the cyclone separator to prevent bed materials from escaping with the exhaust air. The exhaust is collected by another SS pipe that is surrounded by a water jacket for cooling. The exhaust is allowed to flow through a flow control valve and an orifice plate that has a differential pressure transmitter connected across it to calculate the volume flow rate of the exhaust. Entrained solids are recovered in this cyclone separator and returned to the bottom of the riser column through the downcomer of 25 mm internal diameter. The bottom of the downcomer has a graduated transparent section connected to a butterfly valve for visualization of the solid flow and measurement of solid flow rate. The distributor plate used is of straight hole orifice type having 16.9% opening area and is fixed at the bottom of the riser column. Static pressures are measured along the riser height at 13 cm, 25 cm, 37 cm, 49.5 cm, 69.5 cm, 90.5 cm, 118 cm, 142 cm and 176 cm, above the distributor plate. Fine wire mesh (BS 400) and cigarette filters are used at the pressure tapings to minimize pressure fluctuations and prevent leakage of sand. Experiments were performed both with and without using wire mesh and cigarette filters. It was

found that there was some negligible amount of difference in pressure readings in the two cases, but the use of these filters could not be avoided as they were necessary to restrict the leakage of solid particles through the pressure tappings. Pressure drops are measured with piezo resistive type pressure transmitters (accuracy ± 0.2%) which are fitted to the riser section at the above mentioned location using SS tubes of 10 mm diameter and self-sealing ferruled fittings.

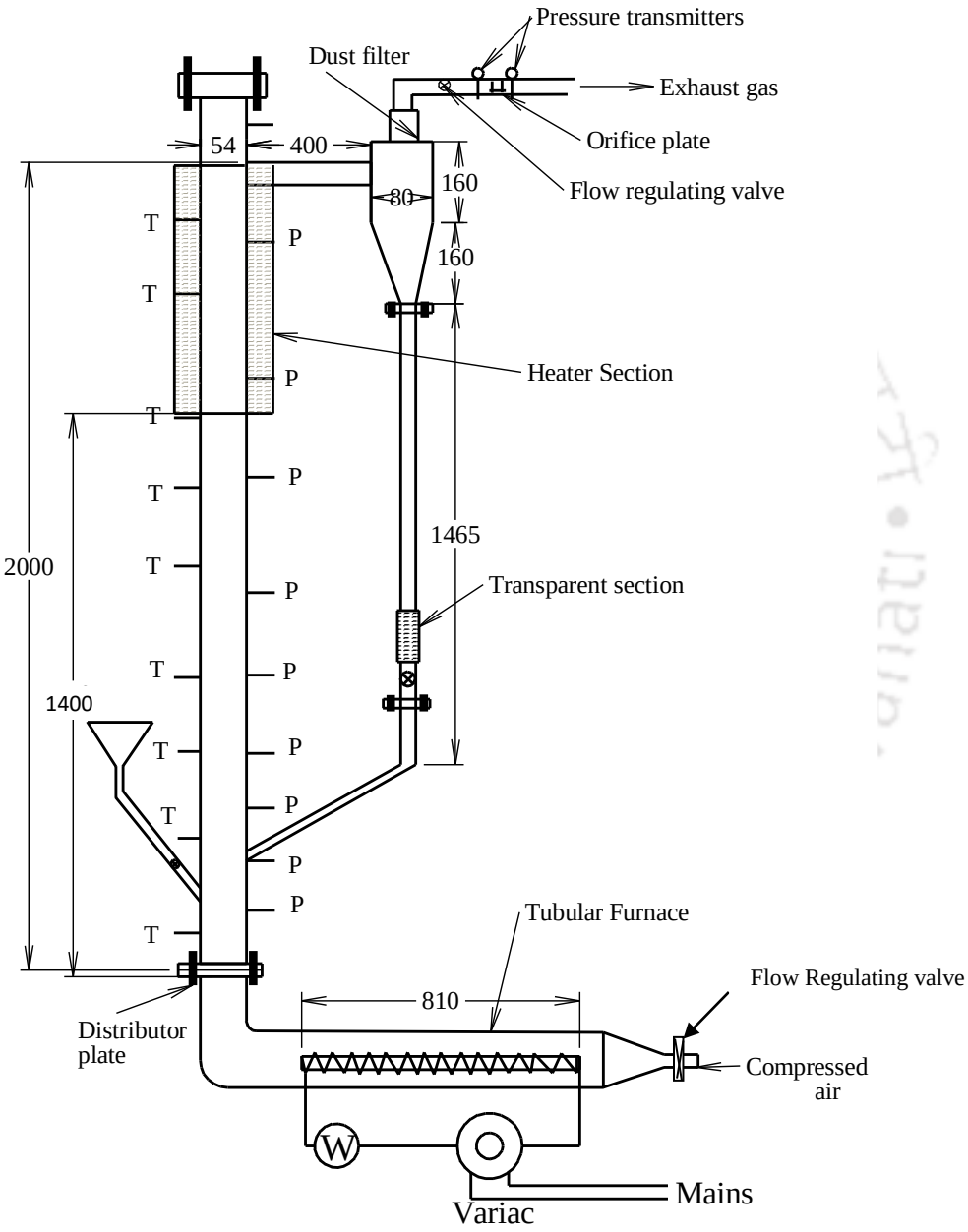

Fig.3.1 Schematics of experimental setup of the PCFB

A tubular furnace is used for the studies along the riser to heat the air before entering the bed from the compressor. This furnace is fabricated out of a SS tube of 54 mm inner diameter and consisting of kanthal heating coil wrapped around a ceramic tube. An autotransformer and a wattmeter are used to regulate the power supply to the furnace. This furnace remains switched off during the studies on the upper splash region. The upper region of the riser column at a height 1.4 m from the distributor plate is considered for the experiments on the upper splash region. The surface area of this section is electrically heated with kanthal heating coils (rated power of 1000 Watt and resistance of 46 Ohms) wrapped around it and insulated with ceramic wool. Mica sheet of 1 mm thickness is used as electrical insulation over which the heater coil is wrapped. The power supply to the coils is regulated by an autotransformer and a wattmeter in the same way as that for the hot bed furnace. The fluidizing air is supplied from a compressor and is regulated by a flow control valve and measured using an attached rotameter and a compressed air flow meter with an accuracy of ± 0.3%. The variations were introduced manually through flow regulating valves and power regulating autotransformers. The changes from one value to another was brought about in less than 10 seconds for all experiments related to heat transfer and hydrodynamics. The time interval for input variations were also recorded and displayed for all purposes. However, for the heat recovery experiments, the variations were brought about through stepped and ramp changes both and the time interval for these changes were also recorded. For repeated runs, the exact replication of the variation brought about manually is not possible, but utmost care was taken to maintain the same.

Figure 3.2 shows the photograph of the experimental set up. The ceramic insulated heater section at the upper region of the riser, the thermocouple wires, the pressure tappings, the downcomer along with the transparent section are seen in this photograph. It may be mentioned that The initial fabrication of the PCFB was already done by an earlier researcher of the Institute. The author has made some modifications and improvement on the setup to make it suitable for transient studies. Some of the modifications done were: fabrication of the SS downcomer to replace the earlier downcomer that had a transparent section. Fabrication of the tubular furnace, replacement of the rough flanged joints with more polished flanged joints to make the setup airtight and suitable for high pressure studies. Wrapping of thermal insulation on the whole rig to minimise heat loss was also done by the author. The modified instrumentation using highly sensitive and accurate sensors on the set up was also done for performing transient studies. Piezo

resistive pressure sensors of higher accuracy (± 0.25% of full scale) and sensitivity, K- type thermocouples of accuracy ± 0.4 % and response time 0.003 sec. were incorporated. Special air tight fittings of stainless steel were also additionally used to attach the pressure transducers and thermocouples. Further, the heat recovery experiments were done on a completely new downcomer that was fabricated by the author. The heat exchanger attached to the downcomer was also fabricated by the author

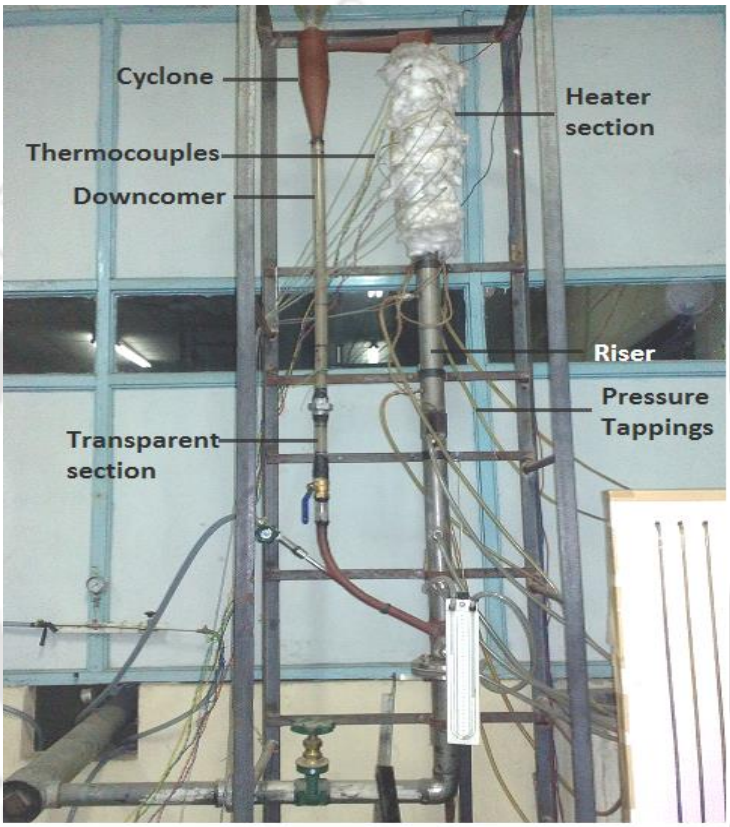

Fig. 3.2. Photograph of the experimental PCFB unit.

A detailed schematic of the heater probe in the upper splash region used for the studies is given in Fig. 3.3.

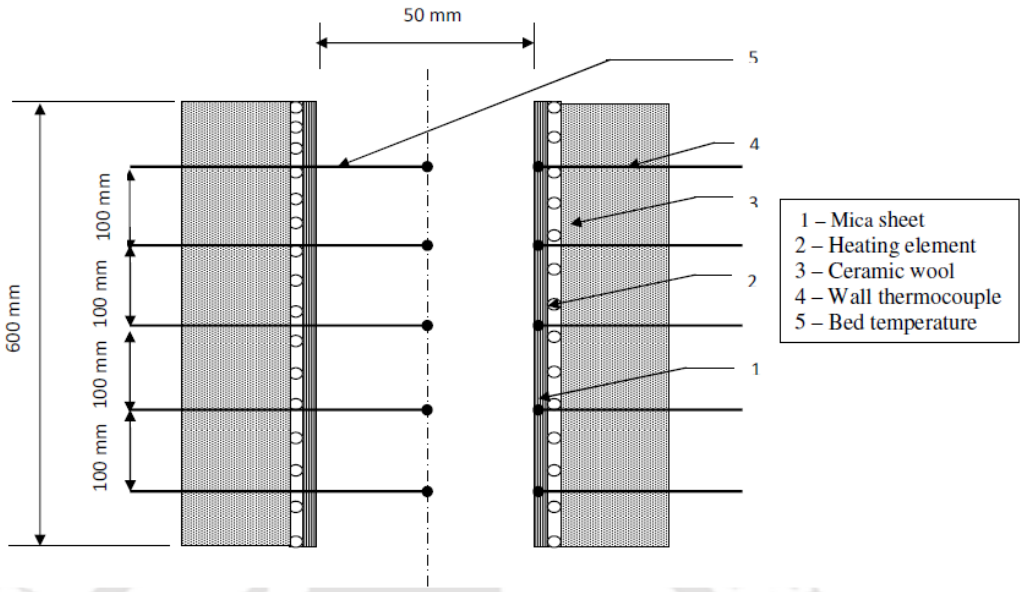

Fig. 3.3 Schematic diagram of heat transfer probe

K- type thermocouples of ±0.4% accuracy are used to measure the surface and bed temperatures. The locations of the thermocouples from the distributor plate are 1500, 1600, 1700 1800 and 1900 mm, respectively. Five numbers of similar thermocouples are also installed to measure the radial temperature variations in the bed at a non-dimensional distance (d/D) OF 0.2, 0.4, 0.6 and 0.8 (Fig.3.4) at a height of 1.6 m from the distributor plate, respectively as shown in Fig. 3.4.

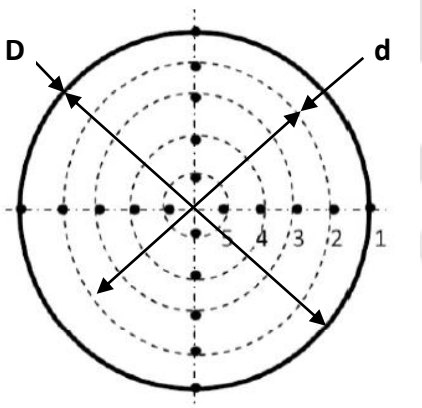

Fig. 3.4. Location of thermocouples for measurement of bed temperature at various radial distances (d/D).

3.3 EXPERIMENTAL PROCEDURE

The experiments on the upper splash region are carried out initially. For this, a measured quantity of inventory is fed into the unit through the top of the cyclone separator which falls down by gravity to the bottom of the riser through the downcomer and the butterfly valve in wide open condition. Regulated amount of fluidizing air is supplied from a compressor of peak pressure 10 bar to the PCFB unit through the flow control valve. Regulated power is supplied to the coil of the heat transfer proble through an autotransformer. The supplied current and voltage are measured using voltmeter and ammeter. A multifunction meter is also used to measure the supplied power to the coil. Adequate electrical and thermal insulation are provided. The axial heat loss by conduction is also prevented by providing ceramic wool insulation in between the joints. Agilent 34972A LXI data acquisition/ switch unit is used for measurement and record of temperature and pressure. Sand and pulverized bituminous coal are used as bed inventory for the study. The particle size of both sand and coal are in the range of 355 to 455 microns which is obtained by standard BIS sieves. The density of the sand and coal used is 1690 kg/m^3 and 600 kg/m^3 , respectively. Experiments are performed with pure sand and also with 2.5%, 12.5% and 20% coal blended with sand. Two different constant heat flux of 1500 W/m^2 and 2000 W/m^2 with primary fluidizing air flow rates of 6.6 l/s, 5.1 l/s and 3.1 l/s, respectively are used. In all the experiments the heat transfer coefficients at various locations along the axial direction are evaluated. The temperature measurements at the heater section are taken with K- type thermocouples (Range: -150 to + 1350°C and Sensitivity: 41 µV/°C).

The wall-to-bed heat transfer coefficient is estimated from the measured local surface to bed temperatures as given below

$$h_i = \frac{q}{T_{si} - T_{bi}} = \frac{V \times I}{A_h (T_{si} - T_{bi})} \tag{3.1}$$

where i represents any location along the riser height and A_h is the heat transfer probe surface area, where i is the thermocouple position.

The construction details of a K-type metal-sheathed thermocouple used for transient temperature measurement are shown in Fig. 3.5. The measuring tip is just exposed to outside and the tip of the thermocouple is silver brazed carefully for preventing the leakage of air into the

thermocouple during measurement. A metal-sheathed tube is drawn into two SS-316 tubes, which are filled with magnesium oxide (MgO) insulation, and further they are connected to the K-type thermocouple wires in the second SS tube which are fitted using self sealing ferruled joints.

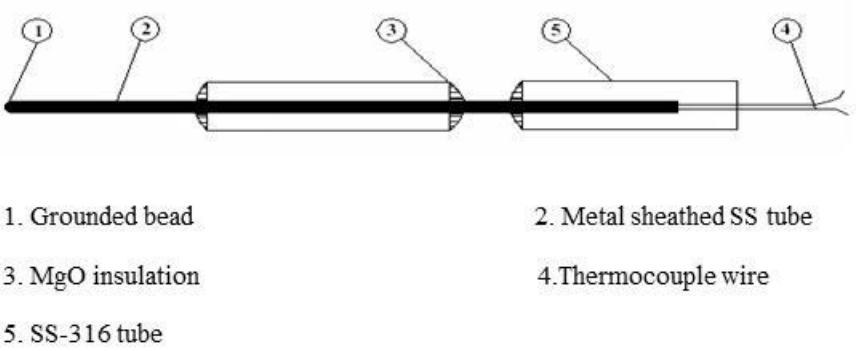

Fig. 3.5. Schematic diagram of K type metal sheathed thermocouple

The same data acquisition system is used for recording the pressure at various locations for the hydrodynamic experiments. Static pressure along the riser is measured by using piezo resistive pressure sensors. The pressure sensors are all calibrated using a dead weight hydraulic tester before fitting them to the PCFB. High precision pressure gauge (Swegelock make) is used for the measurement of the compressor delivery pressure. The data is collected all throughout the experiment till the process reached steady state. For thermal equilibrium, temperature rise is monitored, and for hydrodynamic equilibrium, circulation rate is monitored. Same procedure is followed with every change in operating parameters. Finally, the transient axial and radial heat transfer co efficient, transient temperature profiles and bed voidages are investigated for four different proportions blending of pulverized coal in sand such as 0%, 2.5%, 12.5% and 20%. Three more sets of experiments are performed with heat flux of 1500W/m^2 to observe the transient behavior resulting from sudden increase and decrease in flow rate of fluidizing air. Two of them are performed with sand for flow rate of fluidizing air suddenly changing from 5.1 l/s to 3.1 l/s and in a reverse from 3.1 l/s to 5.1 l/s. The other experiment is performed with 2.5% blending of pulverized coal for the fluidizing air flow suddenly changing from 5.1 l/s to 7.1 l/s. For generating the transient conditions, flow control valve is used to suddenly change the flow rate of fluidizing air. The temperature data capture rate for these experiments is 1 Hz. The

volume flow rate of bed material is noted manually after every 3 to 4 minutes. All the experiments are repeated (three) times and the average data calculated.

The bed voidage ε is calculated using the following formula

$$\varepsilon = 1 - \frac{10 \times \Delta h}{\rho_s \times L_m} \tag{3.3}$$

where Δh is the difference in pressure readings between two consecutive pressure transmitters measured in cm of water column

ρ_s is the solid density in kg/m^3

and L_m is the distance between two consecutive pressure tappings in m.

The Eq. (3.3) can be rewritten as

$$\varepsilon = 1 - \frac{\Delta P}{\rho_s \times L_m} \times 1019.44 \tag{3.4}$$

where ΔP is the difference in pressure readings between two consecutive pressure transmitters measured in bar.

The suspension density is calculated using the formula

$$\rho_{sus} = \rho_s (1 - \varepsilon) + \varepsilon \rho_g \tag{3.5}$$

where ρ_{sus} is the suspension density, ρ_s is the density of solid, ε is the voidage and ρ_g is the density of gas

For the experiments in whole riser column, the heater probe at the upper splash region is kept switched off. Then the heat transfer experiments are performed for which the power supply to the tubular furnace coil located below the distributor plate (Fig. 3.1) is activated with the help of an autotransformer and fixed to a constant power input for heating the inlet air issued from the compressor. Similar K-type thermocouples used in the cold bed experiments are used to measure the surface and bed temperatures along the riser. The locations of the thermocouples from the distributor plate are 9.5 cm, 31 cm, 53.5 cm, 70 cm, 98 cm, 117 cm, 134 cm, 164 cm and 182 cm, respectively. Agilent 34972A LXI data acquisition switch unit is used for measurement .Inventories of 400 g sand, 500 g sand and 500 g sand with 12.5% coal blend is used as bed material. The properties of sand and coal are the same as those used in the experiments involving

the upper splash region. Experiments are performed for each of the inventories for transients in heat inputs, transients in exhaust flow rates and transients in operating pressure. In all the experiments, heat transfer coefficient is evaluated. The temperature and pressure measurements are captured after every 1 (one) second. The solid circulation rate is measured manually by calculating the time required for a certain volume of the solid particles to accumulate in the downcomer section by observing through a small transparent section in the downcomer after every 3 to 4 minutes. Solid circulation rate of 0.95 to 4.5 kg/m^{2}s was maintained in the experiments. All the experiments are repeated 3 (three) times and the average data are calculated. The following equation is used for calculating the heat transfer co efficient in the riser column.

$$h_i = \frac{q}{T_{bi} - T_{si}} = \frac{V \times I}{A_h (T_{bi} - T_{si})} \tag{3.2}$$

The sudden changes that are introduced in the experiments are power input of 0.9 kW, 1 kW and 1.2 kW, operating pressure of 2 bar and 3 bar and exhaust flow rates of 3 l/s and 5 l/s. For generating the transient conditions, pressure regulator is used to change the operating pressure; auto transformer is used to change the heat input and the exhaust control valve to change the exhaust flow rate. Finally, the transient heat transfer co efficient and transient temperature profiles are investigated for the three different types of inventories. The combination of the parameters is shown in details in the result section.

3.4 EXPERIMENTS ON HEAT RECOVERY FROM THE DOWNCOMER OF THE PCFB

The present study on transient heat transfer in a PCFB involves the laboratory scale PCFB set up as described in the previous section. In this section the fabrication of two types of heat exchangers and the experimental procedure in recovering the heat from the downcomer will be discussed

3.4.1 WATER JACKET TYPE HEAT EXCHANGER WITH FINS

The schematic diagram of a water jacket type heat exchanger with fins is given below in figure 3.6. The SS downcomer with a transparent tube at the bottom which is used in the experiments as described in section 3.1 is replaced with a fully metallic one made of the same material. 20

(twenty) numbers of C shaped baffles or fins are welded onto it at regular intervals with consecutive baffles on opposite sides to provide a helical path for the water flow as shown in the figure 3.7.

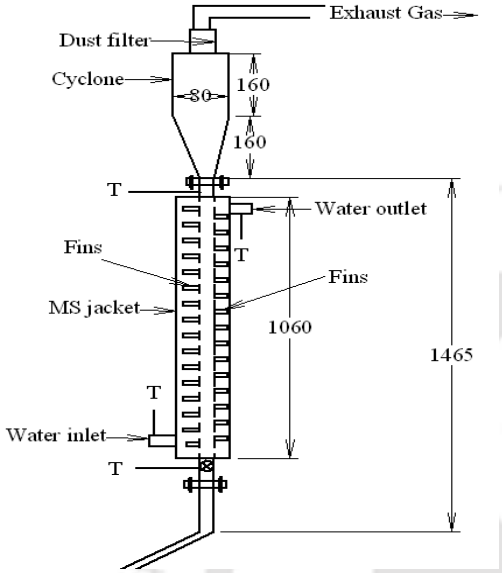

Fig. 3.6 Schematic of water jacket type heat exchanger

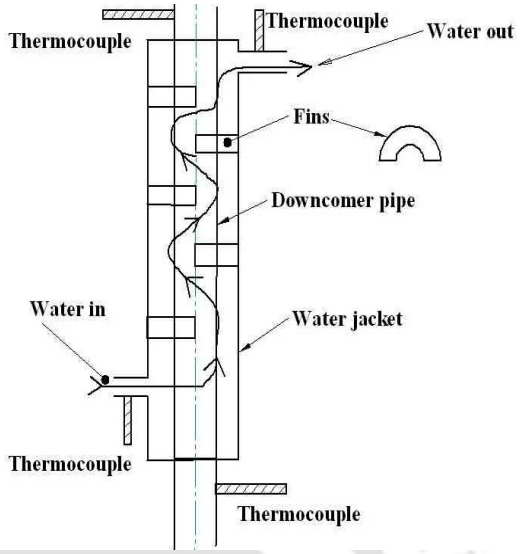

F.g 3.7 Schematic of the path of water flow

It is then inserted into a MS pipe of 55mm internal diameter and 1060 mm length concentrically as shown in the Fig. 3.6. The ends are closed by welding MS sheets of 3mm thickness. Two holes are drilled near the ends to provide for water inlet and outlet. The ports are connected to tubes to facilitate flow of water. Flow rate of water is measured with the help of water rotameter. K type thermocouples are fitted at the ports and also at the top and bottom part of the downcomer to measure the inlet and outlet temperatures of water and fluidized particles respectively. Tap water at room temperature is connected to the heat exchanger to absorb the heat carried by the fluidized particles in the downcomer. The whole set up is thermally insulated with ceramic wool.

3.4.2 SPIRAL TUBE TYPE HEAT EXCHANGER

The schematic of a spiral tube type heat exchanger is given below in Fig. 3.8. The downcomer is replaced with a SS pipe of 54mm inner diameter. A copper tube of 5 mm inner diameter is

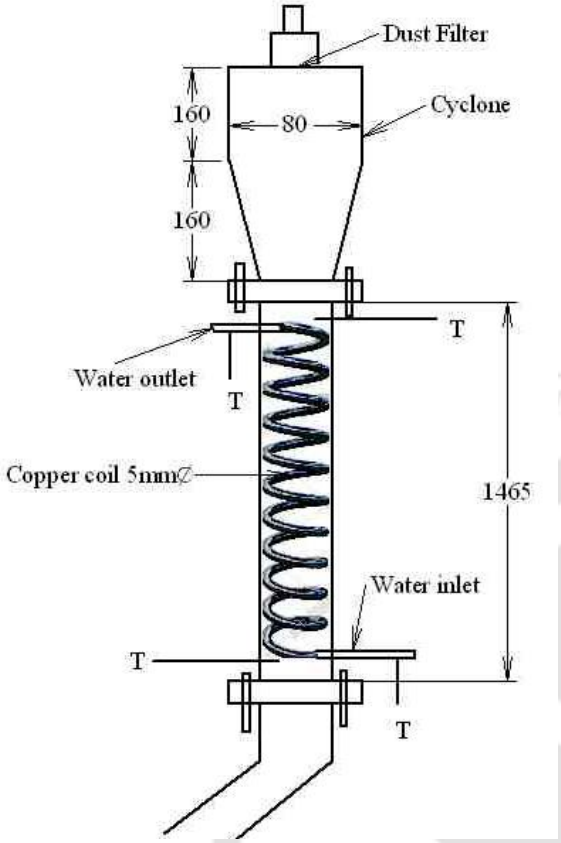

Fig. 3.8 Schematic of a spiral tube type heat exchanger

Fig. 3.9 Photograph of the copper coil used in the heat exchanger

wound around a steel rod with the help of a lathe machine to turn it into a spiral tube as shown in the Fig. 3.9. It is then inserted into the downcomer as shown in Fig. 3.8. Number of turns of the coil is 35. The two ends of the coil are brazed to two holes at the upper and lower ends of the downcomer which are subsequently fitted to copper pipes to act as water inlet and outlet. A photograph of the spiral tube type heat exchanger is shown in Fig. 3.10.

Fig. 3.10. Photograph of spiral tube heat exchanger

Flow rate of water is measured in similar way as that of the water jacket type heat exchanger. Here also the whole heat exchanger is covered with ceramic wool to provide thermal insulation. This heat exchanger has the benefit of enhanced residence time of water in the heat exchanger. The down comer in this case is replaced with a larger diameter pipe to account for the loss of volume in the downcomer with the insertion of the copper tube.

The heat absorbed by the water will be calculated using the formula as follows

$$Q_c = m_c C_{pc} (T_{c,o} - T_{c,i}) \quad (3.6)$$

Where m_c is the mass flow rate water, C_{pc} is the specific heat of water water, $T_{c,o}$ and $T_{c,I}$ are the temperature of water at outlet and inlet respectively.

3.4.3 EXPERIMENTAL PROCEDURE FOR HEAT RECOVERY FROM THE DOWNCOMER OF PCFB

The same inventory of sand used in experiments described in the earlier section is fed into the unit. The heat recovery experiments are performed for which regulated amount of fluidizing air is supplied from a compressor of capacity 10 bar to the PCFB unit through the flow control valve. In order to achieve a higher typical bed temperature at the top of the downcomer in the order of 350 °C to 480 °C, an additional heating coil of 1 kW capacity is inserted into the riser column. Power supply to both the tubular furnace and the heater coils are simultaneously activated with the help of 2 (two) autotransformer and fixed to a constant value. Water is supplied to the heat exchanger through a rotameter. The fluidizing air flow rate is measured by a compressed air flowmeter. The data acquisition system for the temperature measurement is also

switched on to capture data after every 5 seconds. The data is collected all throughout the experiment till the process reached steady state. For thermal equilibrium, temperature rise is monitored. Further experiments are carried out for transient conditions. The procedure for investigating heat recovery during transient conditions is same as that for the steady state with the difference that sudden changes in power input and superficial velocities are introduced during the experiment. The procedure for introducing these changes has already been discussed in section 3.3. These changes are introduced in two ways viz ramp increase and decrease as well as step increase and decrease. The combination of the parameters used and transients introduced along with the types will be discussed in details in the result section of the heat recovery experiments in chapter 6. The temperature data capture rate for the experiments involving transient conditions is 1 Hz.

3.5 SUMMARY OF THE CHAPTER

In this Chapter, development of the PCFB experimental set up and its experimentation have been discussed. The development of heat exchangers and their experimentation in heat recovery has also been discussed. The results of the experiments carried out as per the procedure described in this chapter are presented in the subsequent Chapters.

Chapter – 4

RESULTS AND DISCUSSION ON TRANSIENT HYDRODYNAMIC STUDIES

4.1 INTRODUCTION

Based on the experimental procedure described in the Chapter 3, series of experiments were carried out to investigate the bed hydrodynamics on the experimental setup described in the same Chapter. Result of the experimental investigation with significant outcome is presented in this Chapter.

4.2 INVESTIGATION OF TRANSIENT BED VOIDAGES

The transient experiments on bed hydrodynamics are conducted at various operating conditions by introducing stepped changes or transients to the input parameter which are exhaust flow rate and operating pressure. The experimental matrix showing the combination of parameters and transients in input are given in the Table 4.1

TABLE 4.1 LIST OF COMBINATION OF PARAMETERS AND INPUT TRANSIENTS FOR BED HYDRODYNAMICS STUDY

SL NO	BED INVENTORY AND WEIGHT	OPERATING PRESSURE	FLUIDIZING AIR FLOW RATE	EXHAUST FLOW RATE	INPUT TRANSIENT
1	Sand 400 g	2 bar	4.8 l/s , 4.5 l/s	4 l/s to 2 l/s in 10 s	Exhaust flow rate decreased in step
2	Sand 400 g	2 bar	4.5 l/s , 5.1 l/s	2.5 l/s to 5 l/s in 10 s	Exhaust flow rate increase
3	Sand 500g	2 bar	4.8 l/s , 4.5 l/s	4.8 l/s to 2.6 l/s in 10 s	Exhaust flow rate decrease
4	Sand 500 g	2 bar	4.8 l/s , 5.1 l/s	3.1 l/s to 4.8 l/s in 10 s	Exhaust flow rate increase
5	Sand 400 g + Coal 50 g	2 bar	4.8 l/s , 4.5 l/s	4.5 l/s to 3.3 l/s in 10 s	Exhaust flow rate decrease
6	Sand 400 g + Coal 50 g	2 bar	4.8 l/, 5.1 l/s	2.8 l/s to 5.1 l/s in 10 s	Exhaust flow rate increase
7	Sand 500 g	3 bar to 2 bar in 10 s	6 l/s , 4.8 l/s	5.7 l/s, 3.1 l/s	Operating pressure decrease
8	Sand 500 g	2 bar to 3 bar in 10 s	4.8 l/s ,6 l/s	4.5 l/s , 5.7 l/s	Operating pressure increase

Bed voidage ε, were calculated along the riser height at 8 (eight) different locations such as 19 cm, 37.25 cm, 59.5 cm, 80 cm, 104.25 cm, 130 cm, 159 cm and 191.75 cm above the distributor

plate. The static pressures are measured using piezo resistive type pressure transmitters and the difference in pressure readings between two consecutive pressure tapings is noted.

4.2.1 VARIATION OF BED VOIDAGE PROFILE WITH TRANSIENTS IN EXHAUST FLOW RATES

The variation of bed voidage profile at various riser heights for sudden changes in exhaust flow rates at an operating pressure of 2 bar for inventories of 400g, 500g sand and 500g sand blended with 50g coal are shown in Figs 4.1 through 4.8. It is observed that the voidage profiles have a certain degree of fluctuations of about ± 0.012 at every point of time which is around ±1.5% variation from the average value. In the first experiment with a bed inventory of 400 g sand and an operating pressure of 2 bar, the transient in input in the form of a sudden stepped decrease in the exhaust flow rates from 4 to 2 l/s as shown in Fig. 4.1(c) is introduced. This results in a corresponding output in the form of voidage change shown in the Fig 4.1 (a) and 4.1 (b). The two air flow rates (4.5 l/s and 4.8 l/s) in Table 4.1 and Fig. 4.1 corresponds to the two different exhaust flow rates of 2 l/s and 4 l/s, respectively. During experiment, it is observed that the change in the exhaust flow rate also causes change in the inlet air flow rate. It is observed that the voidage at lower heights of the riser viz 19 to 59.5 cm are not significantly affected by the transients. However, in Fig. 4.1 (b) drastic changes in voidages at the upper regions of 104.25 cm and 159cm are seen. Here the voidage fluctuation is 48%(approx) from an average value of 0.64 to 0.95 The pattern of changes in the output are similar to the pattern of change in the input. The sudden increase in voidage values at the upper region with a decrease in exhaust flow rate may be due to reduced solid circulation resulting from reduced velocity of the circulating air. Hence solid concentration decreased at the upper portion of the riser leading to an increase in voidage values. But the effect was observed to be insignificant in the lower portion of the bed as the transient in the exhaust is introduced far away from the lower region at the exhaust of the cyclone.

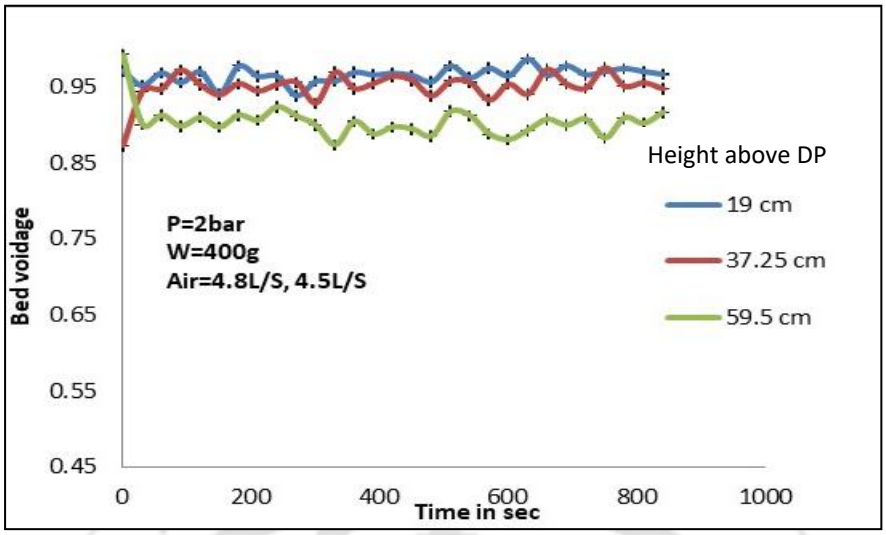

(a)

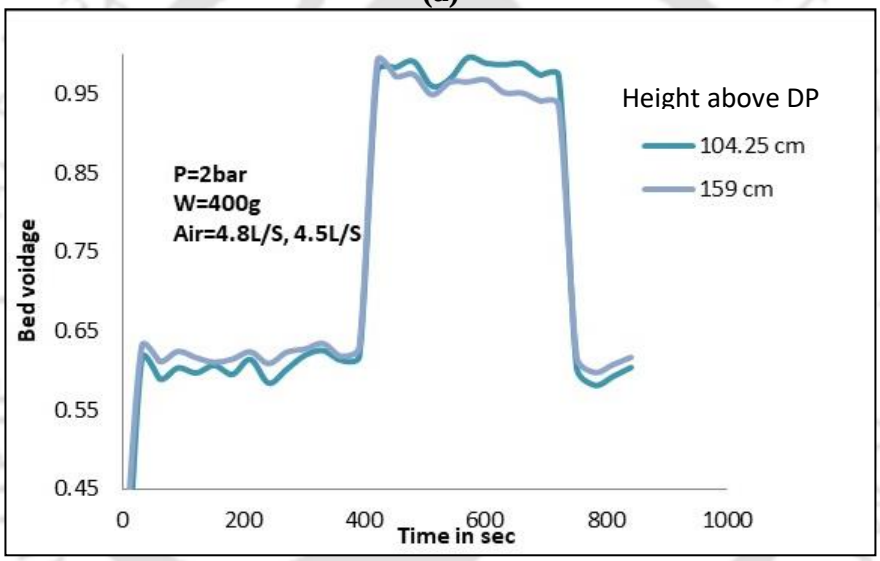

(b)

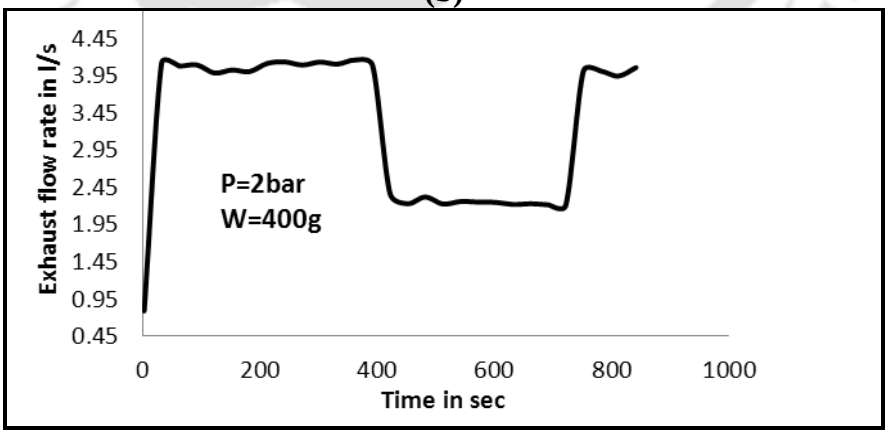

(c)

Fig. 4.1 Transient bed voidages along the (a) lower portion with error bars (b) upper portion of riser height for (c) sudden decrease in exhaust flow rates as the transient input

The reverse of the above is shown in the Fig. 4.2. The Fig 4.2(a) and (b) shows the resulting outputs in the voidage profiles for 400g sand resulting from the input transient shown in Fig. 4.2(c). which is a sudden increase introduced in the exhaust flow rate.

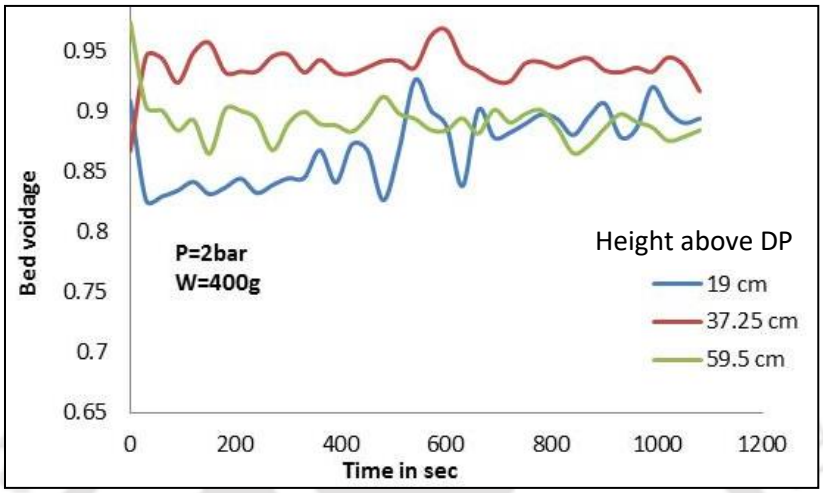

(a)

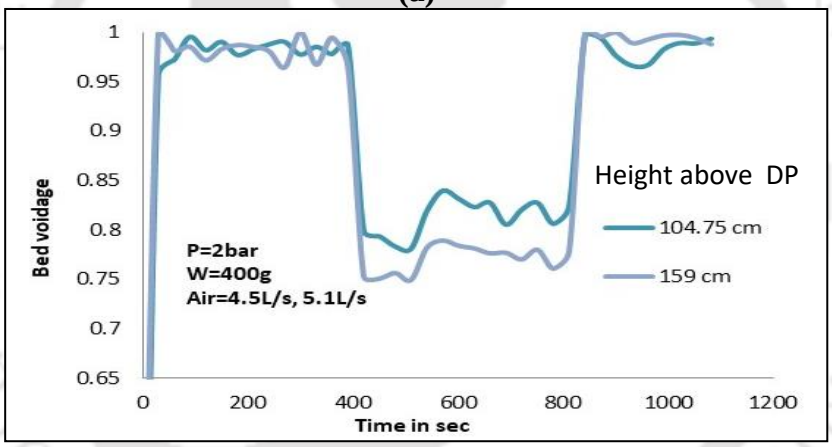

(b)

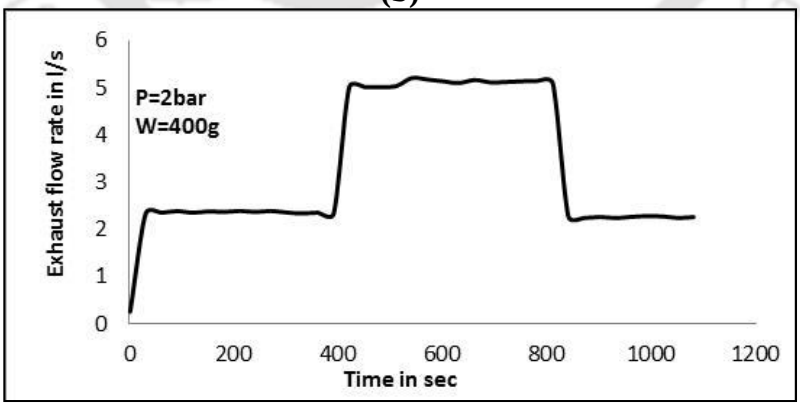

(c)

Fig. 4.2 Transient bed voidages along the (a) lower portion (b) upper portion of riser height for (c) sudden increase in exhaust flow rates as the transient input

In this case also it is observed that the voidages at riser heights of 104.25 cm and 159cm drops drastically by about 22% from an average value of around 0.97 to around 0.8 and 0.75 respectively when the exhaust flow rate was suddenly increased from 2.5 to 5 l/s. It is also observed that the voidages at the lower parts of the riser viz 19 to 59.5 cm are not significantly affected by these changes in exhaust flow rates. It may be because when the exhaust flow was suddenly increased, the solid circulation was increased due to resulting higher velocity of the circulating air and hence solid concentration increased at the upper portion of the riser leading to a decrease in voidage values. But the effect was not significant in the lower portion of the bed as the transient input is introduced at the top portion of the bed.

The Fig. 4.3 shows the steady state bed voidages for 400g sand for the different exhaust flow rates used in the above experiments. It is observed that the variation of bed voidage is very high from 0.98 to 0.5 at high exhaust flow rates of 4 l/s compared to a low exhaust flow rate of 2 l/s. where the variation is 0.9 to 0.98.This may be because of more turbulence in the bed at a higher exhaust flow rate. Also it is observed that the average bed voidage is more for lower exhaust flow rate than for higher exhaust flow rates. Moreover, the axial variation in voidage under steady state observed in Fig. 4.3 may be attributed to the valve that was used to control the exhaust flow rate. The valve used was a ball valve and partial openings of this valve might have resulted in backflow of the solid particles in the riser leading to the fluctuations observed.

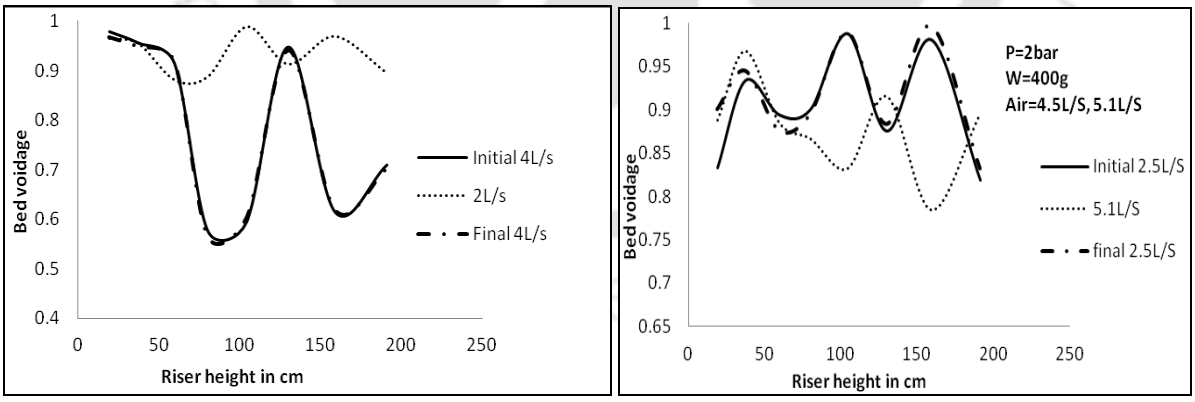

Fig. 4.3 Steady state bed voidages for 400g sand for the initial, intermediate and final conditions of exhaust flow rates

In the experiments with 500g sand as bed material, the transient voidage profiles are shown in the Fig. 4.4 to Fig.4.5. The transient in input in the form of a sudden stepped decrease in the exhaust flow rates from 4.8 to 2.8 l/s is shown in Fig. 4.4(c). The trend of output is almost

similar to the experiment with 400 g sand. Here too the resulting outputs are significant at heights of 159 and 104.25 where the voidage drastically increases by about 20% from an average value of around 0.79 to around 0.95 whereas in lower regions like 19cm height, 37.25cm and 59.5cm the voidage does not change drastically with change in exhaust flow rates. It is also observed that the voidages show a lower values for 500g sand compared to 400g sand.

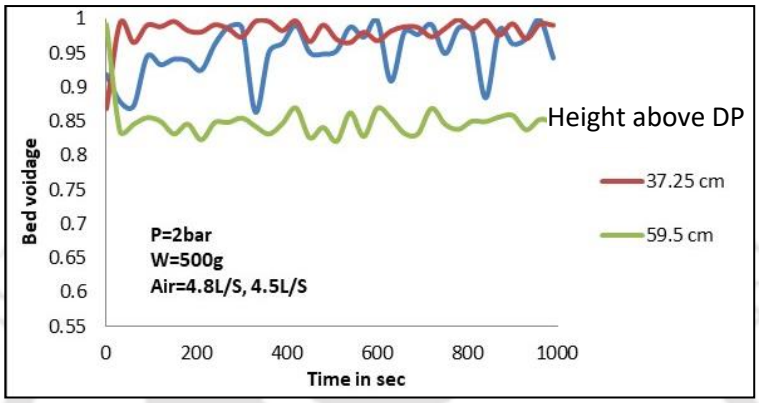

(a)

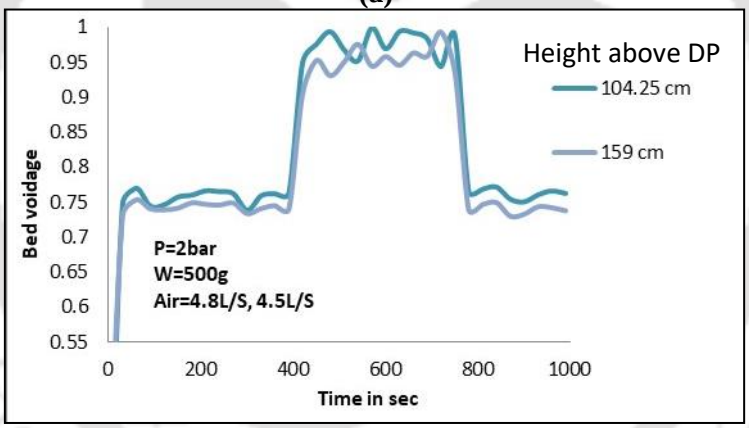

b)

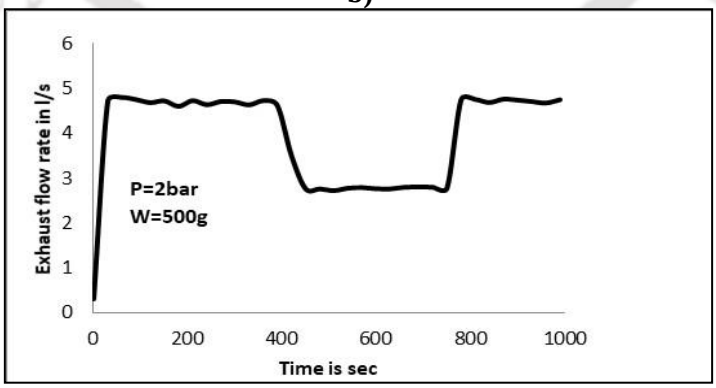

(c)

Fig. 4.4 Transient bed voidages along the (a) lower portion (b) upper portion of riser height for (c) sudden decrease in exhaust flow rates as the transient input

For example at a height of 59.5 cm the voidage for 500g sand is observed to be 0.8 while that for 400g sand is 0.9. This may be due to more concentration of solid in the bed with increase in volume of inventory.

Fig. 4.5 represents the output in bed voidages for 500 g sand along the riser height resulting from the transient in input in the form of a sudden stepped increase in the exhaust flow rates from 3.1 to 4.8 l/s.

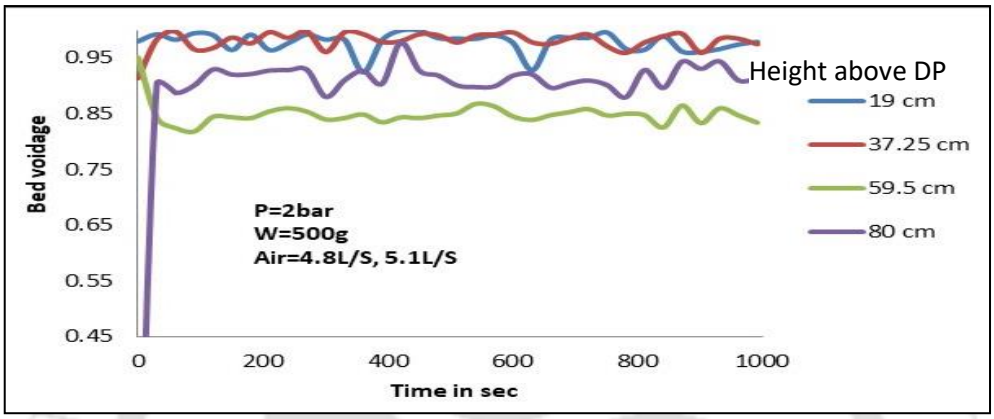

(a)

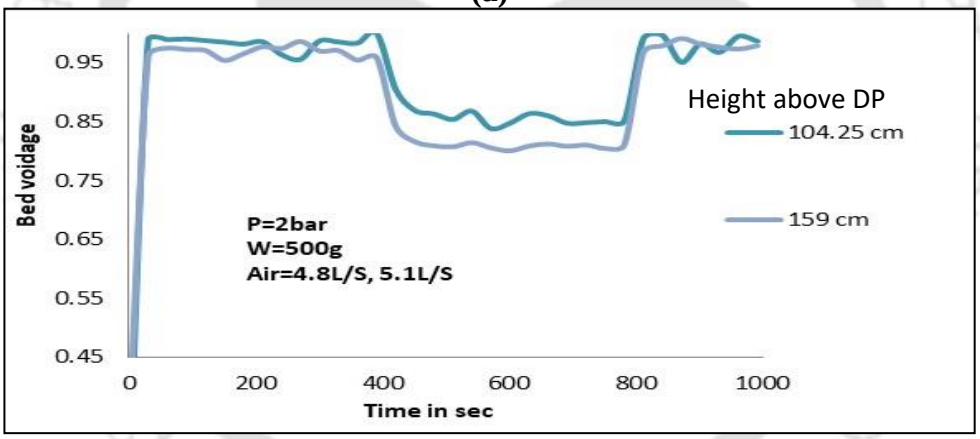

(b)

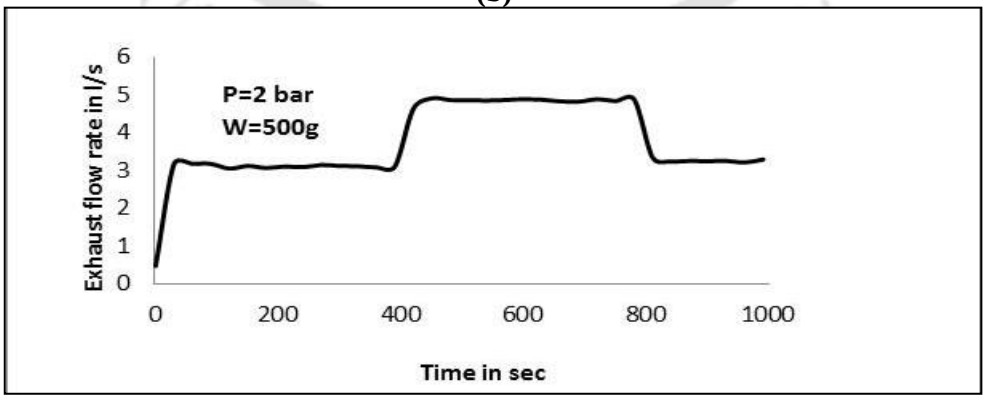

(c)

Fig. 4.5 Transient bed voidages along the (a) lower portion (b) upper portion of riser height for (c) sudden increase in exhaust flow rates as the transient input

It is observed that the major changes in bed voidage takes place at a height of 159 and 191 cm, respectively. The voidage at 159 cm suddenly decreases by about 15% from 0.95 to 0.8 which is due to better solid circulation associated with higher exhaust flow resulting in better movement of solid from the bottom to the top. The voidages at the lower portion of the riser are observed to be unaffected by the sudden changes in exhaust flow rates. In the lower region the voidage is highest at 19 and 37.25 cm with a value of 0988 and lowest at 59 cm with a value of 0.8.

The steady state bed voidages for these experiments are compared in Fig. 4.6 for the three exhaust flow rates for 500 g sand. It is observed that the variation of bed voidage is very high from 0.75 to 0.95 at high exhaust flow rates of 4.8 l/s compared to a low exhaust flow rate of 2.7 l/s. where the variation is 0.8 to 0.95.This may be because of more turbulence in the bed at a higher exhaust flow rate. Also it is observed that the average bed voidage is more for lower exhaust flow rate than for higher exhaust flow rates.

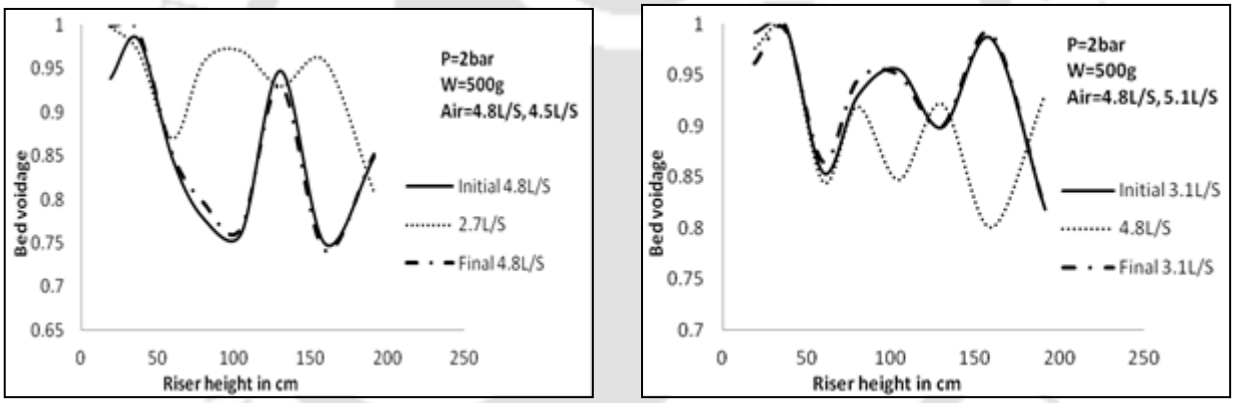

Fig. 4.6 Steady state bed voidages for 500g sand for the initial, intermediate and final conditions of exhaust flow rates

The experiments performed with 10.0% coal blends also show a similar behaviour in the voidage profiles as is evident from the Fig. 4.7 and Fig 4.8. Figure 4.7 shows the transient bed voidages along the riser height for 10% coal blends with sudden decrease in exhaust flow rate from 4.5 to 3.3 l/s. Here it is observed that at heights of 191.25, 80, 159 and 104.25 cm the voidage drastically rises from 0.8, 0.75, 0.74, and 0.75 respectively to a value of 0.9, 0.85, 0.96 and 0.96 respectively. This variation is about 12% for the first two locations and 28% for the other two. The voidage at the other locations mostly near the lower region are not significantly affected by the transients in exhaust flow rates.

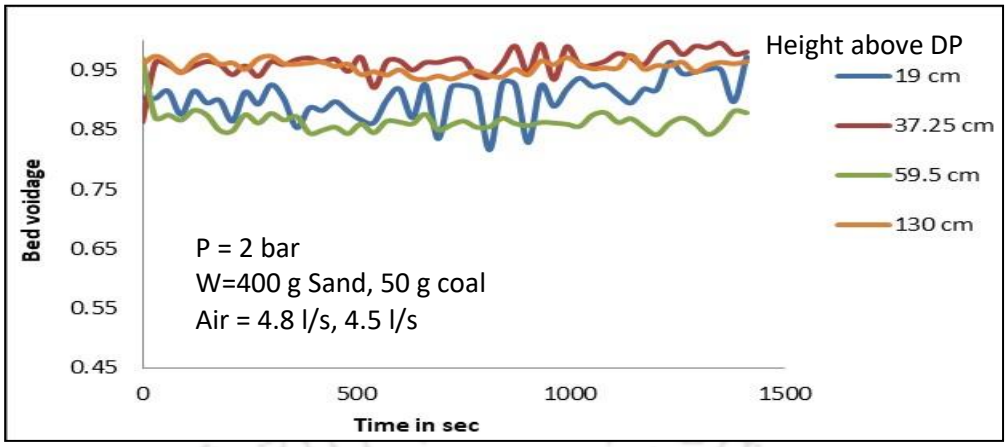

(a)

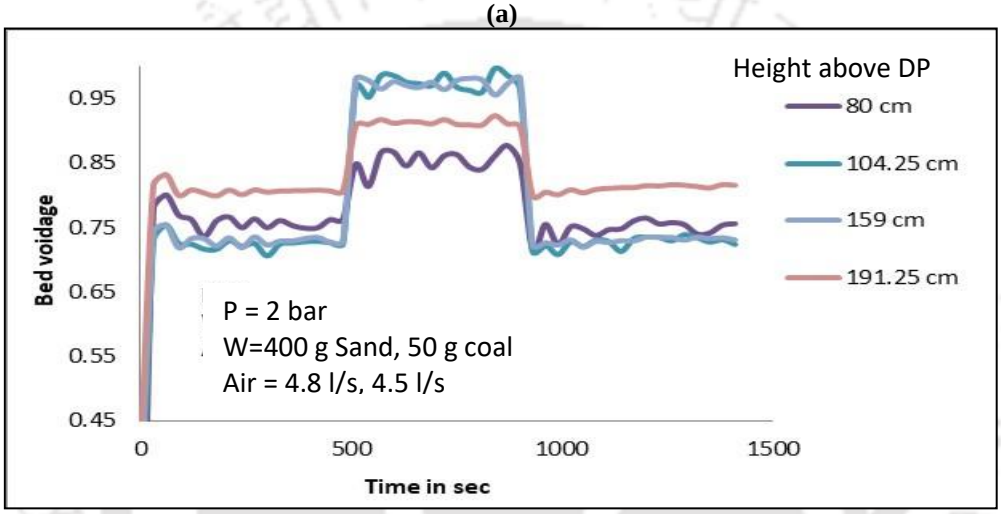

(b)

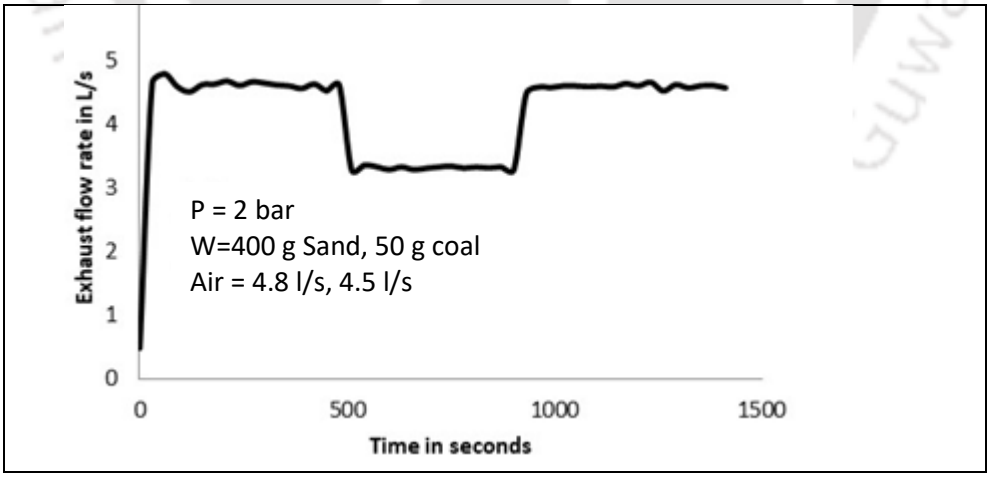

(c)

Fig. 4.7 Transient bed voidages along the (a) lower region (b) upper region of the riser height for sand with 10.0% coal blend for (c) decrease in exhaust flow rate as transient input

In these regions the voidage is highest at 37.25 cm with a value of around 0.98 and lowest at 59.5 cm aith a value of around 0.85. It is also observed that these variations differ from that of the variations observed with pure sand.

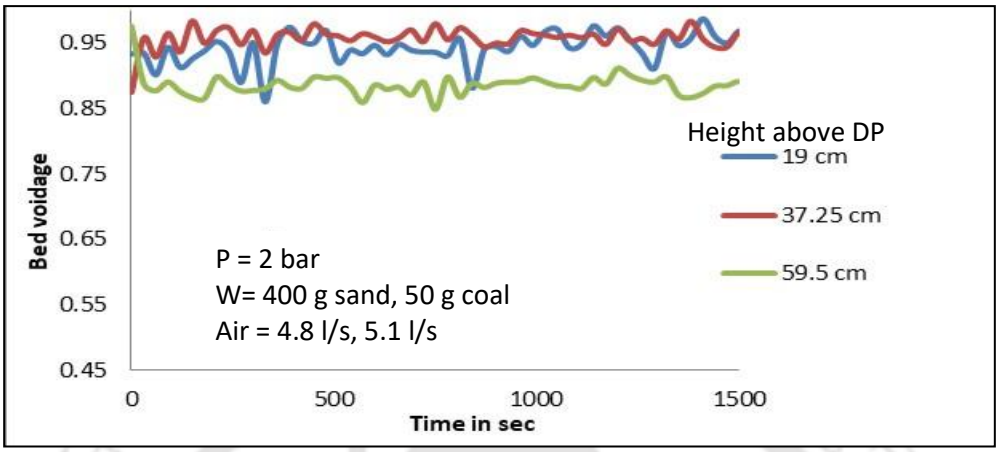

(a)

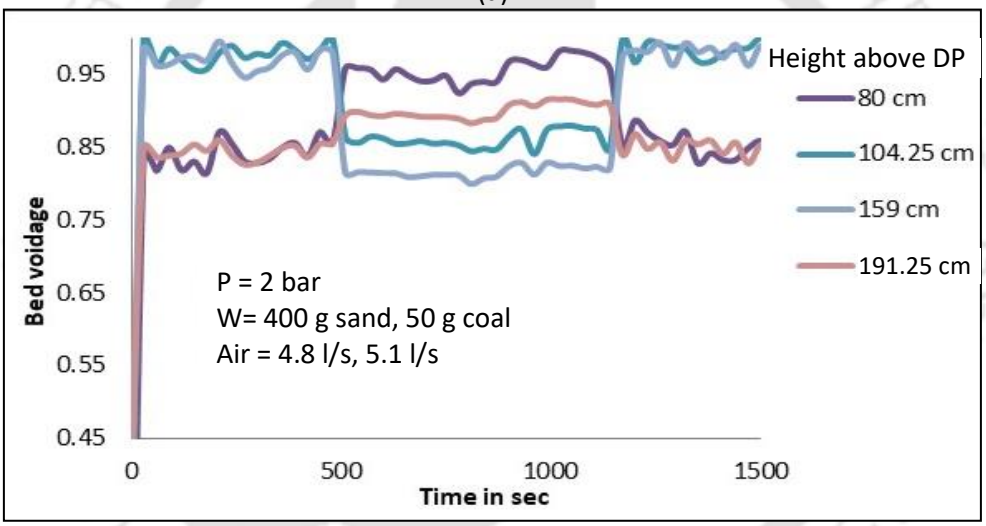

(b)

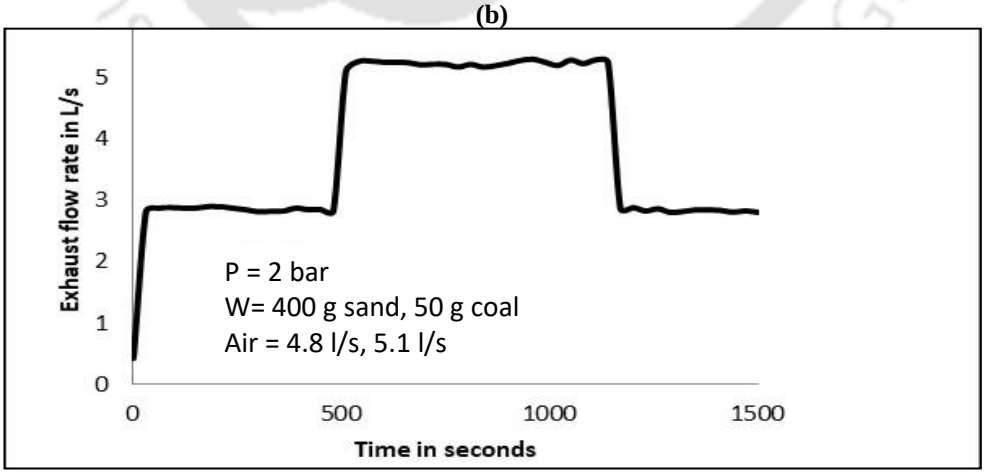

(c)

Fig. 4.8 Transient bed voidages along the (a) lower region (b) upper region of the riser height for 500g sand with 10.0% coal blend for (c) increase in exhaust flow rate as transient input

Figure 4.8 shows the output in transient bed voidages along the riser height for 10% coal blends resulting from the transient in input in the form of a sudden stepped increase in the in exhaust flow rate from 2.8 to 5.2 l/s.

Here it is seen that the major changes takes place in the height of 159 and 104 cm where the voidages drops from 0.98 to 0.8 and 0.85 respectively which is about 14% drop. At a height of 191.25 cm, the voidage is seen to increase slightly by around 7% from a value of around 0.86 to 0.93. The voidages at the lower regions from 19 to 80 cm are not significantly effected by the transients in exhaust flow rates. This may be again because the change is exhaust takes place near the upper region of the riser at the outlet of the cyclone.Similar experiments were also performed with 1 bar as operating pressure and almost similar trends were observed.

4.2.2 VARIATION OF BED VOIDAGE PROFILE WITH TRANSIENTS IN OPERATING PRESSURE

The output in transient bed voidages profiles for 500g sand for a transient input in the form of sudden changes in operating pressure are presented in the Figs. 4.9 and 4.10. The Fig. 4.9 shows that with a sudden increase in operating pressure the bed voidages at heights of 191, 159, 104.25 and 80 cm drops from 0.85, 0.98, 0.98 and 0.9 respectively to values of 0.8, 0.68, 0.7 and 0.75 respectively.This accounts for 5%, 30%, 28% and 16% change respectively. The pattern of the changes in the output in these regions is similar to the patern in the changes in the input transient. This occur at the upper regions of the riser. The bed voidages at the lower region viz 19, 37.25 and 59.5 cm remain unaffected at around 0.95, 0.98 and 0.85, respectively. This may be due to the fact the increase in pressure results in a increase in pressure drop along the riser which results in more solid particles being lifted to the upper region resulting in increased solid concentration at the upper regions and decrease in voidage. The results of hydrodynamics under the sudden variation of exhaust flow and pressure show that the bed voidage in the upper part of the bed changes in tandem with the input parameter, while that in the lower part remains unchanged. This may be due to the fact thst at the lower regions the voidage is very high comparatively which indicates that it is mostly gas in the lower regions for all the cases. This may indicate that at the superficial velocity in which the experiments are conducted, the solid partlcles are

concentrated in the upper region only mostly above 80 cm and hence the voidage changes take place above this region only.

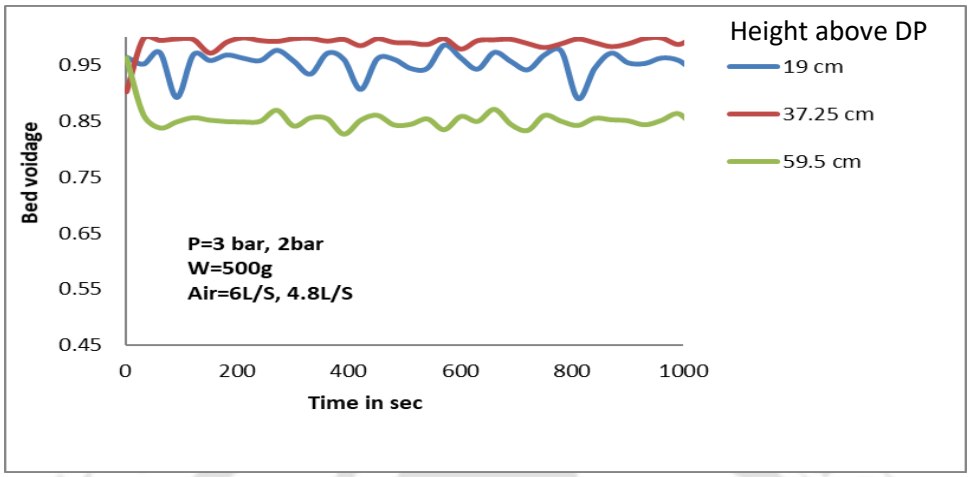

(a)

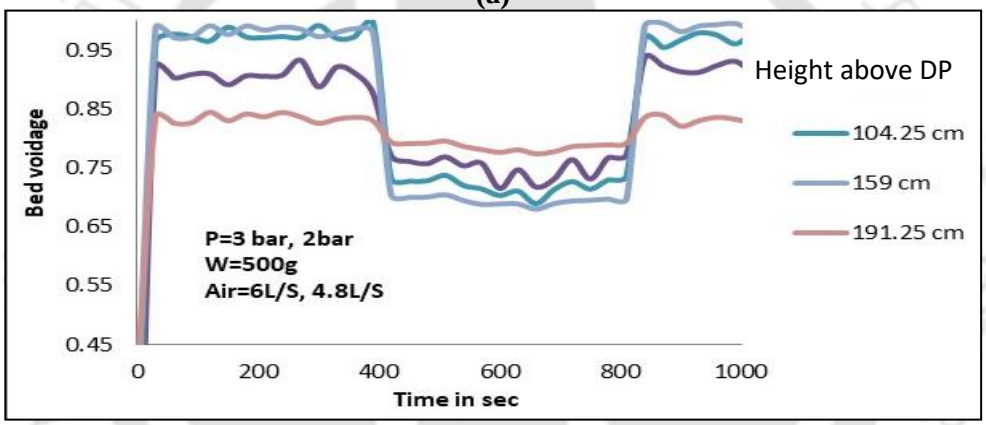

(b)

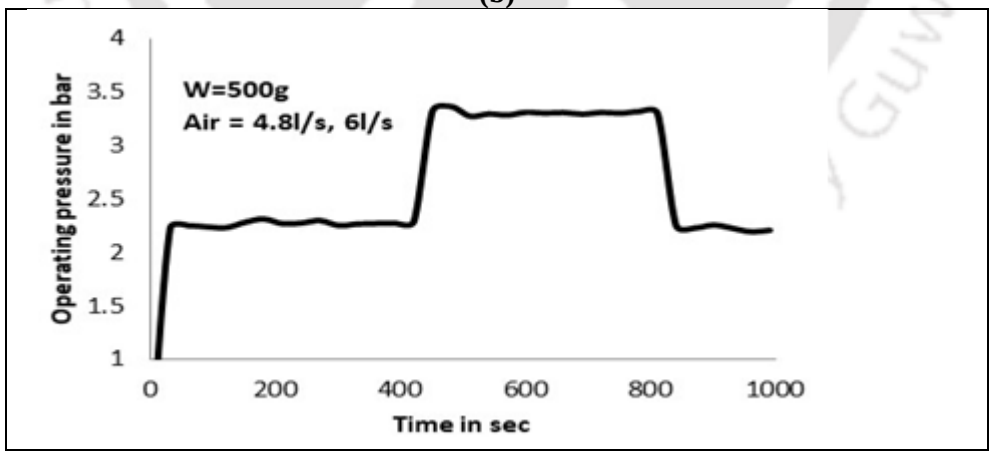

(c)

Fig.4.9 Transient bed voidages for 500g sand along the (a) lower portion (b)upper portion of the riser with (c) sudden decrease in operating pressure as the transient input

The trend is reversed when the operating is decreased suddenly as seen from the Fig. 4.10

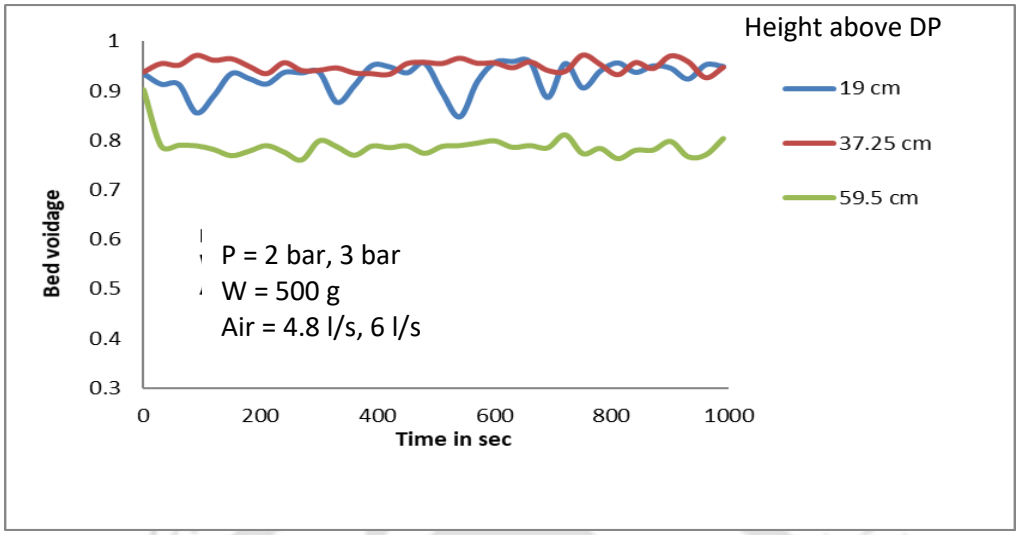

(a)

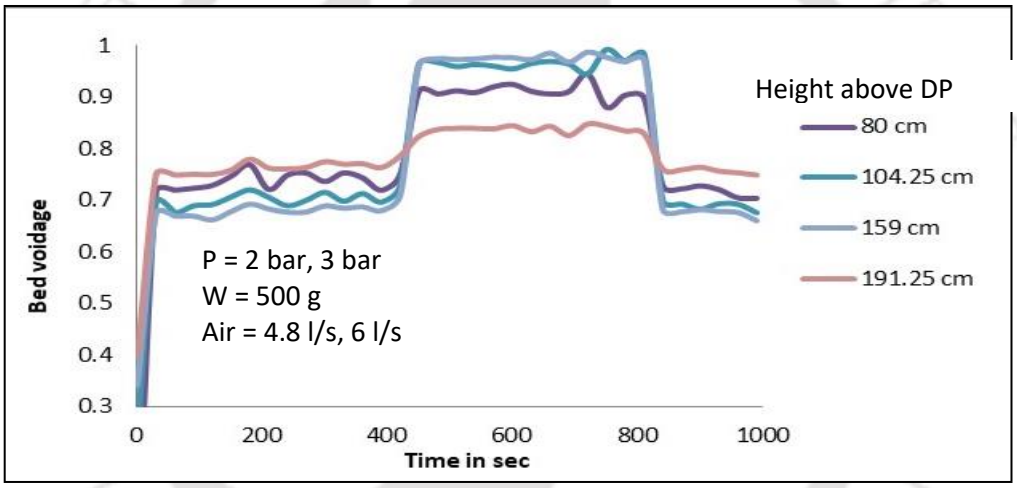

(b)

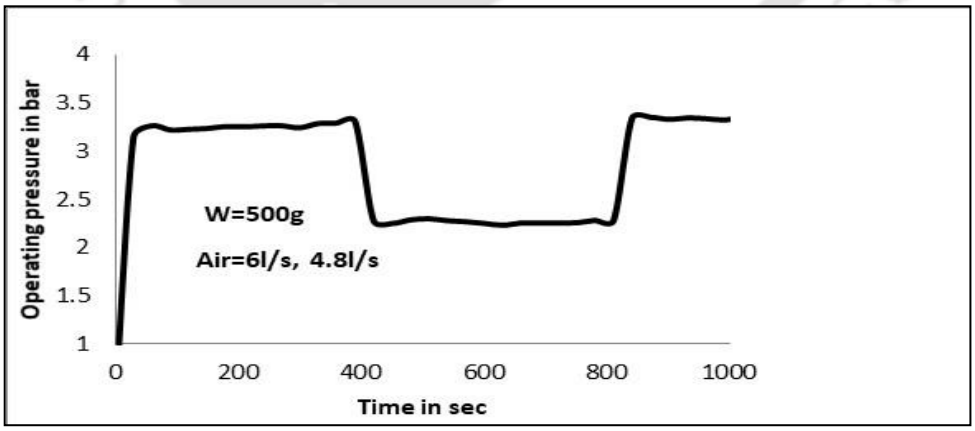

(c)

Fig 4.10 Transient bed voidages for 500g sand along the (a) lower portion (b)upper portion with (c) sudden increase in operating pressure as the transient input

Here it is seen that the bed voidages at the upper regions viz 191.25, 159, 104.25 and 80 cm increases from values of 0.75, 0.68, 0.69 and 0.74 respectively to values of around 0.81, 0.97, 0.98 and 0.98 respectively which is a change of about of 8, 42, 42 and 32%, respectively with respect to the average. The voidages at the lower region this time again remains almost steady at 0.9 to 0.95 and are not effected drastically by the transients in operating pressure. It may be that with decreased operating pressure resulting in less pressure gradient, less solids are carried to the upper region.

The steady state bed voidages for these experiments are compared in Fig 4.11 for the three operating pressures.. It is seen that on an average the bed voidage is less for higher operating pressure and more for lower operating pressure. The steady state bed voidage profiles are validated with those obtained by Kalita et *al*. (2013). The results are observed to be in agreement.

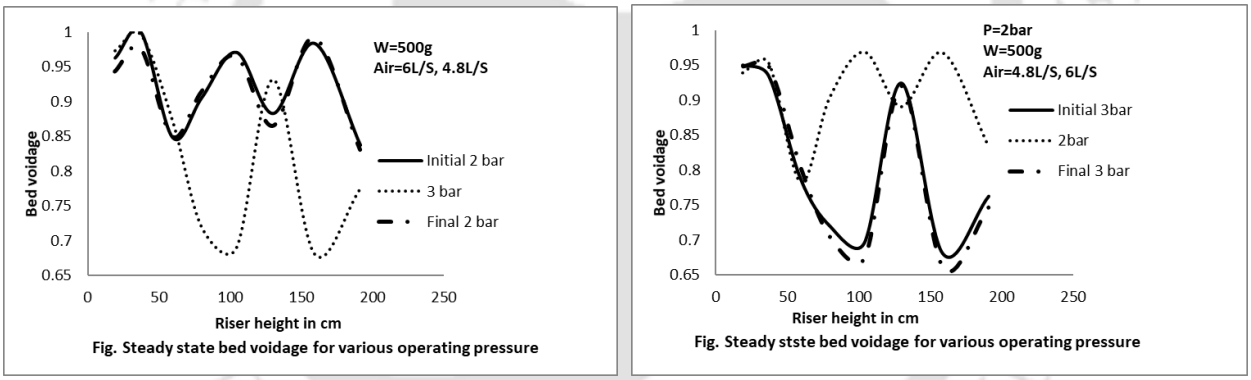

Fig. 4.11 Steady state bed voidages for 500g sand for the initial, intermediate and final conditions of operating pressures

4.3. BED VOIDAGES FOR VARIOUS COAL BLENDS UNDER STEADY STATE CONDITION

The comparative steady state voidage profiles for various percentage blends are shown in the following Fig. 4.12. It is observed that the voidage for all the percentage blends are lower near the bottom of the riser. The voidage values at this particular location decreases with increasing percentage blend of coal. This may be due to the increase in weight of inventory with increasing percentage of coal which require higher force to overcome the weight of the bed.

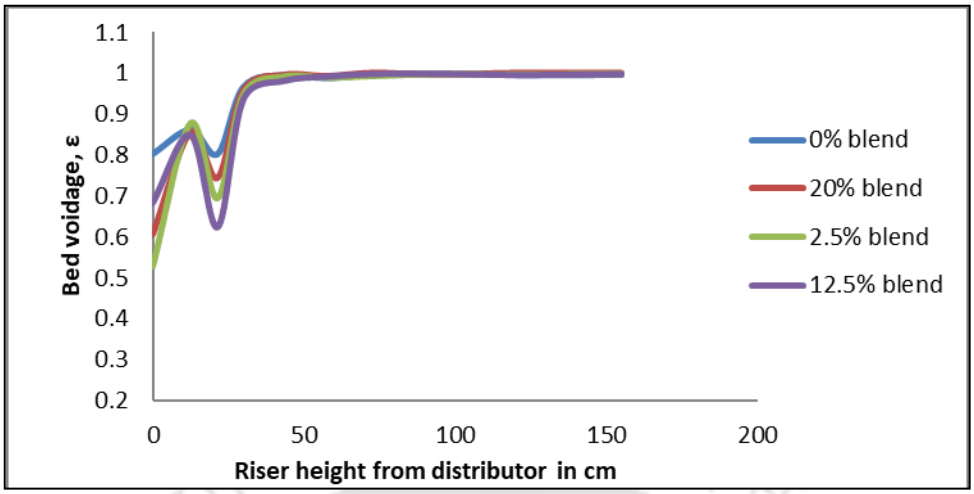

Fig. 4.12 Steady state bed voidages for varying coal blends

The fluctuations in axial bed voidage shown in Fig. 4.12 differ from that observed earlier results (Fig. 4.3 and 4.6). It is due to the reason that in case of the experiments whose data are shown in Fig 4.12, the exhaust was kept fully open without attaching any control valve that was used for the experiments whose results are shown in Fig. 4.3 anf 4.6

4.4 FFT OF TRANSIENT BED VOIDAGE

.The Fig. 4.13 shows the transient bed voidage from the experiment conducted wth 10.0% as bed material .

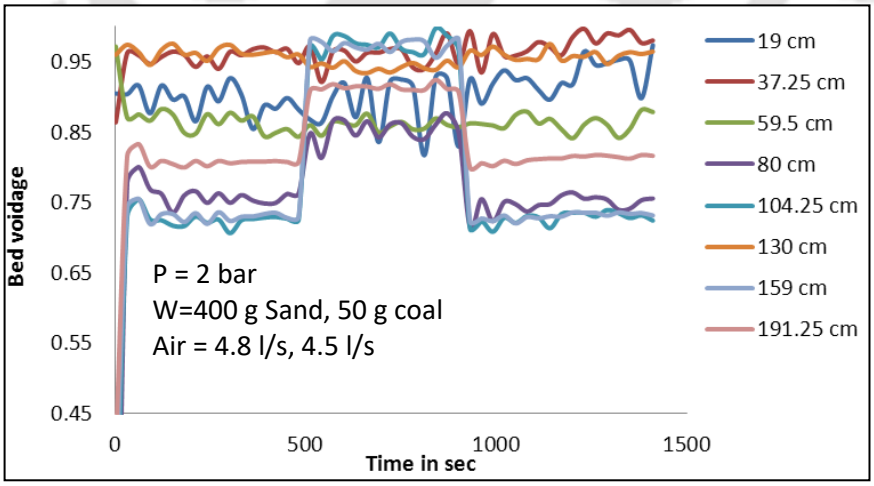

Fig 4.13 Transient bed voidages along the riser height for sand with 10.0% coal blend for changes in exhaust flow rates (high to low to high)

The transient voidage profile at the bottom region of 19 cm height above the distributor plate and the top region at 191.25 cm are taken for analysis through fast fourier transformation. The FFT graphs are presented in Fig. 4.14 and 4.15, respectively.

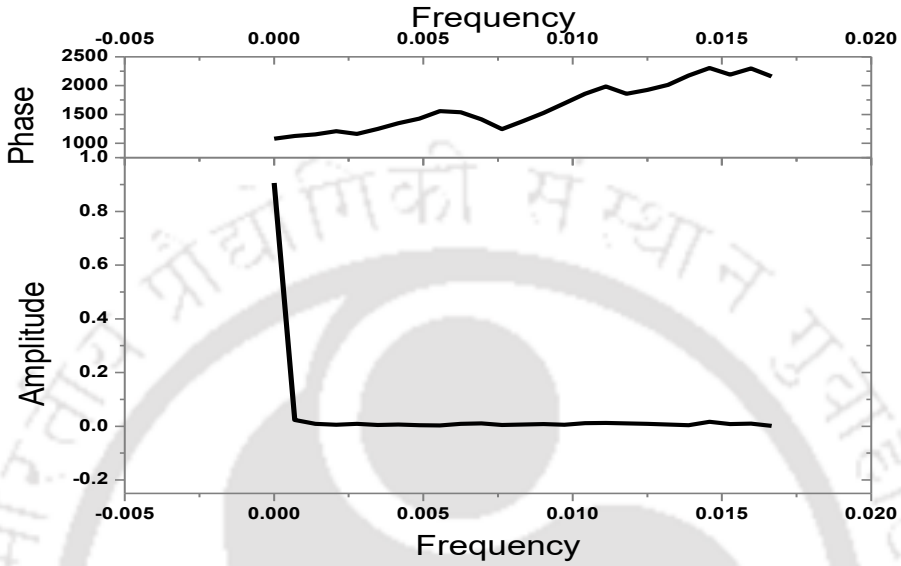

Fig. 4.14 FFT of voidage datas at 19 cm height showing Frequency vs phase and amplitude

From the Fig. 4.14 it is observed that the voidage signal at 19cm height which is a lower region of the riser is a monotonic signal. The phase vs frequency graph shows a variation in phases which may be due to the continous fluctuations in the voidage values as discussed in the earlier sections and shown in Fig. 4.13. The FFT of the voidage values at the upper region of the riser at a height of 191.25 cm is shown in the Fig. 4.15. Here also, the signal of monotonic type. The phase variation with frequency shows a single sharp spike with negligible magintude of other variations. This may be due to the comparatively lower magnitude of fluctuations in this region as seen in the Fig. 4.13. The sharp spike may be a representation of the sudden change in the voidage with the sudden change in exhaust flow rate value [Viswanathan (2017)]. Effect of location of adjacent pressure sensors gave multiple phases in each of the fixed input regime of the plot.

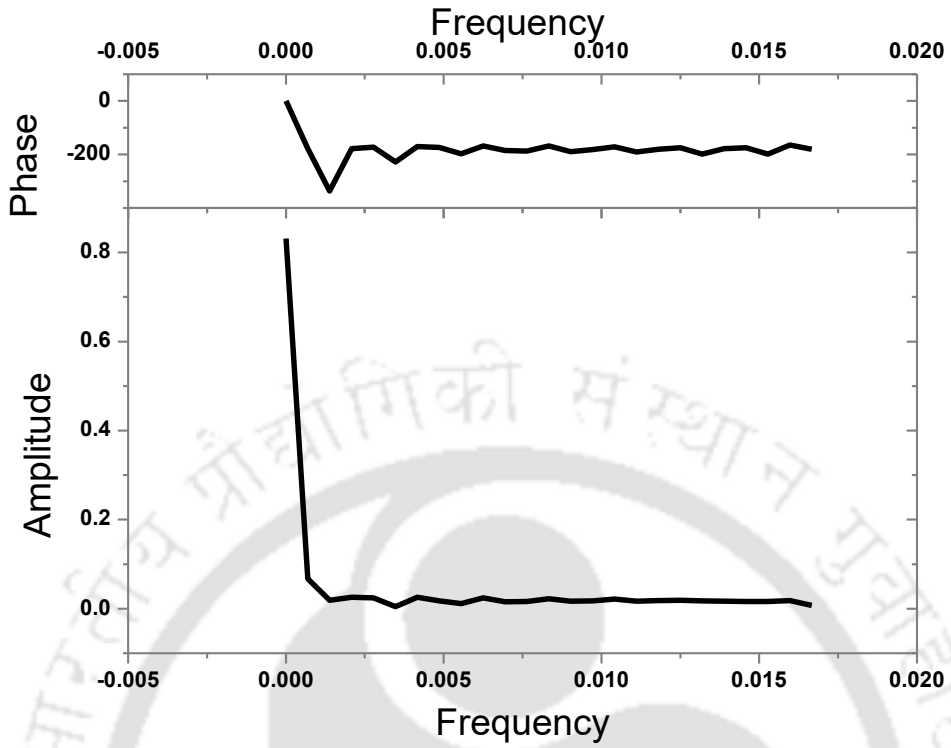

Fig. 4.15 FFT of voidage datas at 191.25 cm height showing Frequency vs phase and amplitude

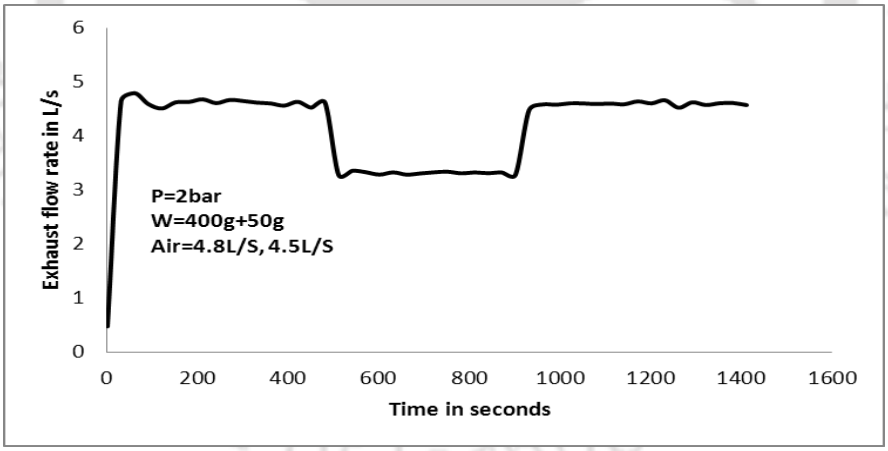

Fig. 4.16 Sudden changes in exhaust flow rate (high to low to high) as transient input

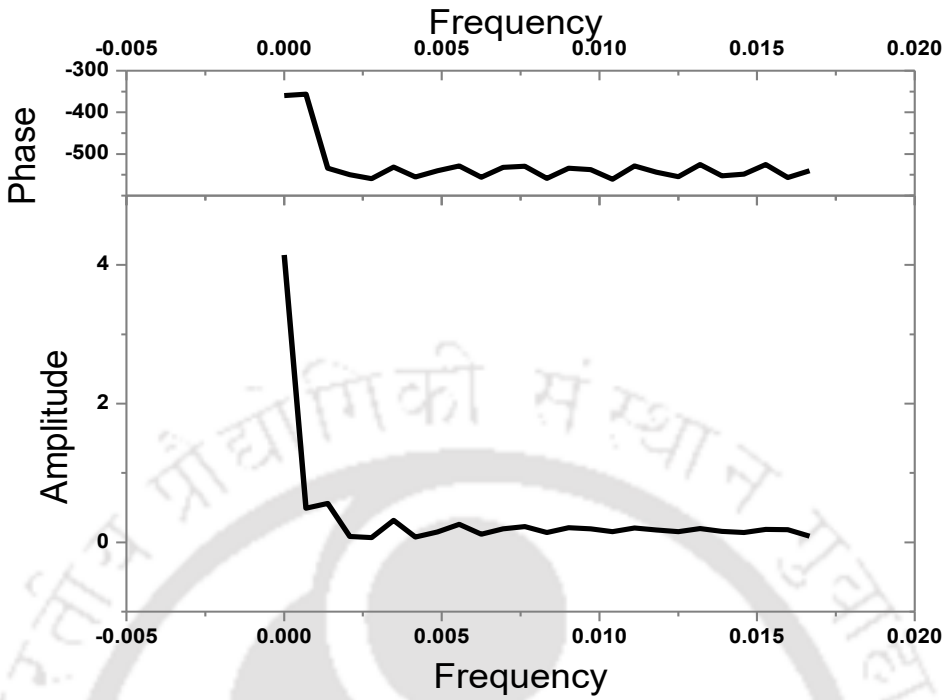

Fig. 4.17 FFT of sudden changes in exhaust flow rate datas showing Frequency vs phase and amplitude

The FFT for the exhaust flow rate input as seen in Fig. 4.17 shows various oscillations but of very low magnitude. These oscillations are also seen in the original exhaust flow rate graph as observed in Fig. 4.16.

4.5 SUMMARY OF THE CHAPTER

Series of experiments were carried out to investigate the effect of various transient input parameters on the bed hydrodynamics for bed inventories of 400g, 500g sand and 500g sand with 10% coal blends. The S-Shaped bed voidage has been observed at all the operating conditions and all percentage of blending. Drastic changes in voidage values were observed mostly in the upper region of the riser column for transient conditions in the operating parameters. With addition of coal blends to the bed inventory, the voidage slightly drops at the lower part of the riser. Also the voidage is observed to be lower for low air flow rate than for higher air flow rate near the bottom of the riser. The difference is negligible towards the upper part of the riser. The steady state voidage profiles at different operating pressure are similar to those reported by Kalita *et al*. (2013) The next Chapter presents the results of the experiment carried out to investigate the heat transfer during various transient conditions.

Chapter – 5

RESULTS AND DISCUSSION ON TRANSIENT HEAT TRANSFER STUDIES ON PCFB

5.1 INTRODUCTION

In the present Chapter transient heat transfer characteristics in a PCFB unit are studied with variation of input transient parameters such as operating pressure, superficial velocity of air, heat flux and exhaust flow rates. Results of the study are discussed in the pertaining sections.

5.2 TRANSIENT STUDIES ON THE UPPER SPLASH REGION OF PCFB

To get first hand information on transient heat transfer characteristics in the upper splash region of PCFB, experiments on the PCFB are conducted at various operating conditions by introducing stepped changes or transients to the fluidizing air flow rate. The experimental matrix showing the combination of parameters and transients in input are given in the Table 5.1

TABLE 5.1 LIST OF COMBINATION OF PARAMETERS USED IN THE EXPERIMENTS AND TRANSIENTS INTRODUCED

Sl NO	Bed inventory and weight	Operating pressure	Fluidizing air flow rate	Heat input	Input transient
1	Sand 400 g	2 bar	5.1 l/s	1.5 kW/m^2 , 2 kW/m^2	None
2	Sand 400 g blended with 12.5% coal.	2 bar	5.1 l/s	1.5 kW/m^2 , 2 kW/m^2	None
3	Sand 400 g blended with 2.5% coal.	2 bar	5.1 l/s	1.5 kW/m^2 , 2 kW/m^2	None
4	Sand 400 g blended with 12.5% coal.	2 bar	5.1 l/s	1.5 kW/m^2 , 2 kW/m^2	None
5	Sand 400 g blended with 20% coal.	2 bar	5.1 l/s	1.5 kW/m^2 , 2 kW/m^2	None
6	Sand 400 g	2 bar	5.1 l/s to 7.1 l/s in 1 s 7.1 l/s to 3.0 l/s in 1 s	1.5 kW/m^2	Fluidizing air flow rate
7	Sand 400 g blended with 2.5% coal.	2 bar	5.1 l/s to 6.6 l/s in 1 s 6.6 l/s to 3.0 l/s in 1 s	1.5 kW/m^2	Fluidizing air flow rate

5.2.1 INVESTIGATION OF TRANSIENT HEAT TRANSFER FROM STARTUP TILL STEADY STATE IN THE UPPER SPLASH REGION OF PCFB

Axial heat transfer coefficient has been measured at the upper splash region of the riser. The variation of temperature of the bed and surface of the riser with time and the variation of heat transfer co efficient along the axial and radial direction with time were studied. The variation of bed temperatures and riser surface temperatures with time for a heat influx of 1.5 kW/m^2 and fluidizing air flow rate of 5.1 l/s for a bed of sand are shown in Fig 5.1 and 5.2, respectively. The corresponding transient heat transfer coefficient (HTC) along the axial direction are also shown in Fig 5.3 and the temperature variation along the radial direction are shown in Fig.5.4 From the graphs it is seen that the steady state is reached after about 5000 seconds since start up. Fig 5.1 shows the bed temperature to rise to a maximum of 50 ^oC at a height of 1.8 m from the distributor plate and to about 36 ^oC at a height of 1.5 m from the distributor plate. The corresponding riser surface temperature is 130 ^oC and 70 ^oC, respectively. The maximum heat transfer coefficient is observed at the topmost region of the riser at a height of 1.8 m from the distributor while that at the lower parts are comparatively low. Similar trends have been observed by Kalita *et al*. (2013). The maximum value being 22 W/m^{2}K at a height of 1.8 m and 19 W/m^{2}K at a height of 1.4 m. It is thus observed that the HTC is 15% higher at the topmost region than at the bottom region of the heat transfer probe. The higher heat transfer near the riser exit may be due to an increase in solid concentration near the exit as the drag force acting on the bed material lifts the particles to the top zone. Further at pressurized condition the gas phase convective heat transfer is also high due to high density of gas at the upper zone.

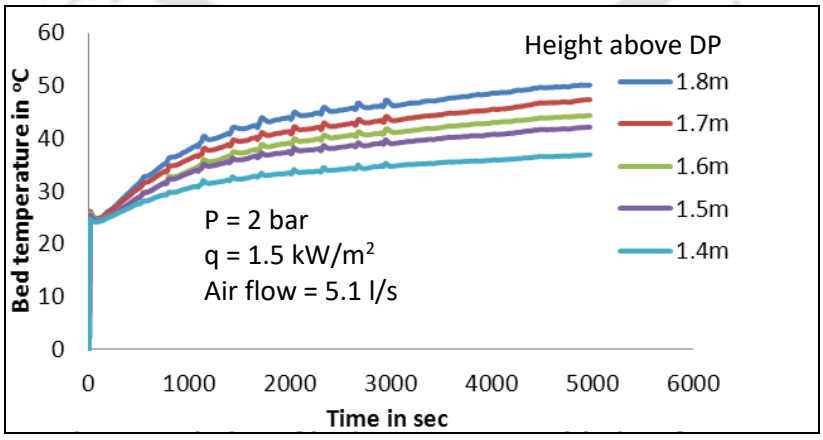

Fig 5.1 Variation of bed temperature with time along the riser height for 400 g.

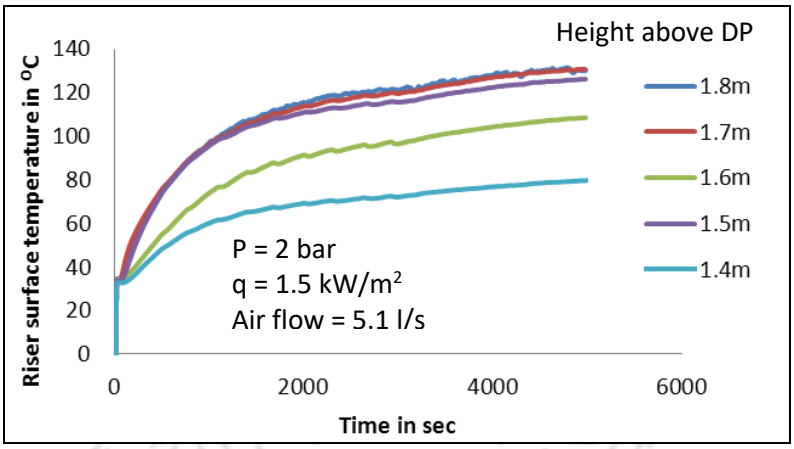

Fig 5.2 Variation of riser surface temperature with time along the riser height for 400 g sand

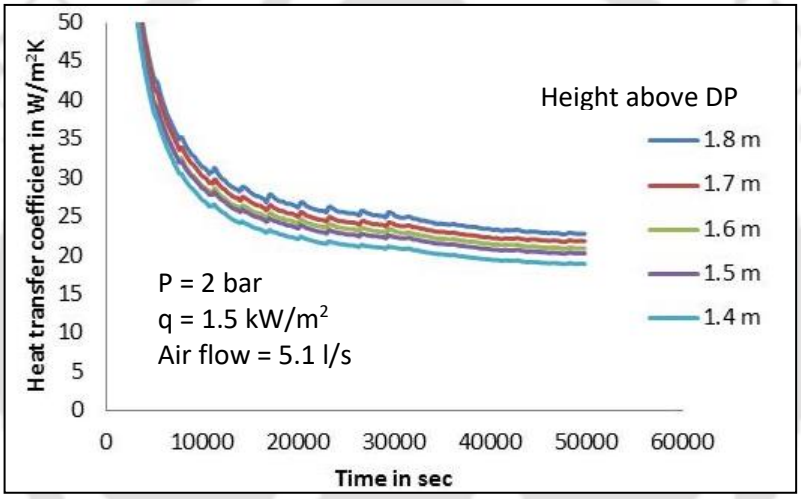

Fig. 5.3 Transient heat transfer coefficient along the axial direction with time for 400 g sand

From the Fig 5.4 it is observed that the bed temperature is more near the riser wall (85 ^{o}C) than at the core which is about 35 ^{o}C. Thus the bed temperature is higher by 142% at the wall than at the core. This is obvious as in the probe, heating is done from the wall. Similar observations were made by Kalita *et al*. (2013) who attributed it to the presence of higher concentration of larger particle clusters near the wall of the riser. The higher heat transfer coefficient towards the upper region of the riser may be due to the increased concentration of solid particles at that region in comparison to that at the lower region. The higher heat transfer near the riser exit may be due to an increase in solid concentration near the exit as the experiments were done in pressurized condition. Additionally, at the topmost region of the riser the solid particle has to change direction and move at an angle of 90 ° towards the cyclone which may result in the

formation of vortex at the top and increased solid concentration. Also the repeated drops observed in all the graphs are due to stoppage in flow of sand caused by closing of the ball valve in the transparent downcomer section during repeated measurements of solid flow rate.

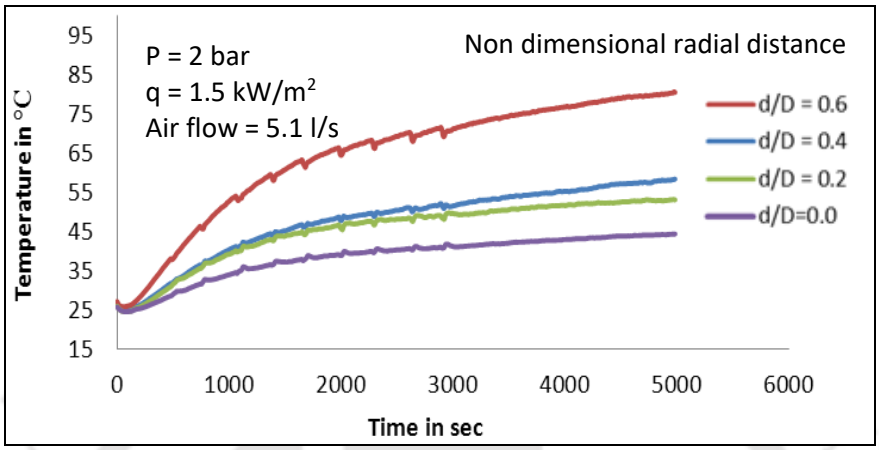

Fig 5.4 Variation of bed temperature with time along the radial direction for 400 g sand.

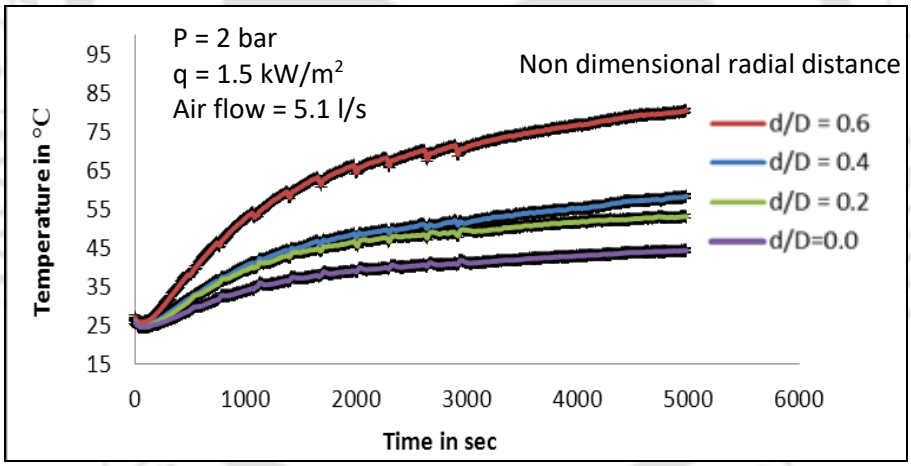

Fig 5.5 Variation of bed temperature shown with error bars with time along the radial direction for 400 g sand.

5.2.2 HEAT TRANSFER WITH VARIOUS COAL AND SAND BLENDS

Comparision of the heat transfer coefficients along the axial direction for various percentage blends of sand and coal are presented in the Figs. 5.6 to 5.7. It is observed that 12.5% blend and 2.5% blend has a comparatively better heat transfer coefficient than the 0% and 20% blend. For 12.5% coal blends, the heat transfer coefficient to vary from 20 to 24 W/m^{2}K along the riser height while for pure sand it varies from 19 to around 22 W/m^{2}K.

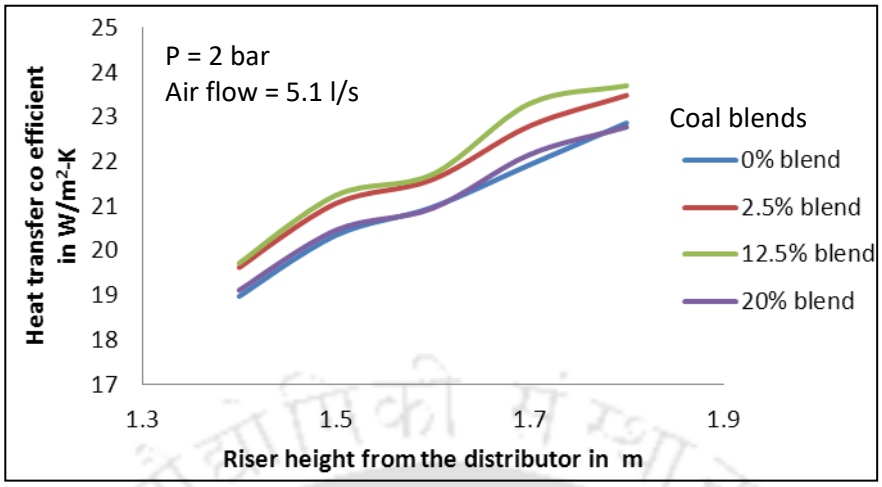

Fig. 5.6 Variation of heat transfer coefficient along the axial direction at q=1.5 kW/m^2

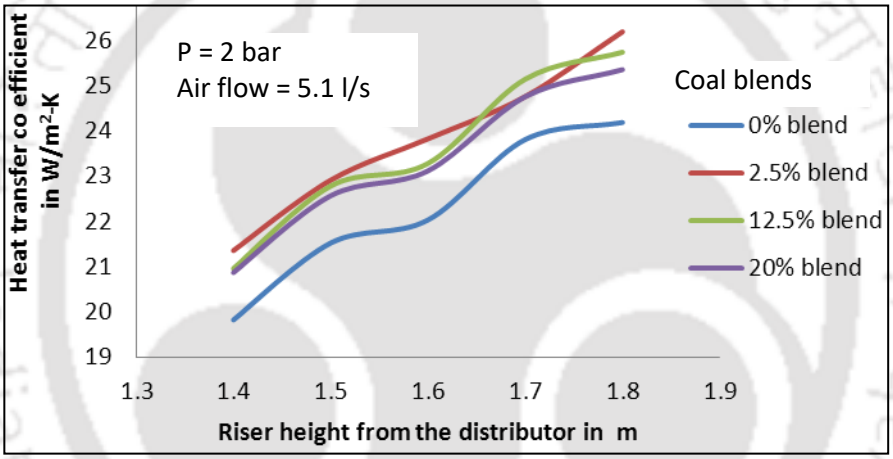

Fig. 5.7 Variation of heat transfer coefficient along the axial direction at q=2 kW/m^2

A comparision of steady state heat transfer coefficient along the axial direction of the riser for a heat flux of 1.5 kW/m^2 and 2.0 kW/m^2 can be made from the above figures for all the percentage blends of sand and coal. The heat transfer coefficient is observed to be higher for a heat flux of 2 kW/m^2 than for 1.5 kW/m^2 for all the percentage blends by an average of about 1.5 W/m^2-K for all the cases.

5.2.3 INVESTIGATION OF TRANSIENT HEAT TRANSFER DURING SUDDEN CHANGE IN FLOW RATES OF FLUIDIZING AIR

The results of the experiments related to sudden increase and decrease in the fluidizing air flow rate are shown in the Fig 5.8. It is observed that with the sudden increase in the flow rate of the

fluidizing air fom 5.1 l/s to 6.6 l/s as the transient input shown in Fig 5.8 (c), the resulting output i.e the temperature of both bed and the riser wall suddenly decreases for a moment and then reaches a steady atate after about 1000 seconds as observed from the Fig. 5.8(a) and 5.8(b). Correspondingly the output heat transfer coefficient shows a sudden decrease by about 5 W/m^2K for about 10 seconds and subsequent increase by 6 W/m^2K in about 500 seconds. This may be due to the fact that a sudden increase in flow rate of the fluidizing air results in a sudden convective cooling of the bed temperature which results in a drop in heat transfer coefficient. But subsesequently at higher velocities of air the intermixing of solid particles increases due to increased turbulence and this effect overrides the earlier sudden cooling effect resulting in an increase in heat transfer coefficient. But still later the heat transfer coefficient is observed to finally decrease again. The final decrease may be due to the fact that at higher fluidizing air flow rate, the axial heat transfer through convection increases, thereby having a cooling effect on the bed which increases the ΔT. Thus the denominator in the formula for heat transfer co efficient "h" increases consequently decreasing its value. Another factor may be the loss of solid particles at higher flow rate.The trend is same at all the riser heights with the heat transfer being more near the riser exit. The reaseon has been explained in the section 5.3. The difference of heat transfer coefficient between the top and the bottom regeion is about 4 W/m^2K. where the heat transfer coefficient at the 1.8m height is 39 W/m^2K and that at the 1.4 m height is about 24 W/m^2K.

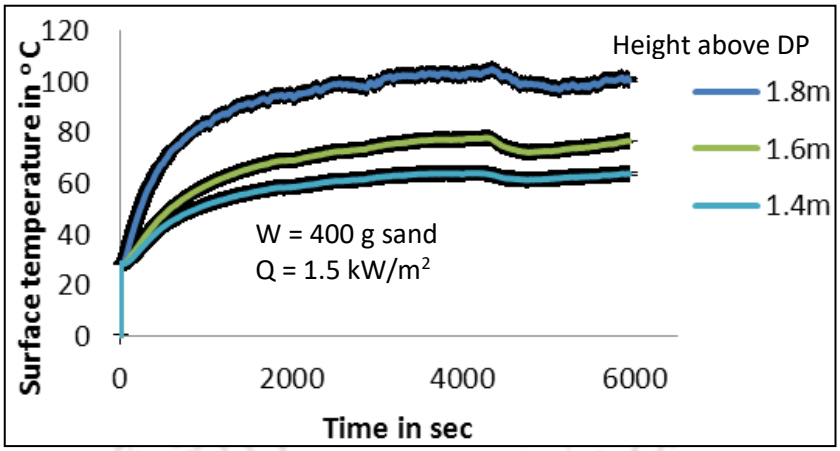

(a)

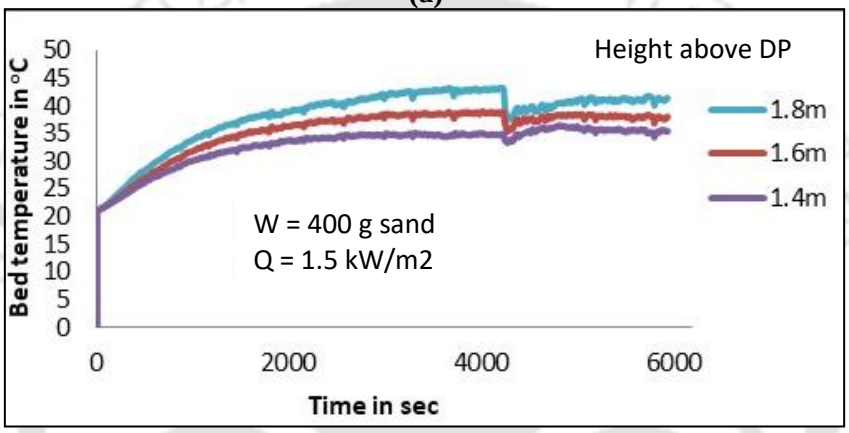

(b)

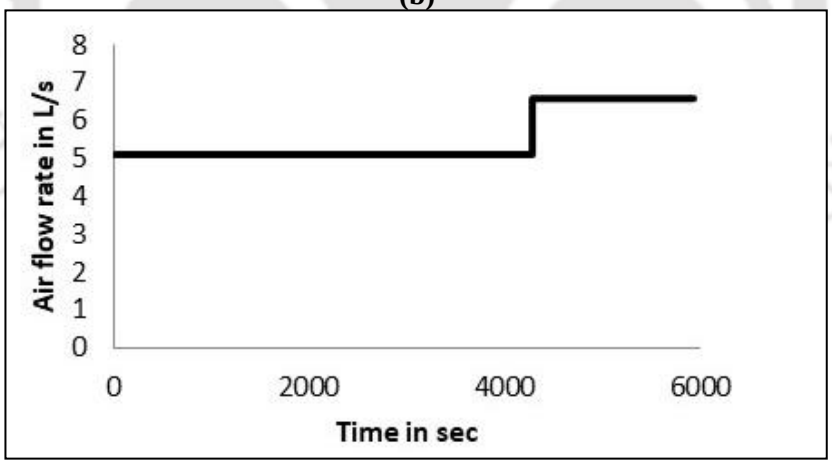

(c)

Fig. 5.8 Transient (a) surface temperature with error bars (b) bed along the riser height for sudden (c) increase in air flow rate as the transient input

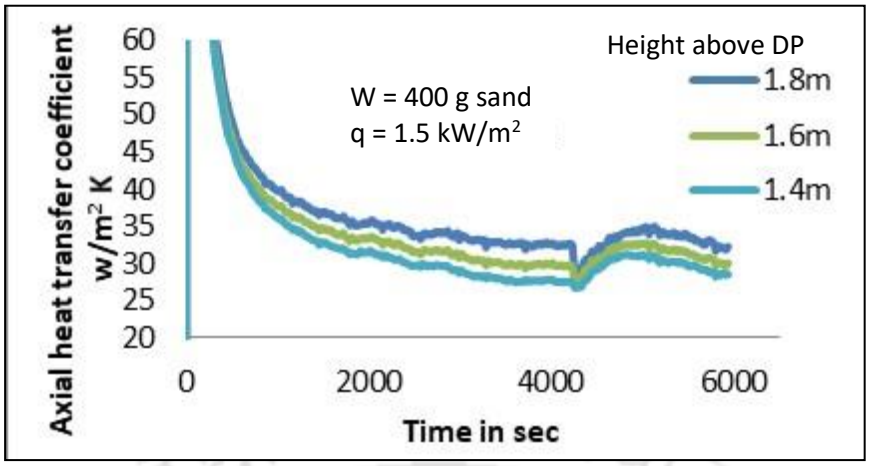

(a)

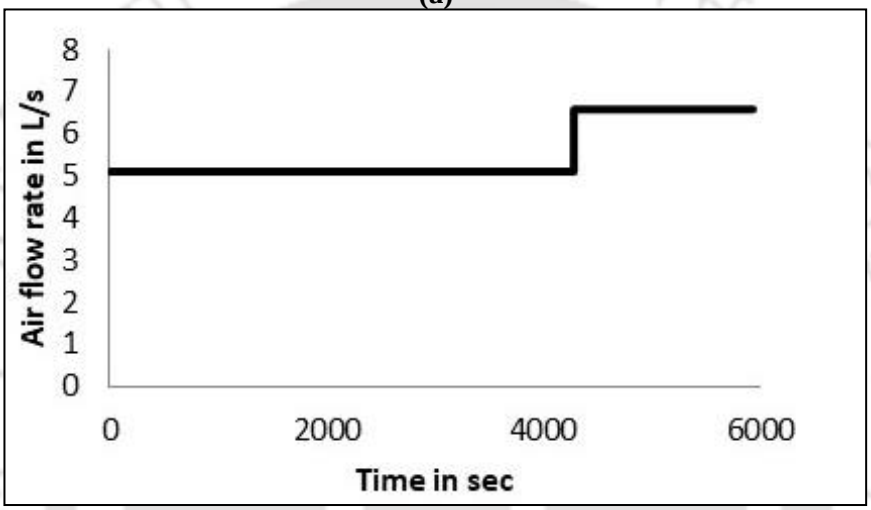

(b)

Fig 5.9 (a)Transient heat transfer coefficient along the riser height for (b) sudden increase in air flow rate as the transient input

Similar results were observed when the experiment was performed with 2.5% coal blend with a sudden increase in the flow rate of the fluidizing air from 5.1 to 6.6 l/s as the transient input. Fig. 5.10 shows the transient bed and surface temperature profile along with the transient input while the Fig. 5.11 presents the transient heat transfer coefficient along the axial direction along with the input transient introduecd with 2.5% coal blends as inventory ansd a heat input of 1.5 kW/m^2. From the figure it is clear that there is a sudden decrease in both the bed and surface temperature and a corresponding instantaneous drop in the heat transfer coefficient for around 10 seconds and then a sharp increase. The instantaneous drop in heat transfer coefficient is about 2 W/m^{2}K at all the regions as seen in Fig. 5.11(a). The subsequent increase is about 10 W/m^{2}K at all the regions.

The maximum heat transfer coefficient being 32 W/m^{2}K at a height of 1.8m while the lowest is about 28 W/m^{2}K at a height of 1.4 m.

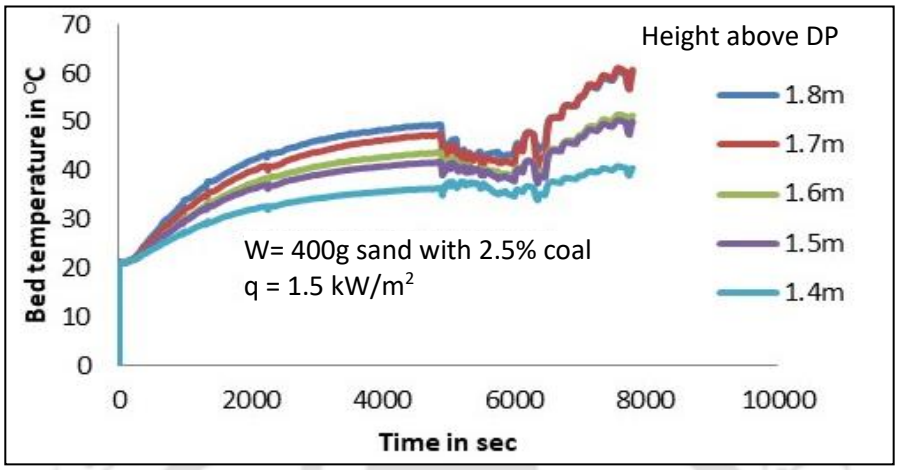

(a)

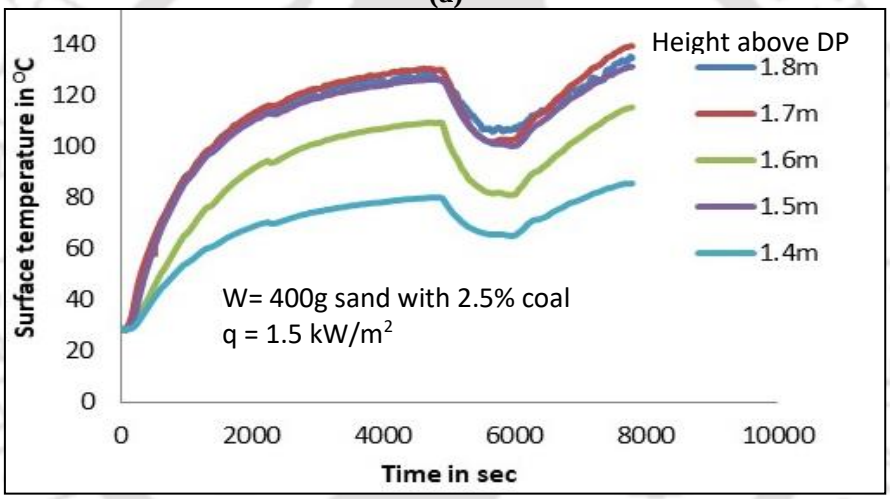

(b)

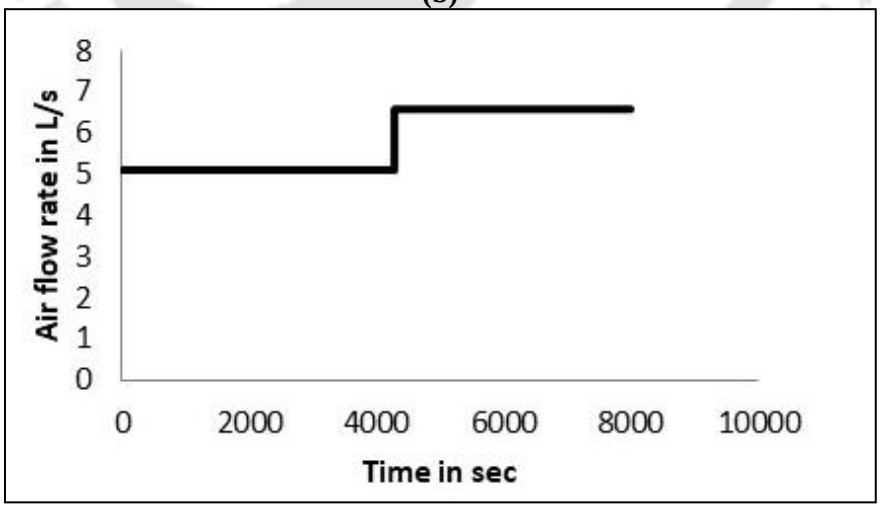

(c)

Fig. 5.10 (a) Transient bed temperature (b) transient surface temperature for (c) sudden increase in air flow rate as the transient input

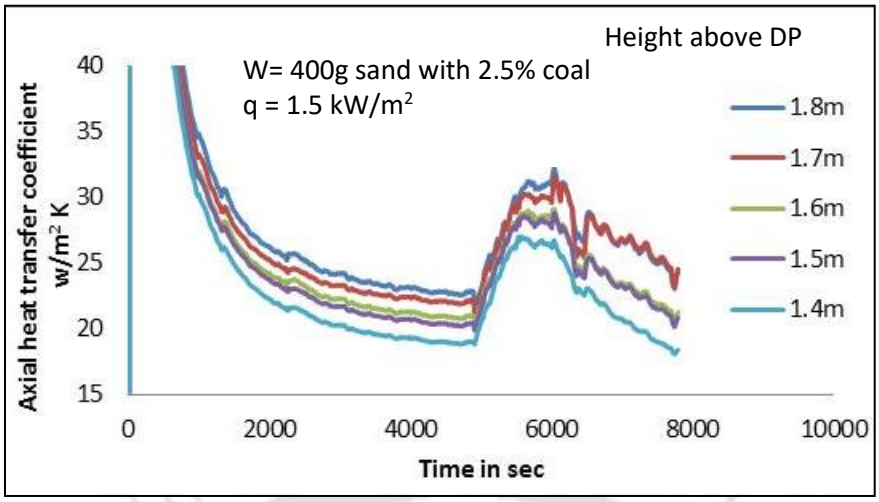

(a)

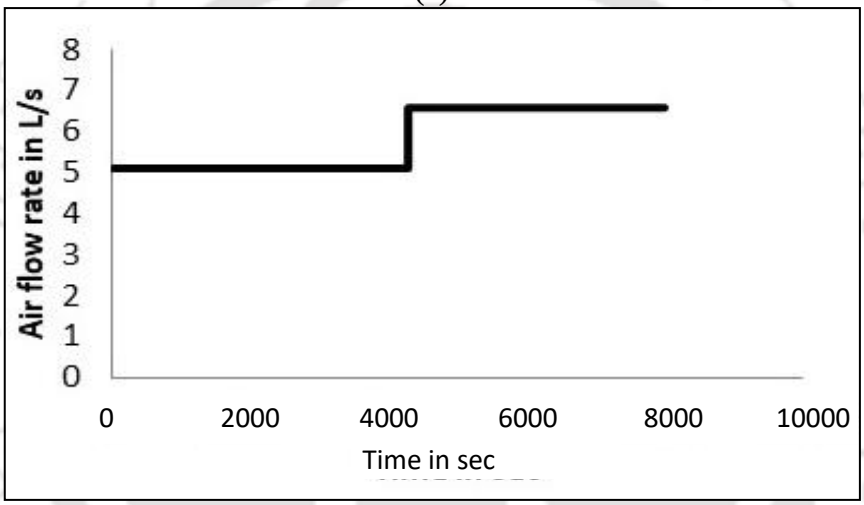

(b)

Fig. 5.11 (a) Transient heat transfer coefficient along the axial direction for (b) sudden increase in air flow rate as the transient input

In a reverse transient input as the above where a sudden decrease in the rate of fluidizing air flow from 5.1 l/s to 3.0 l/s is the transient input as shown in Fig. 5.12(c), an opposite result is achieved. It is observed that the temperature of both bed and the riser wall suddenly increases for a moment and then reaches a steady atate after a few seconds as observed in Fig 5.12 (a) and 5.12(b). Correspondingly the heat transfer coefficient shows a sudden increase for a few seconds and then steadily decrease to a lower steady value as shown in Fig 5.13 (a).

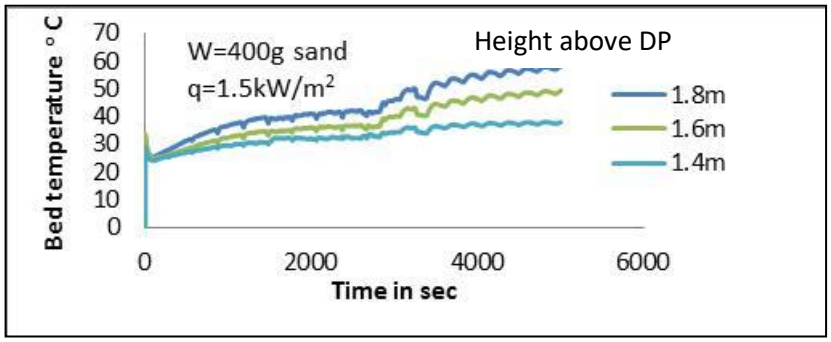

(a)

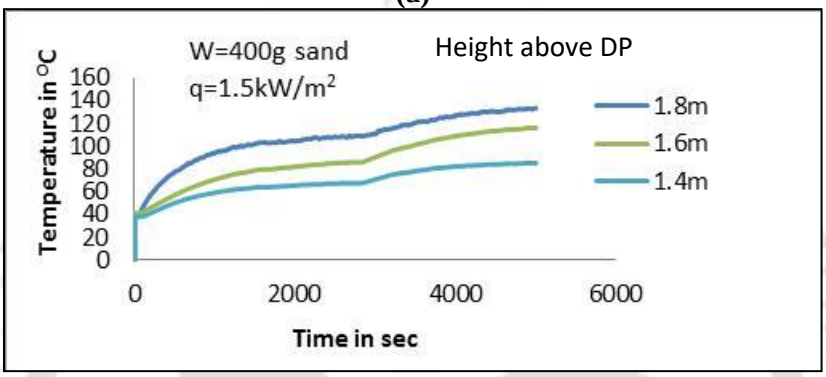

(b)

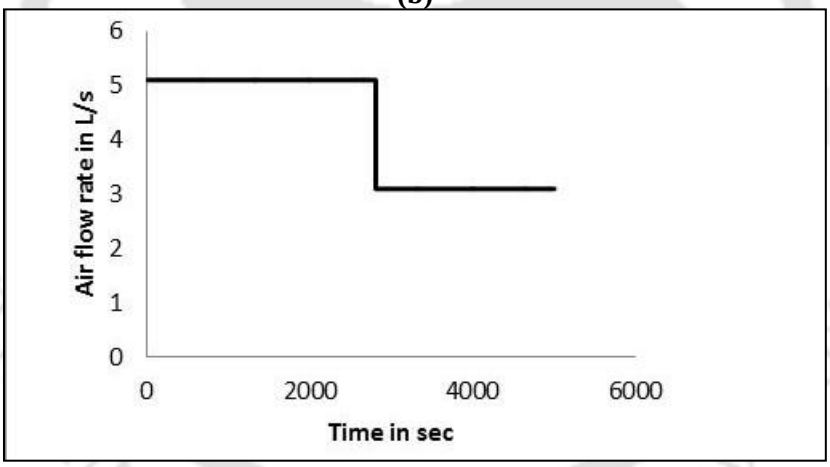

(c)

Fig 5.12 (a) Transient bed temperature (b) transient surface along the riser height for (c) sudden change in air flow rate rate as the transient input

This may be due to the fact that a sudden decrease in flow rate of the fluidizing air results in a sudden heating of the bed temperature which results in a rise in heat transfer coefficient. But subsesequently at lower velocities of air the intermixing of solid particles decreases due to decreased turbulence and this results in a consequent decrease in heat transfer coefficient.

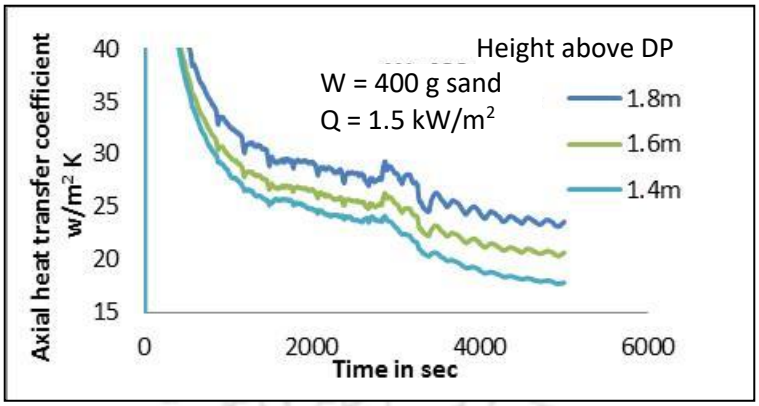

(a)

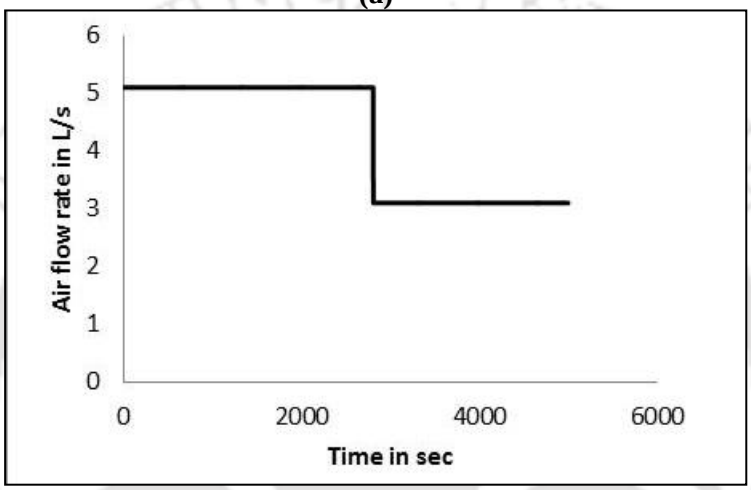

(b)

Fig. 5.13 (a) Transient heat transfer coefficient along the riser height for (b) sudden change in air flow rate

The comparision of the variation of heat transfer coefficient along the axial direction when the fluidizing air flow rate was changed are shown in the Fig. 5.14. Thus as discussed above it is observed that the heat transfer is higher at higher fluidizing flow rates of air and comparatively lower at lower flowdizing air flow rates. For an air flow rate of 5.1 l/s it is observed that the heat transfer coefficient varies from 24 to 29 W/m^{2}k along the riser height while a lower air flow rate of 3.1 l/s the same varies from 24 to 27 W/m^{2}K along the riser height. The increase in heat transfer coefficient at higher air flow rates may be due to increase in the intermixing of solid particles caused by enhcnced turbulence associated with higher flow rates as explained by Kalita *et al*. (2013)

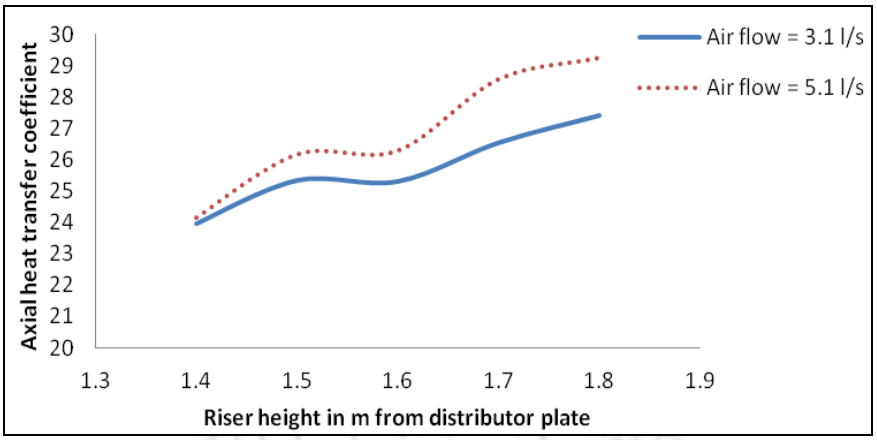

Fig 5.14 Variation of axial heat transfer coefficient at air flow rates of 5.1 and 3.1 l/s

5.3 TRANSIENT STUDIES ALONG THE RISER OF PCFB

The transient experiments on the riser of the PCFB are conducted at various operating conditions by introducing stepped changes or transients to input operating parameters. The combination of parameters and transients introduced are given in the Table 5.1. The transients introduced are shown in bold and each transient were introduced within a time span of 1 second.

Table 5.2 List of combination of parameters used in the experiments and transients introduced (in bold)

Sl No	**Bed material and weight**	**Operating Pressure**	**Power input**	**Fluidizing air flow rate**	**Exhaust flow rate**
1	Sand 400 g	2 bar	**0.9 kW to 1 kW to 1.2 kW**	5.1 l/s	4 l/s
2	Sand 400 g	2 bar	**1.2 kW to 1 kW to 0.9 kW**	5.1 l/s	4 l/s
3	Sand 400 g	2 bar	1.25 kW	5.1 l/s	**4 l/s to 2 l/s to 4 l/s**
4	Sand 400 g	2 bar	1.25 kW	5.1 l/s	**2 l/s to 4 l/s to 2 l/s**
5	Sand 500 g	2 bar	**0.9 kW to 1 kW to 2 kW**	5.1 l/s	4 l/s
6	Sand 500 g	2 bar	**1.2 kW to 1 kW to 0.9 kW**	5.1 l/s	4 l/s
7	sand 500 g	2 bar	1.25 kW	5.1 l/s	**4.7 l/s to 3.1 l/s to 4.7 l/s**
8	sand 500 g	2 bar	1.25 kW	5.1 l/s	**3.1 l/s to 4.7 l/s to 3.1 l/s**
9	Sand 450 g + Coal 50 g	2 bar	1.25 kW	5.1 l/s	**4.7 l/s to 3.1 l/s to 4.7 l/s**
10	Sand 450 g + Coal 50 g	2 bar	1.25 kW	5.1 l/s	**3.1 l/s to 4.7 l/s to 3.1 l/s**
11	Sand 450 g + Coal 50 g	2 bar	**1.2 kW to 1 kW to 0.9 kW**	5.1 l/s	4.5 l/s
12	Sand 450 g + Coal 50 g	2 bar	**0.9 kW to 1 kW to 2 kW**	5.1 l/s	4.5 l/s
13	Sand 500 g	**3 bar to 2 bar to 3 bar**	1.2 kW	6 l/s, 5.1 l/s, 6l/s	5.9 l/s, 4.8 l/s, 5.9 l/s
14	Sand 500 g	**2 bar to 3 bar to 2 bar**	1.2 kW	5.1 l/s, 6 l/s, 5.1 l/s	4.8 l/s, 5.9 l/s, 4.8 l/s

5.3.1 TRANSIENT STUDIES FOR SUDDEN CHANGES IN POWER INPUT

The output in variation of bed temperatures and riser surface temperatures for transient inputs in heat supply from 0.9 kW to 1 kW to 1.2 kW to 0 kW shown in Fig 5.15 (a) and 5.15 (b) . Fig. 5.12(c) shows the transient input in heat. The corresponding transient bed to wall heat transfer coefficient are also shown in Fig 5.16(a). The fluidizing air flow rate is 5.1 l/s, bed inventory is 400 g sand and operating pressure is 2 bar. From the graphs it is seen that the initial steady state is reached after about 2000 seconds after start up. The temperature profile for bed temperature shows the bed temperature to rises to a maximum of 90 ^{o}C at a height of 9.5 cm from the distributor plate and of about 60 ^{o}C at a height of 134 cm from the distributor plate. The corresponding riser surface temperature is 85 ^{o}C and 45 ^{o}C, respectively. It is observed that both the bed and surface temperature show an increase with increase in power input until they reach a subsequent steady state. The bed to wall heat transfer co efficient is seen to suddenly drop by about 50% after an instantaneous increase with increase in heat input but again increase to a steady value almost equal to the initial value in about 2000 seconds at the position 9.5 cm which is nearest to the heater. This is because as the heat supply has been increased instantaneously the temperature of the bed core rises faster than that of the surface thereby increasing the difference between the bed and surface temperature resulting in a sudden drop in the heat transfer coefficient. But as the difference gets narrower the heat transfer coefficient is seen to increase steadily. However the phenomenon is not the same in case of the higher regions farther away from the heater section in the riser where the bed temperature rises in a comparatively slower rate and which is same as that of the surface temperature rising rate. Therefore at these locations the difference between the bed and surface temperature is low and thereby shows sudden increase in heat transfer coefficient by about 20% due to sudden increased heat input. The initial instantaneous increase is due to the sudden increase in input power.

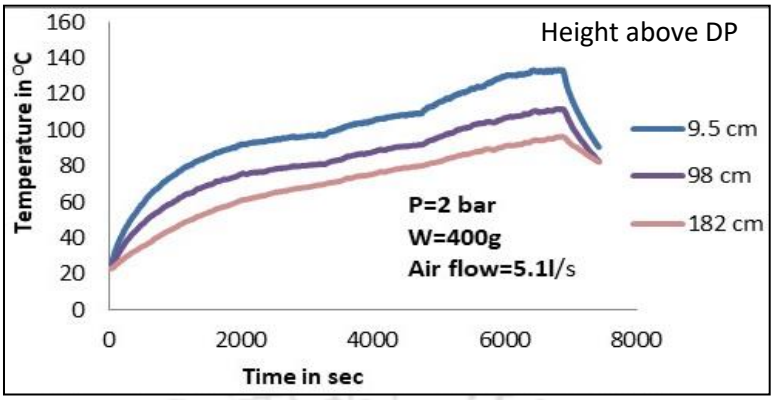

(a)

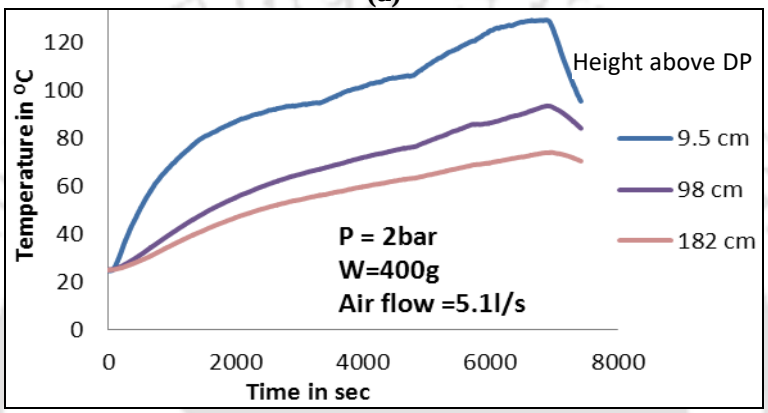

(b)

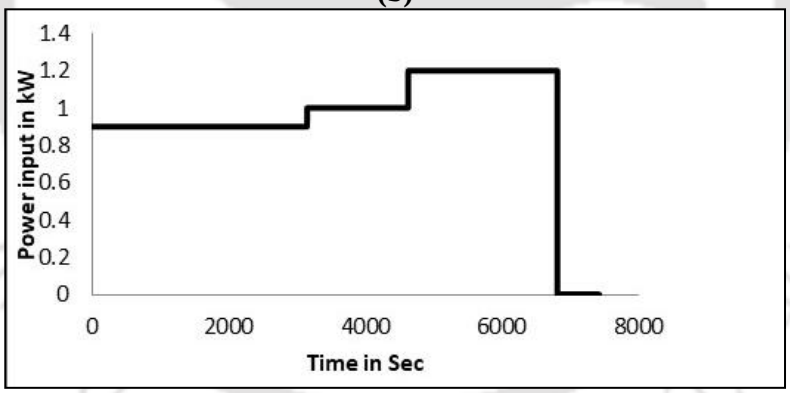

(c)

Fig 5.15 (a) Transient bed temperature (b) surface temperature along the riser height for (c) sudden changes in heat input as the transient input

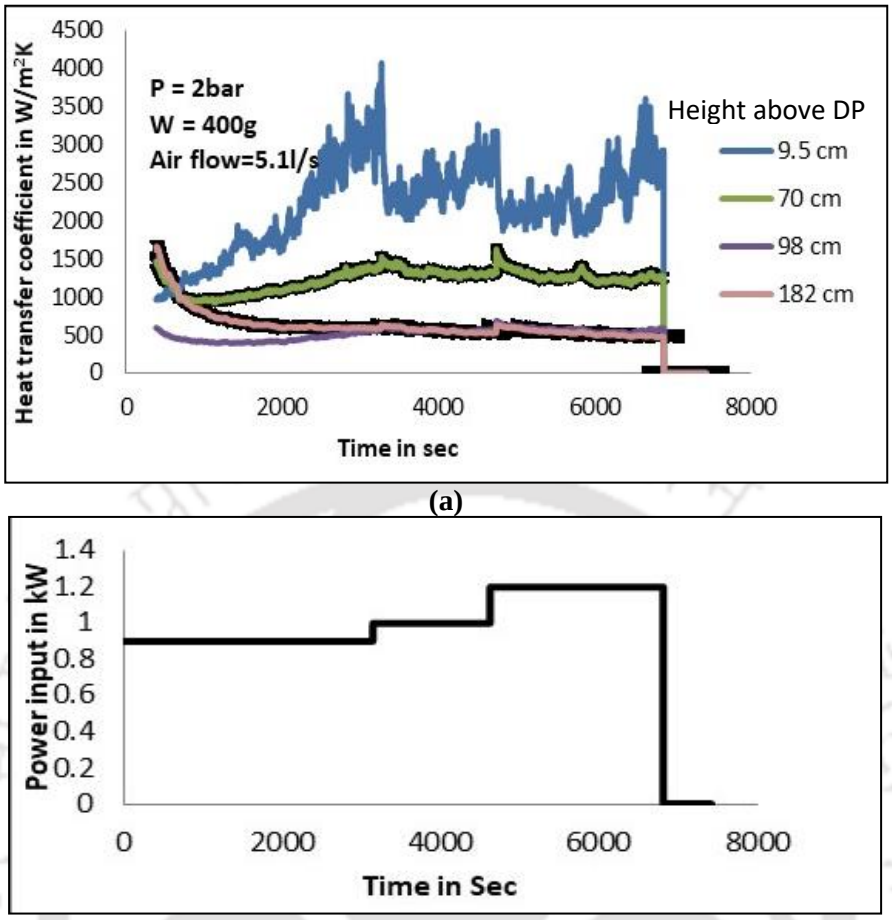

Fig. 5.16 (a) Transient heat transfer co efficient shown with error bars along the riser heights for (b) sudden changes in heat input

Then gradually as the increased heating effect takes place in the bed due to axial heat transfer from the bottom to the top, the temperature difference increases thereby reducing the heat transfer coefficient by 20% again. Still further as heat travels towards the surface bringing up the surface temperature and reducing the bed and surface temperature difference the heat transfer again starts increasing. The maximum heat transfer coefficient is observed at the lowermost region of the riser at a height of 9.5 cm. It is because of its proximity to the heater. The low heat transfer coefficients are observed to be at 98cm and 182 cm. This can be explained from the suspension density profile shown in fig 5.18 where the suspension densities are lowest at these regions whereas the higher heat transfer regions are near 70cm because of higher concentration of sand in these regions resulting in a higher heat transfer coefficient at these regions. The highest value being around 1400W/m^{2}K ignoring the region in close proximity to the heater and lowest being around 400 W/m^{2}K

The voidage profile and suspension density for the above experiments are shown in Fig 5.17 and 5.18, respectively.

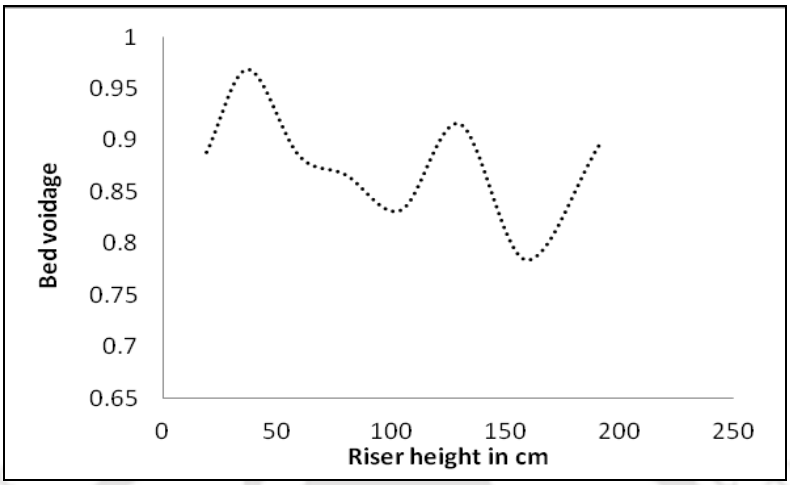

Fig. 5.17 Steady state bed voidage for fluidizing air flow rate of 5.1 l/s, P=2 bar, W=400g

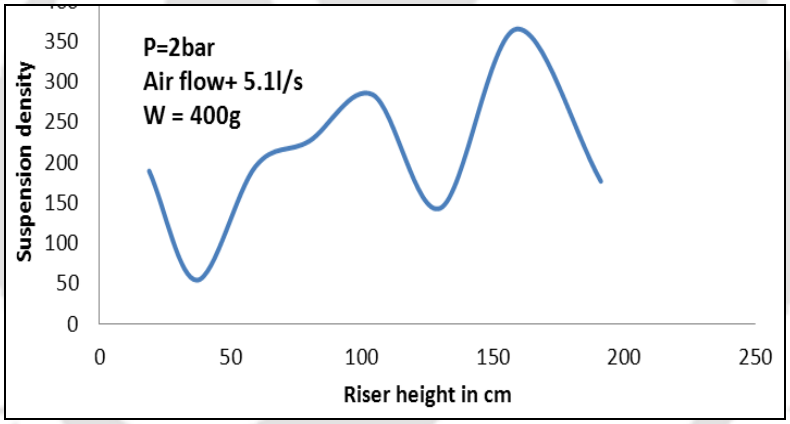

Fig. 5.18 Steady state suspension density for fluidizing air flow rate of 5.1 l/s, P=2 bar, W=400g

The output variation of bed temperatures and riser surface temperatures for reverse case ie sudden changes in heat inputs from 1.2 kW to 1 kW to 0.9 kW to 0 kW as the transient input are shown in Fig 5.19 The corresponding transient bed to wall heat transfer coefficient are also shown in Fig 5.20.

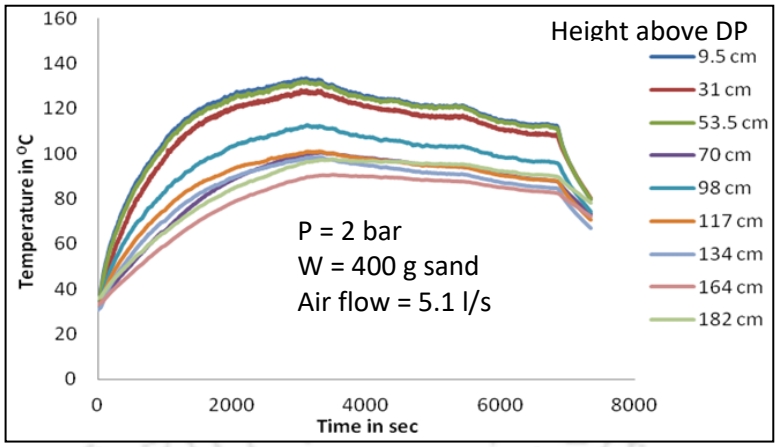

(a)

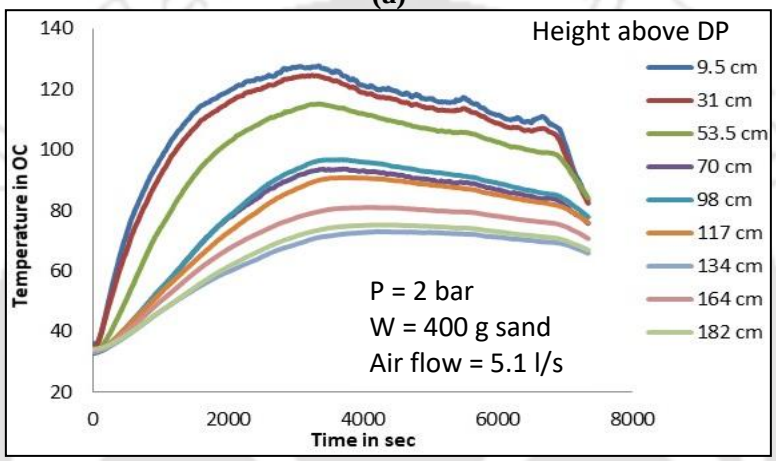

(b)

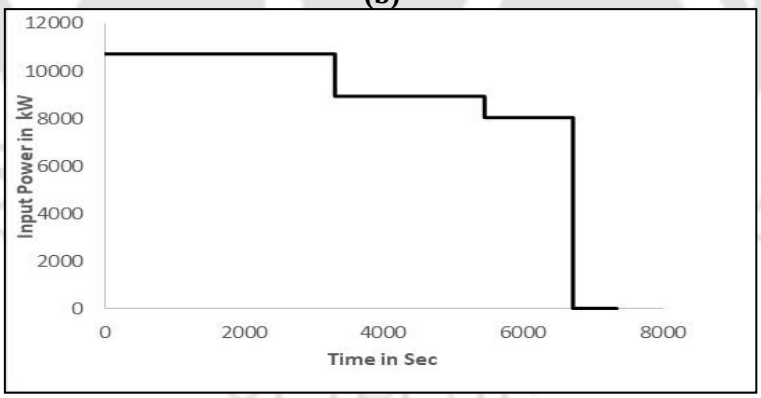

(c)

Fig. 5.19 (a) Transient bed temperature (b) surface temperature along the riser height for (c) sudden changes in heat input as the transient input.

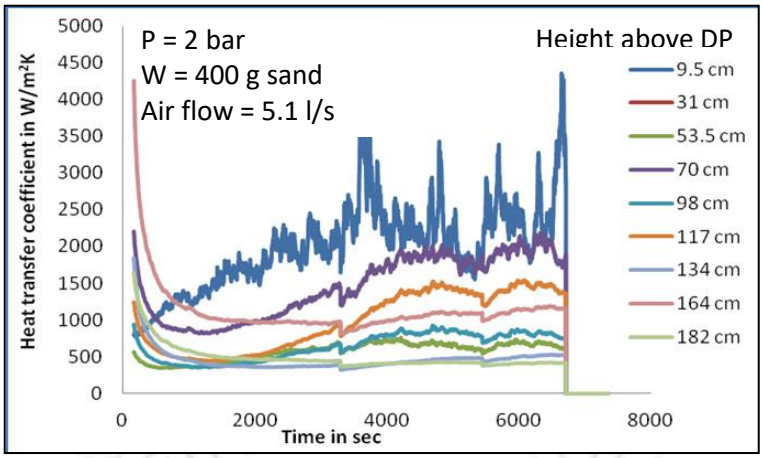

(a)

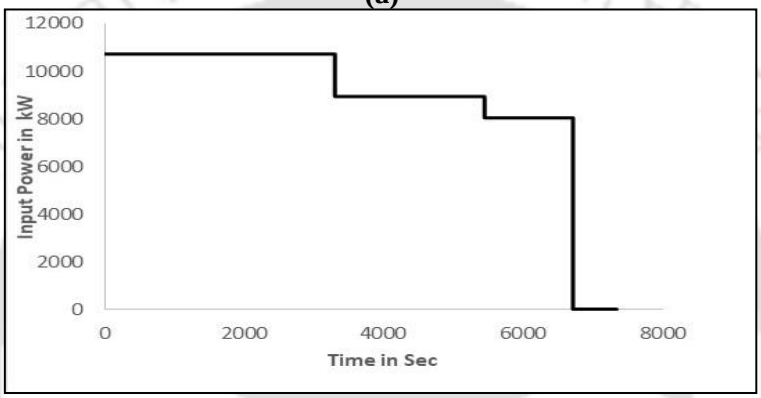

(b)

Fig. 5.20 (a)Transient heat transfer coefficient along the riser height for (b) sudden changes in heat input.

Here the bed to wall heat transfer co efficient is seen to first increase after an instantaneous decrease with decrease in heat input but again decrease. This may be because as the heat input is reduced suddenly the bed temperature falls faster than the surface because of its proximity to the SS tube wall thereby reducing the temperature difference between bed and wall. This makes the heat transfer coefficient to show an increased value. But gradually again as the temperature difference rise due to gradual fall in temperature of the wall, the heat transfer coefficient values again show a decrease in value. The initial instantaneous decrease is due to the sudden decrease in input power. From the Fig. 5.20 (a) it is seen that at a height of 70 cm the heat transfer is maximum ignoring the region of 9.5 cm which is nearest to the heater. At 70 cm height the heat transfer coefficient is seen to vary from 1 to 1.5 and finally to 2 kW/m^2K for the transient heat inputs of 1.2, 1 and 0.9 kW, respectively.

The same sets of experiments were performed for 500 g sand as bed material and the resulting graphs are shown in the following figures. From the Fig 5.21 and Fig 5.22 it is observed that the values of highest and lowest temperature are almost similar to those of 400 g sand. However here

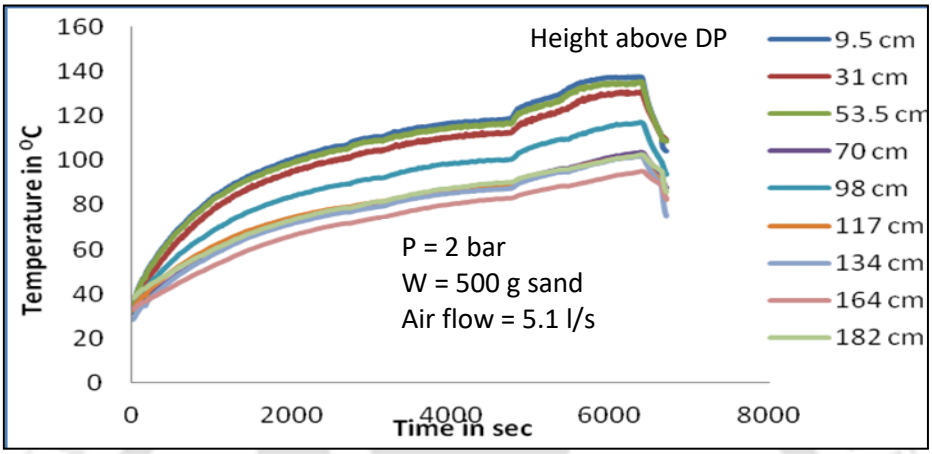

(a)

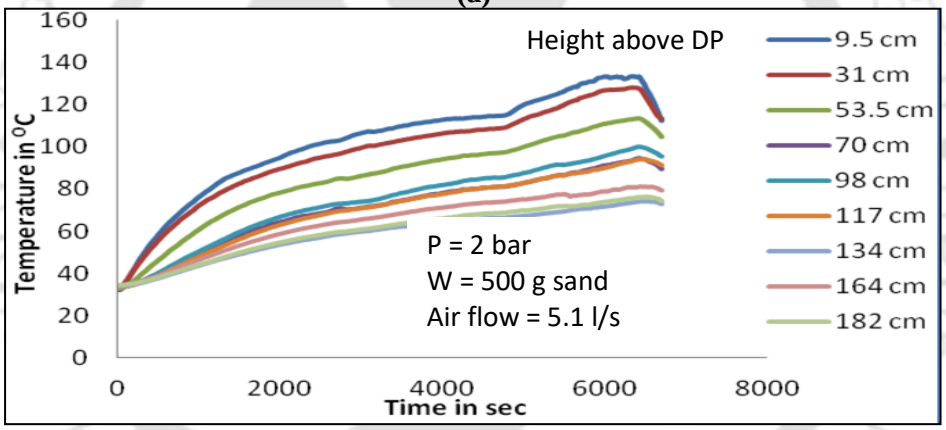

(b)

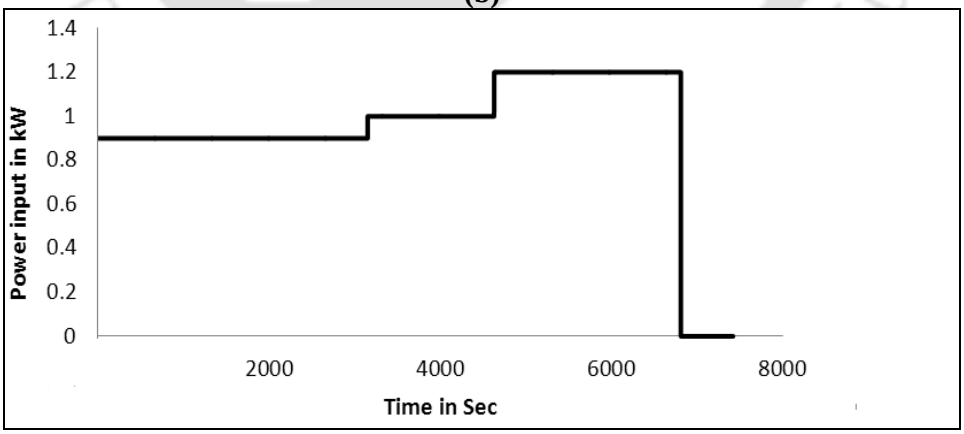

(c)

Fig. 5.21 (a) Transient bed temperature (b) surface temperature along the riser height for (c) sudden changes in heat input as the transient input.

it is observed that similar to the case with 400 g sand the maximum heat transfer coefficient is observed at the lowermost regions of the riser because of its proximity to the heater. Apart from this the regions of higher heat transfer coefficients are at 164 cm, 70 cm and 117 cm where as those of lower heat transfer coefficients are at 182 cm, 134 cm.

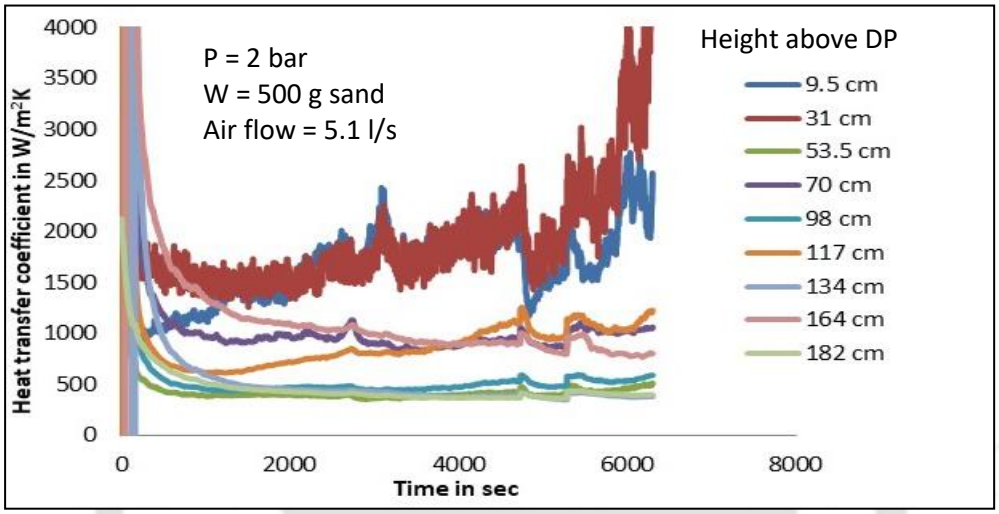

(a)

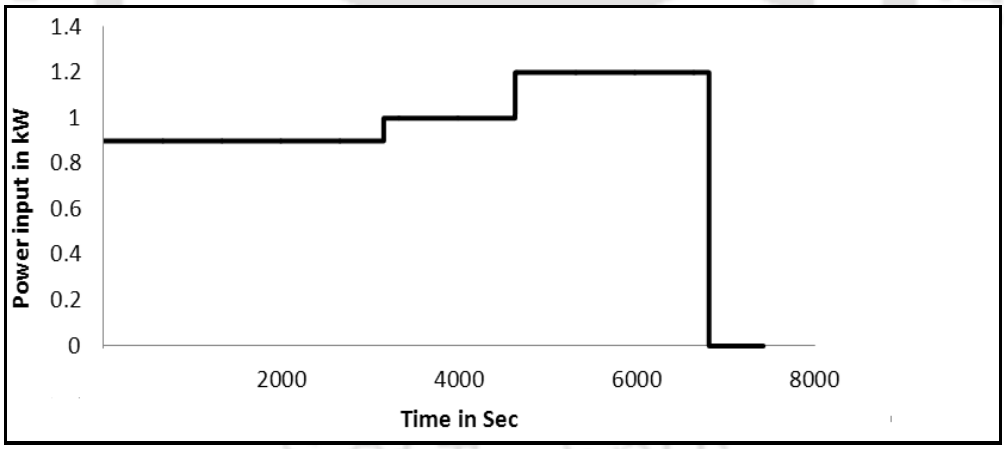

(b)

Fig. 5.22 (a)Transient heat transfer coefficient along the riser height for (b) sudden changes in heat input (0.9 kW-1 kW-1.2 kW)

This can be explained from the corresponding voidage profile given below in Fig 5.23 where concentration of sand are lower at 182 cm, 134 cm and and higher at164 cm, 70 cm and 117 cm. The highest value of heat transfer coefficient being around 1400 W/m^{2}K ignoring the region in close proximity to the heater and lowest being around 400 W/m^{2}K. Thus it is observed that the heat transfer values slightly increase with 100 g increase in bed material.

The same experiment with 500 g sand was performed in the reverse order i.e. with decreasing changes in power input and similar results were obtained.

Fig. 5.23 Steady state bed voidage for fluidizing flow rate of 5.1 l/s, P=2 bar, W=500 g

In another experiment, an amount of 500 g sand with10.0% coal blend was taken as bed material for investigating the transient heat transfer during changes in power input to heating coil as the transient input. The operating pressure and fluidizing air flow rate was kept the same at 2 bar and 5.1 l/s, respectively. The power input to the heater was initially fixed at 0.9 kW and suddenly changed to 1 kW and subsequently to 1.2 kW at 2 different instants of time. The changes in temperature profile and the heat transfer coefficient are given below in the Fig. 5.24. It is observed that the trend of changes in the bed temperature, surface temperature and heat transfer coefficient are similar to that observed for sand. Here it is observed that the highest temperature obtained at the height of 9.5 cm is slightly than that for pure sand. Is is observed ot be around 130 °C while it was around 5 °C higher for pure sand for both the bed and surface temperatures.

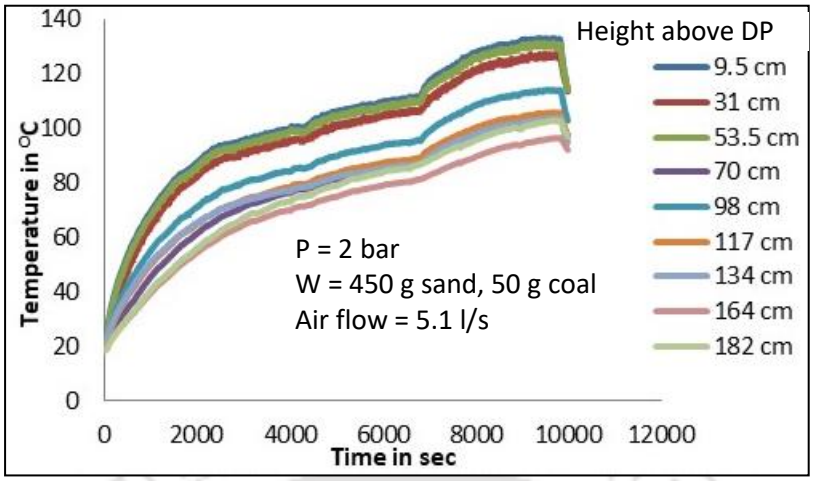

(a)

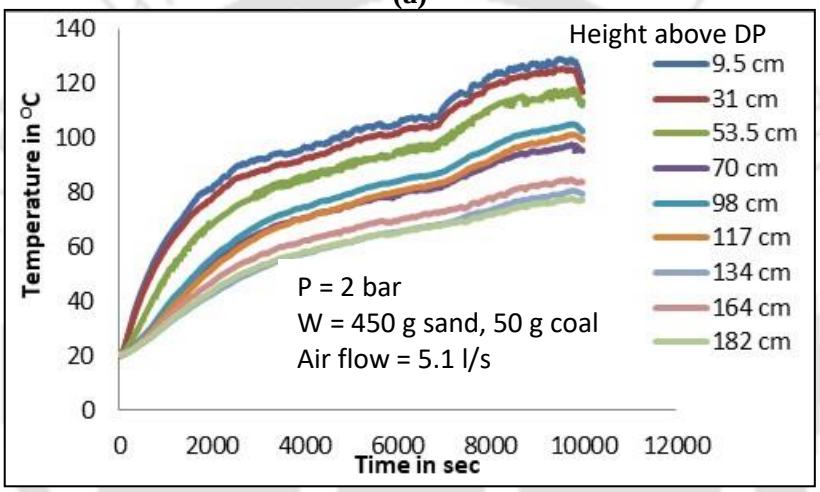

(b)

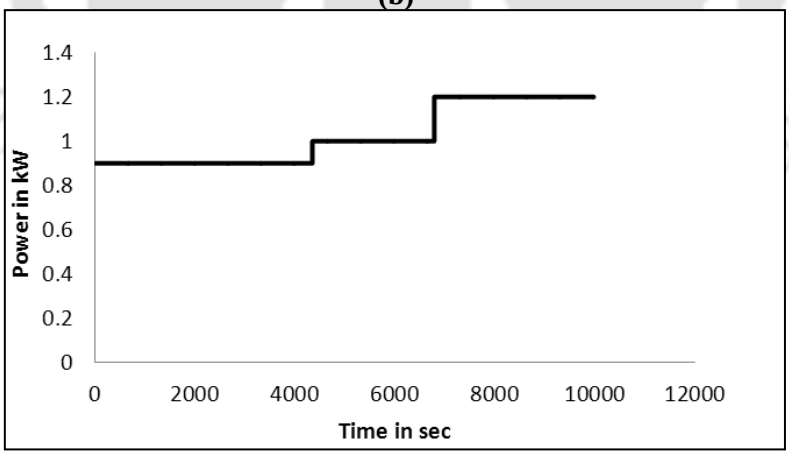

(c)

Fig. 5.24 (a) Transient bed temperature (b) surface along the riser height for (c) sudden changes in heat input (0.9 kW-1 kW-1.2 kW) as the transient input.

However from the Fig 5.25 it is observed that higher values of heat transfer coefficients are obtained at a height of 117 cm which varies from 1.2 kW/m^{2}k to 2.0 kW/m^{2}K. At 164 cm it is

around 1.0 kW/m^{2}K, at 98 cm it changes from 0.9 to 1.0 kW/m^{2}K and at 53.5 cm it varies from 500 to 800 W/m^{2}K with the increase in power input.The difference in heat transfer coefficients at the different height can again be explained with the voidage graph given in Fig. 23 for the same flow rate of air. It is seen that the regions where higher heat transfer takes place are those with less voidage values. Moreover the increase in heat transfer coefficient due to increased power input is due to increased heat flux. It is observed that there are spikes in the graphs of heat transfer coefficients at the transient moments. These are due to sudden increase of the heat influx, but the gradual decrease in the graphs are due to the increase in the bed temperature at a comparatively faster rate than that of the surface temperature which increases the ΔT. But still it can be observed that the values of heat transfer coefficients are higher at higher heat flux.

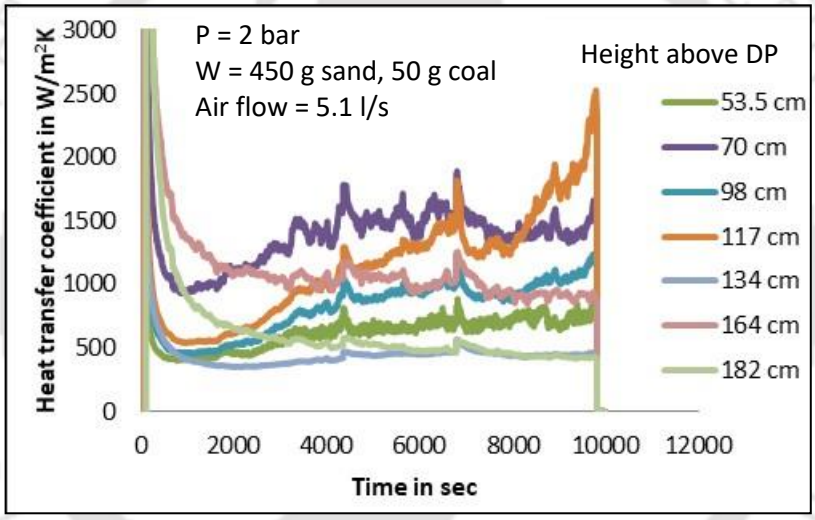

(a)

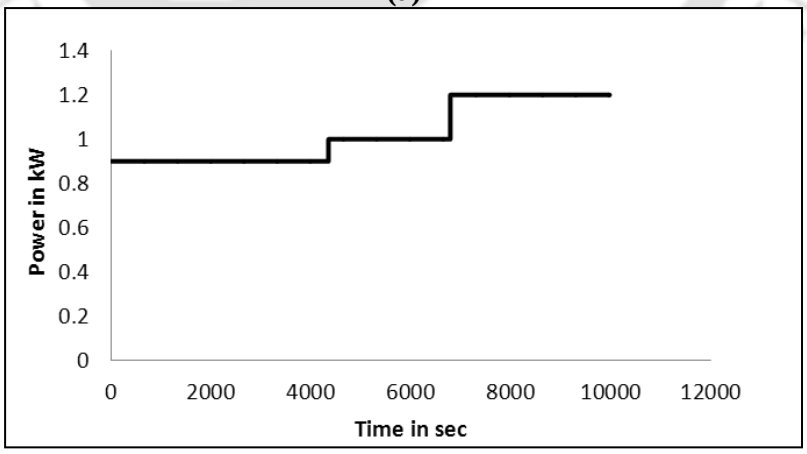

(b)

Fig. 5.25 (a) Transient heat transfer along the riser height for (b) sudden changes in heat input as the transient input (0.9kW-1kW-1.2kW).

5.3.2 TRANSIENT STUDIES FOR SUDDEN CHANGES IN EXHAUST FLOW RATES

The experiments related to transient inputs in exhaust flow rate (low to high to low) yielded significant output variations in temperature and heat transfer coefficients values. The transient temperatures for bed temperature and riser surface temperatures are shown in the following figures 5.26 (a) and 5.26 (b). The transient input is shown in Fig 5.26 (c). The transient heat transfer coefficients are shown in the Fig 5.27 (a). It is observed that with the sudden increase in the flow rate of exhaust air, the temperature of bed suddenly decrease to a lower steady value at the lower region of the riser whereas it increases to a higher steady value at the upper regions. From the Fig. 5.26 (a) it is seen at the lower region of 9.5 cm from the distributor plate, the bed temperature suddenly drops from around 160 °C to around 140 °C with the sudden increase in exhaust flow rate. The same figure shows that bed temperature at the upper regions of 164 and 182 sm shows a slight increase in value by about 1 to 2 °C. The riser surface wall temperature also shows a similar change as seen in Fig. 5.26 (b). Correspondingly the heat transfer coefficient also shows a sudden sharp decrease and gradual increase again at 9.5 cm from distributor plates where as in the upper regions it shows a steady increase. This may be due to the fact that a sudden increase in flow rate of the exhaust air results in a sudden convective cooling of the bed temperature which results in a drop in heat transfer coefficient at the lower region. But subsesequently at higher velocities of air the intermixing of solid particles increases due to increased turbulence and this effect overrides the earlier sudden cooling effect resulting in an increase in heat transfer coefficient. However at the upper region at 98 cm, there is a sudden increase in the heat transfer. This may be due increased concentration of bed materials at that point as seen from the corresponding suspension density profile for the three different exhaust flow rates shown in Fig. 5.28. The heat transfer is seen to be highest at lower most region of 9.5 cm due to its closest proximity with the heater coil. The heat transfer coefficient is observed to show a significant increase at a height of 98 cm from the distributor plate. It increases from a value of around 500 W/m^2K to a value of about 1.0 kW/m^2K while at regions of 164 and 182 cm it is almost same at values of 1.0 and 0.5 kW/m^2K, respectively. It is evident from the suspension density graph shown in Fig. 5.28 where the values of suspension density rises at 98 cm for higher exhaust flow rate while at the opther regions it remains same.

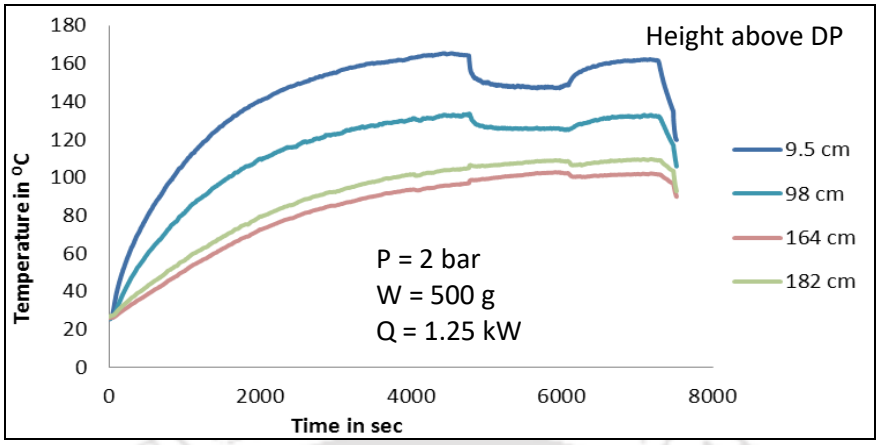

(a)

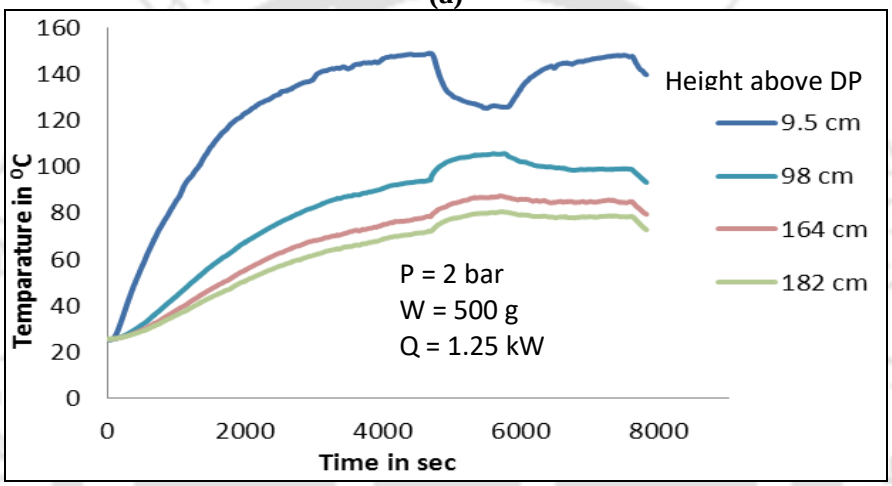

(b)

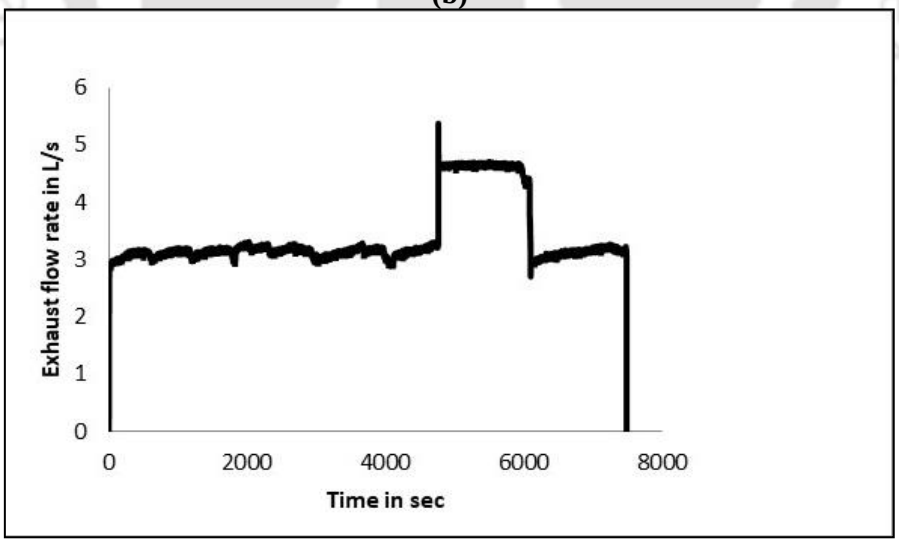

(c)

Fig 5.26 (a) Transient bed temperature (b) surface temperature along the riser height for (c) sudden changes in exhaust flow rate as the transient input

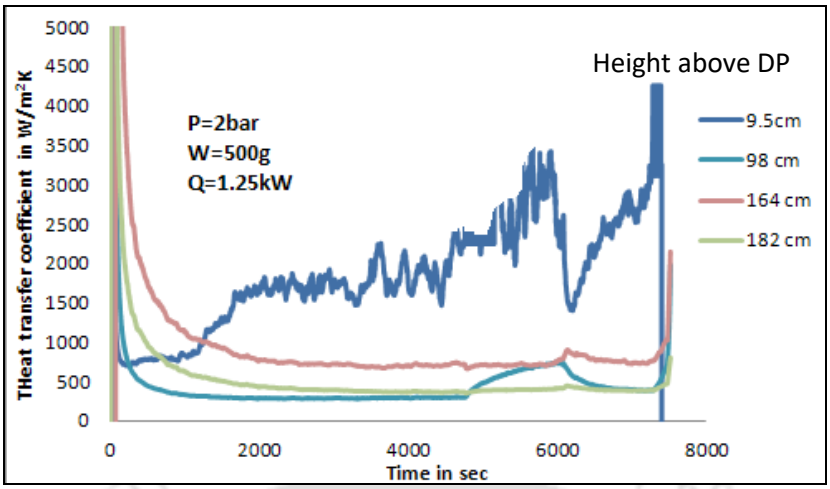

(a)

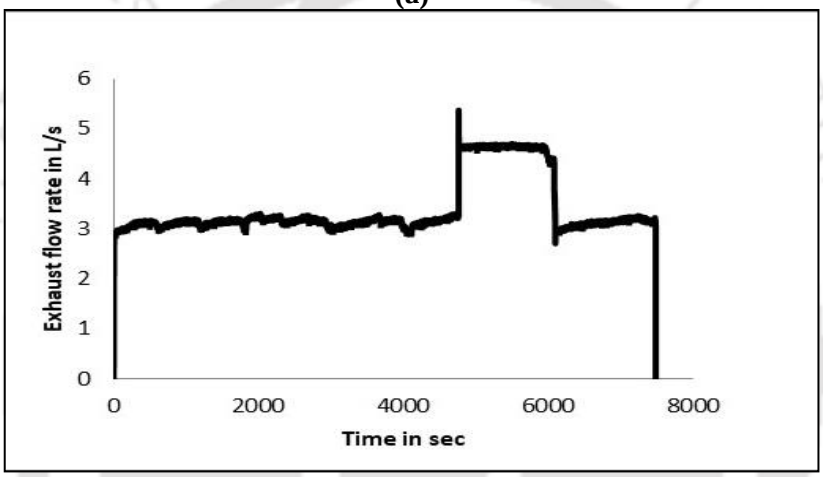

(b)

Fig. 5.27 (a) Transient heat transfer coefficient along the riser height for (b) sudden changes in exhaust flow rates as the transient input

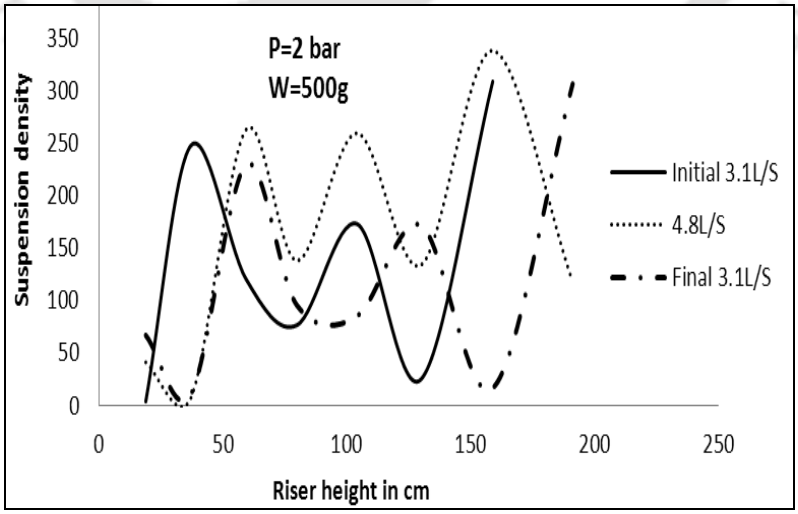

Fig 5.28 Steady state suspension densities for three exhaust flow rates

Experiment with 500 g sand performed with the change in exhaust flow rates in the reverse order i.e starting with high exhaust flow rate and sudden decrease followed by sudden increase showed similar changes in the reverse order as is evident from the Fig. 5.29.

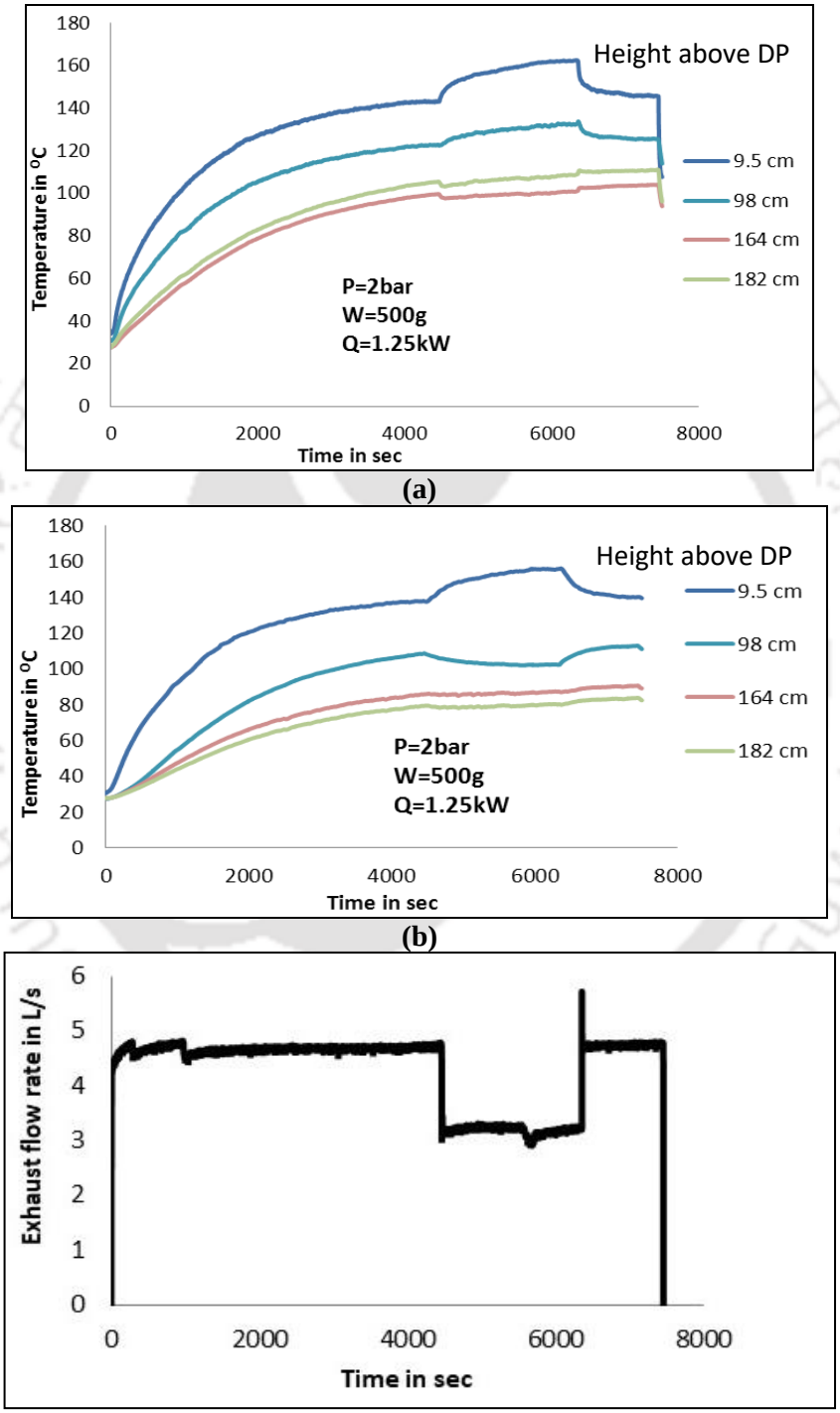

Fig 5.29 (a) Transient bed temperature (b) surface temperature along the riser height for (c) sudden changes in exhaust flow rates.

It is evident from the Fig. 5.29 above that the bed and surface temperatres at the lower regions show an increase in temperature while those at the upper region show an decrease in temperature with sudden drop in exhaust flow rates. For a sudden drop in exhaust flow rate, the bed temperature rises by about 20 and 30 °C at the heights of 9.5 and 98 cm, respectively while they decrease slightly by about 2 °C at the upper regions of 164 and 182 cm. The surface temperature meanwhile show an increase only at the height of 9.5 cm by about 20°C while it shows a decrease at the other regions. The causes of these have already been explained in the above section.

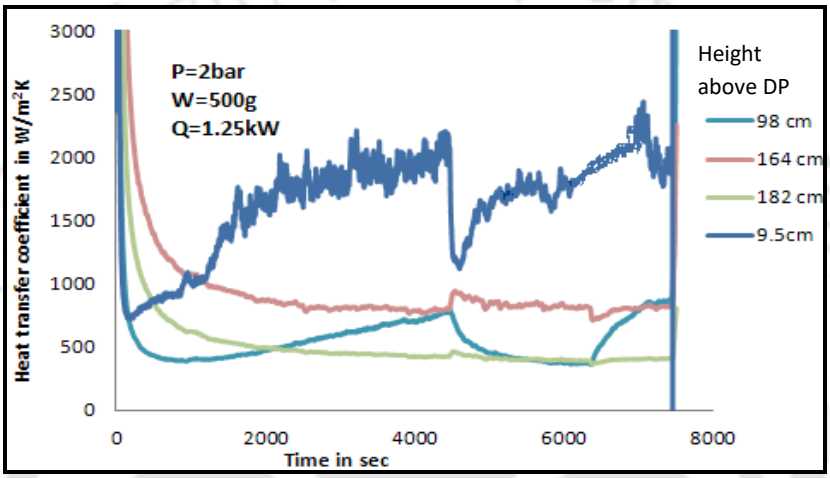

(a)

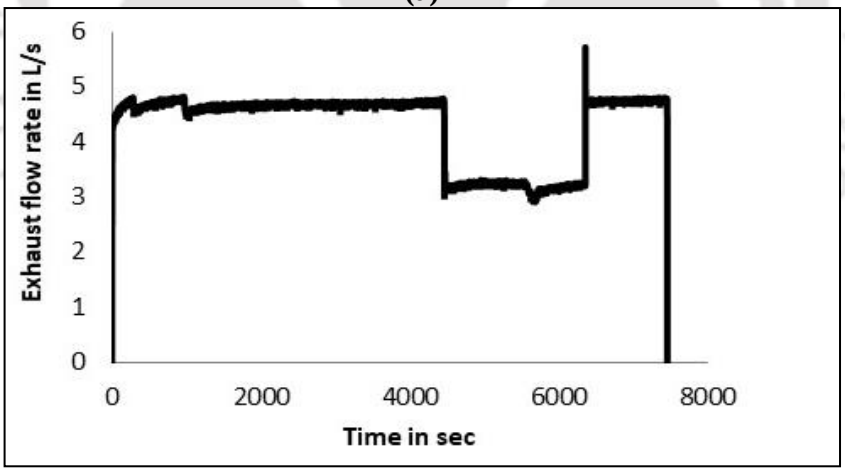

(b)

Fig.5.30 (a) Transient heat transfer coefficient along the riser height for (b) sudden changes in exhaust flow rates

The resulting graphs for heat transfer coefficient as shown in Fig. 5.30 (a) shows that the heat transfer coefficient is here also highest at 9.5 cm height which is due to its closest proximity to the heater coil. It is also seen at the height of 98 cm there is a sudden drop in the heat transfer

coefficient from a value of around 900 W/m^{2}K to around 400 W/m^{2}K. This again can be explained by the suspension density graph shown in Fig. 5.31. It is seen that the seuspension density at 98 cm height shows a sudden drop thereby decreasing the heat transfer coefficient at this point due to decrease in concentration of solid particles. The suspension densities at heights of 164 and 182 cm are seen to be almost same for the two exhaust flow rates.hence the heat transfer coefficient at these regions remains almost steady.

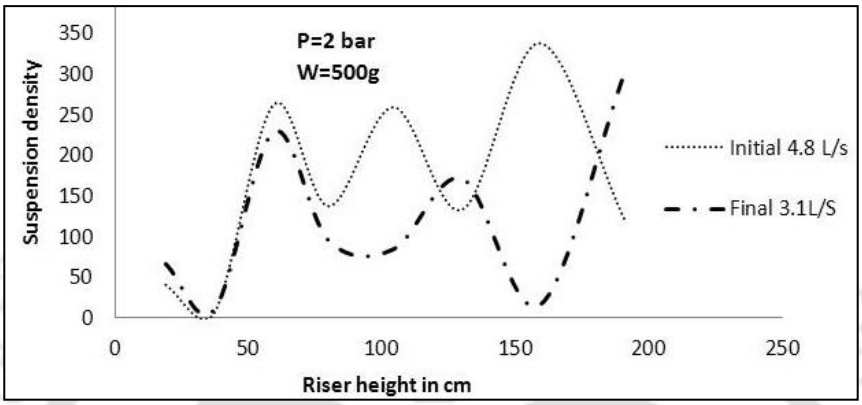

Fig 5.31 Steady state suspension densities for three exhaust flow rates

To study the effect of coal blends, an amount of 500 g sand with 10% coal was taken as bed material for investigating the transient heat transfer during changes in exhaust flow rates. The operating pressure was kept at 2 bar and fluidizing air flow rate was kept at 5.1 l/s. The power input to the heater was at 1.25 kW. The changes in temperature profile and the heat transfer coefficient are given in Fig. 5.32 and 5.33. It is seen that the heat transfer coefficients show a sudden sharp decrease and a steady increase at all regions within the riser column with increase in exhaust flow rates which can be explained by the corresponding suspension density graphs for high and low exhaust flow rates.The sudden sharp decrease and subsequent steady increase are comparable to those for the similar experiment with 500g sand. The suspension density values increase with increased exhaust flow rates as is seen from the Fig. 5.34. The higher values of heat transfer coefficients are seen at those regions where the concentration of bed material are higher. Moreover for example at a height of 70 cm it is seen that the suspension density show a marked increase in value with the sudden increase in exhaust flow rate, hence here the heat transfer coefficient show a sharp increase. Similarly at a height of 134 cm it is seen that the suspension density does not change significantly with an increase in exhaust flow and hence here the heat transfer coefficient too does not show a significant increase. Moreover if we observe the

suspension density graph for the exhaust flow rate of 4.5 l/s we see that the suspension density is highest at a height of 70 cm and lowest at a height of 134 cm. Subsequestly the heat transfer coefficiend at these regions are also highest and lowest, respectively. Thus it was observed that the changes are same as those for pure sand, however the values of heat transfer coefficient in this experiment showed a maximum value of 2000 W/m^2K at a height of 70 cm. and 98 cm which is of a higher value than that for pure sand. Thus it is observed that with coal blend of 10% the heat transfer coefficient at these regions show an increase by about 50%.

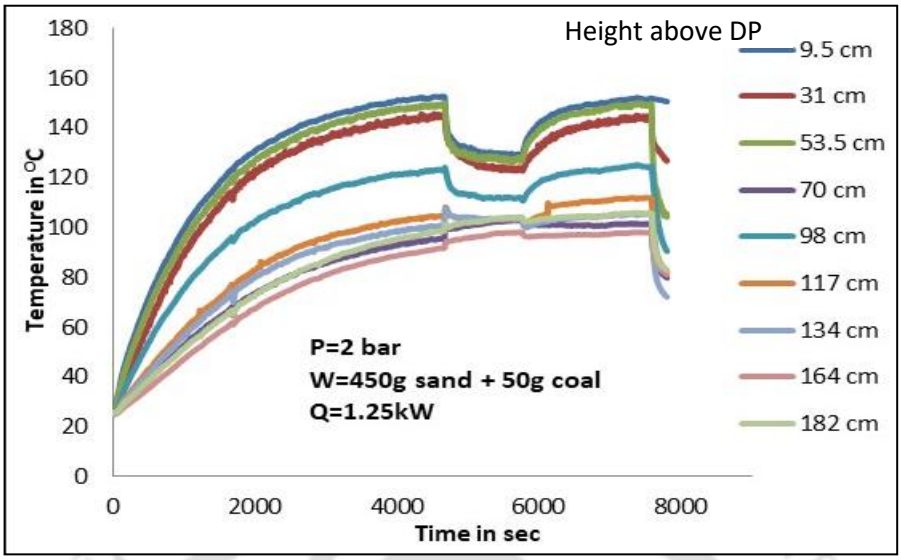

(a)

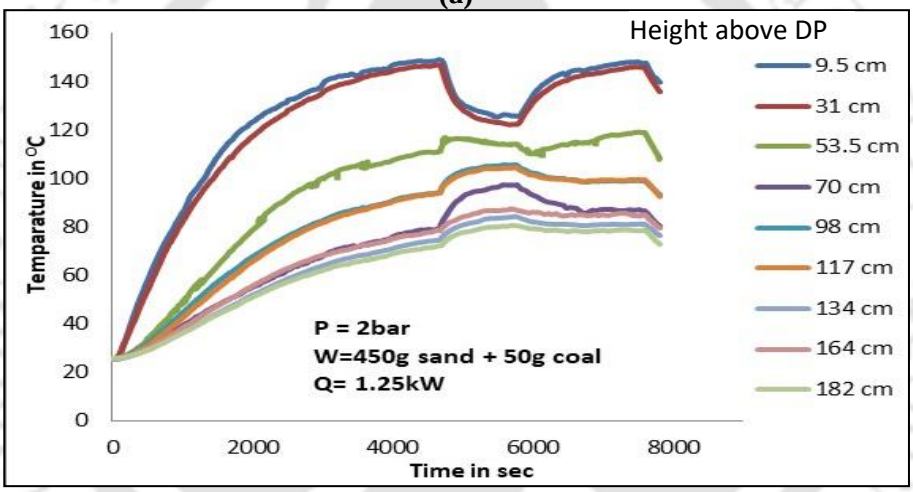

(b)

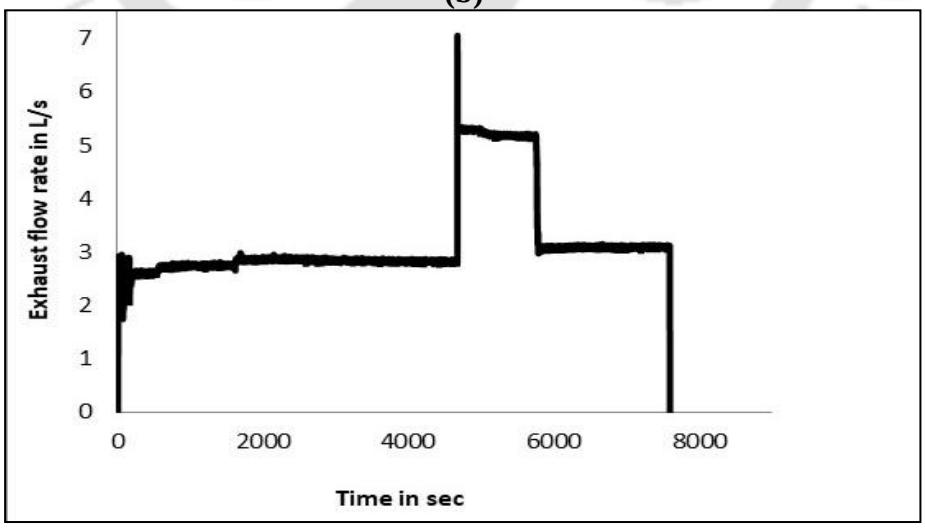

(c)

Fig. 5.32 (a) Transient bed temperature (b) surface temperature along the riser height for (c) sudden changes in exhaust flow rates

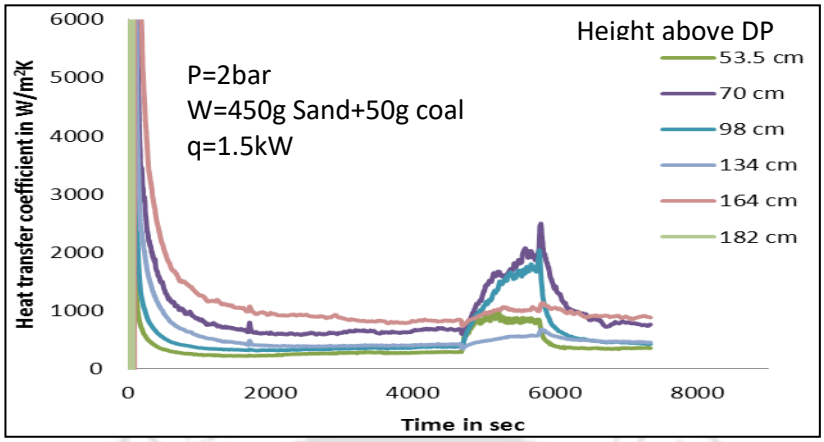

(a)

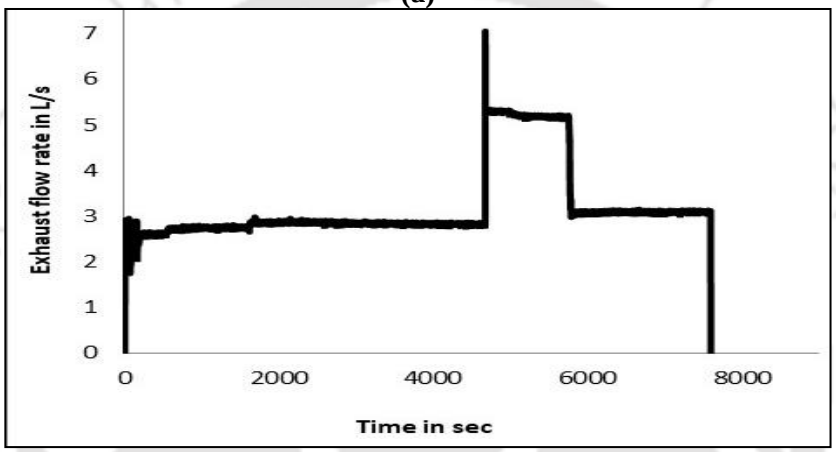

(b)

Fig. 5.33 (a) Transient heat transfer coefficient along the riser height for (b) sudden changes in exhsuat haust flow rates

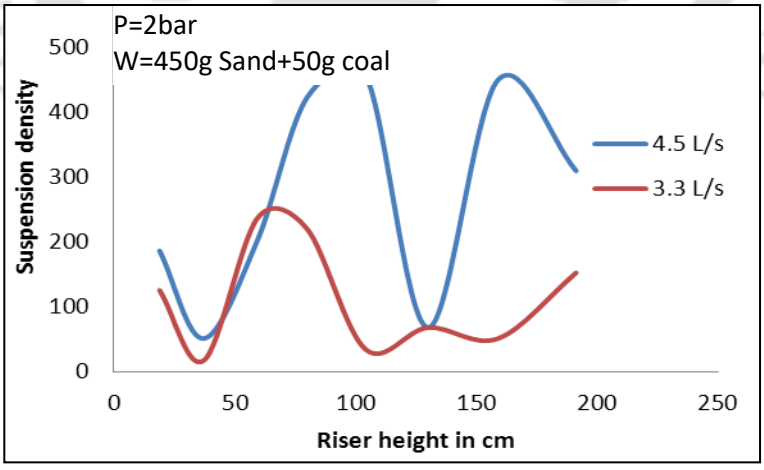

Fig. 5.34 Steady state suspension density for different exhaust flow rates.

5.3.3 TRANSIENT STUDIES FOR SUDDEN CHANGES IN OPERATING PRESSURE

Two experiments were performed with 500g sand as bed material and with power input of 10717w/m^2 where the transient input is operating pressure to observe the transient heat transfer coefficients. The transient graphs are given in the figures below.

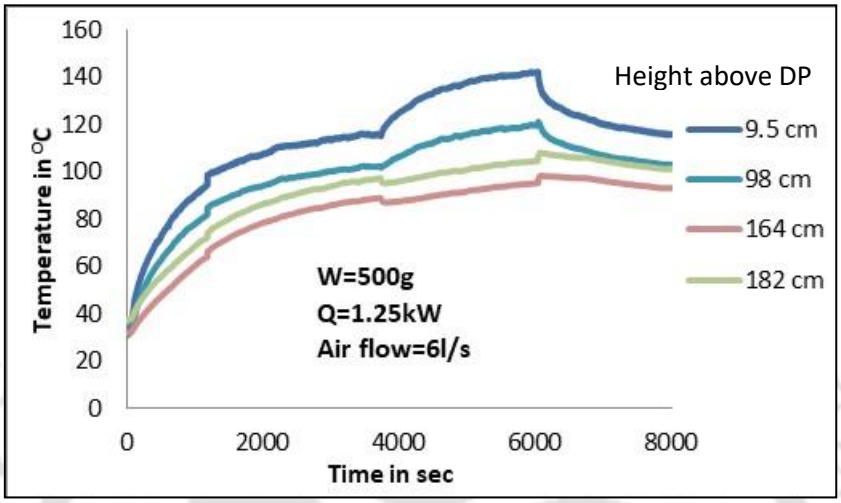

(a)

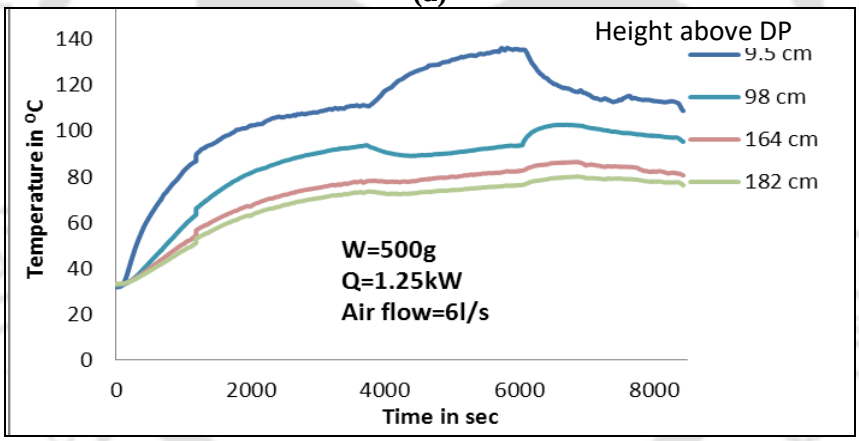

(b)

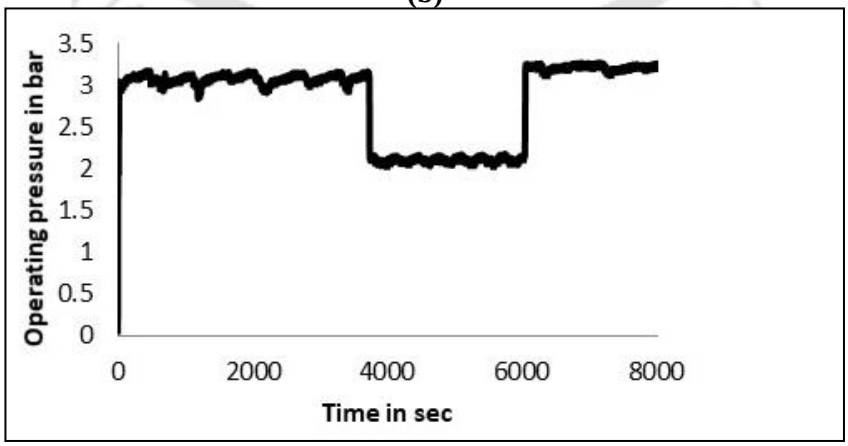

Fig 5.35 (a) Transient bed temperature (b) surface temperature along the riser height for (c) sudden changes in operating pressure as the transient input

It is observed from Fig 5.35(a) and (b) that both the bed and surface temperature increases with the sudden decrease in operating pressure at the lower regions. But the temperature in the upper regions of the riser decrease with decrease in operating pressure. This may be due to the decrease in pressure drop across the riser resulting from a decrease in operating pressure which leads to lesser amount of hot solid particles being transferred to the upper region. This is also obvious in the corresponding heat transfer change in the riser as shown in the Fig 5.36 (a). The phenomenon can be explained from the suspension density graphs for the various operating pressure shown in Fig 5.37

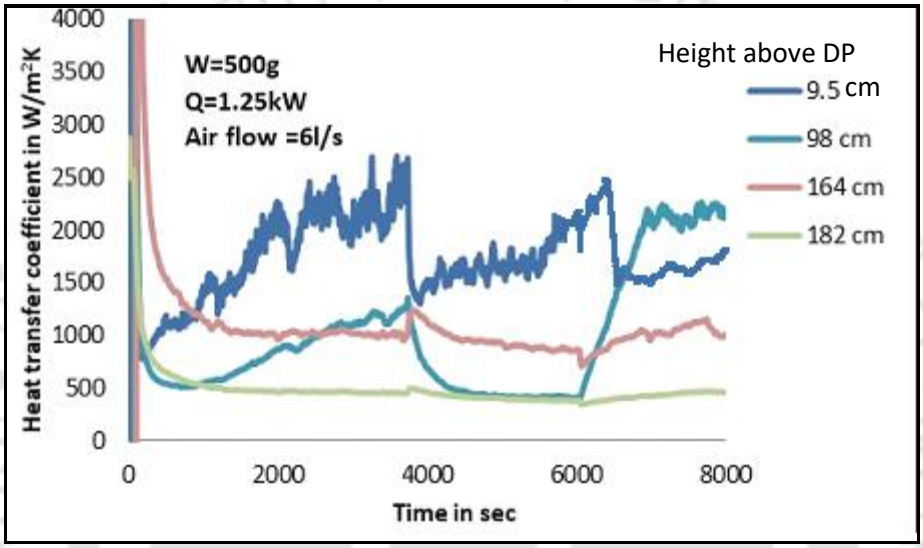

(a)

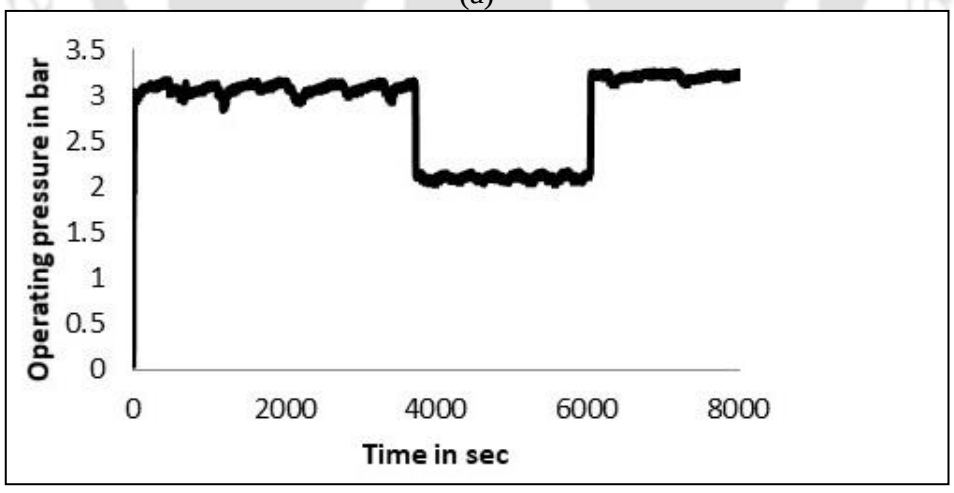

(b)

Fig. 5.36 (a) Transient heat transfer coefficient along the riser height for (b) sudden changes in operating pressure

It is observed that at a height of 98 cm the heat transfer coefficient drops from a value of around 1.4 kW/m^{2}K to a value of about 0.5 kW/m^{2}K with a sudden drop in operating pressure from 3 to 2 bar. The suspension density graph below shows that at this height there is a sharp increase in suspension density when the pressure was dropped to 2 bar. Thus with more solid being carried to this region, there is a sharp increase in heat transfer coefficient. Similar trends are also observed in the other regions of the riser

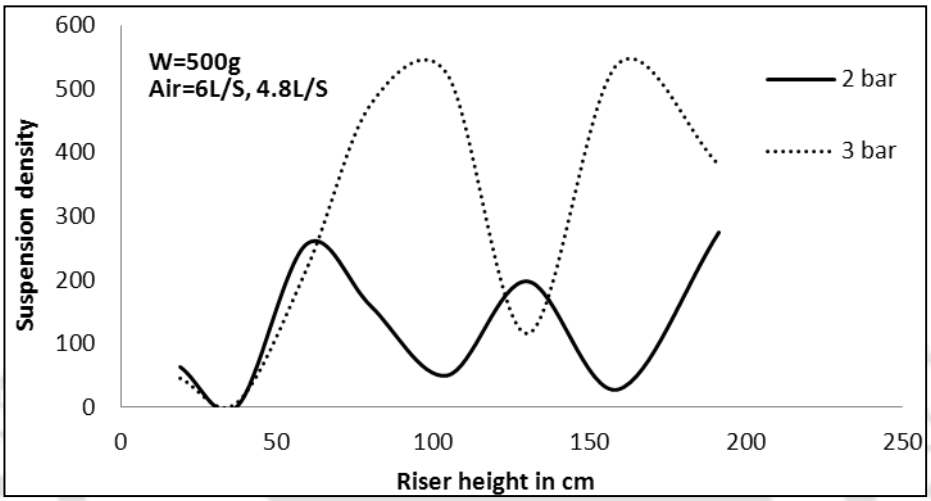

Fig 5.37 Steady state suspension density for various operating pressure

The results of the similar experiment in the reverse order of transient input where the operating pressure was first started with a low value are given below in Fig. 5.38. The heat transfer coefficient is shown in Fig 5.39 and the suspension densities for the three operating pressure are shown in Fig 5.40. The bed temperature, bed surface temperature and the heat transfer coefficients showed changes in the reverse order as that of the previous experiment involving change in operating pressure from a high value to low and high again. The graphs for bed and surface temperature profiles shows that with a sudden increase in operating pressure the temperatures at the lower regions drops and those in the upper region increases. This is because with increase in pressure the pressure drop across the riser rises and hence more hot solid particles are carried to the top region from the bottom in a reverse phenomenon as that of the previous experiment. From the Fig. 5.39 it is observed that there is a sharp rise in the heat transfer coefficient with increase in operating pressure at a height of 98 cm. This can be explained from the suspension density graph in Fig. 5.40 which indicates a sharp rise in suspension density at this point with a rise in operating pressure. The heat transfer coefficient at

164 and 182 cm height also show a slight increase and this is a result of the suspension densities at this regions to show a comparative increase as is evident from the Fig. 5.40.

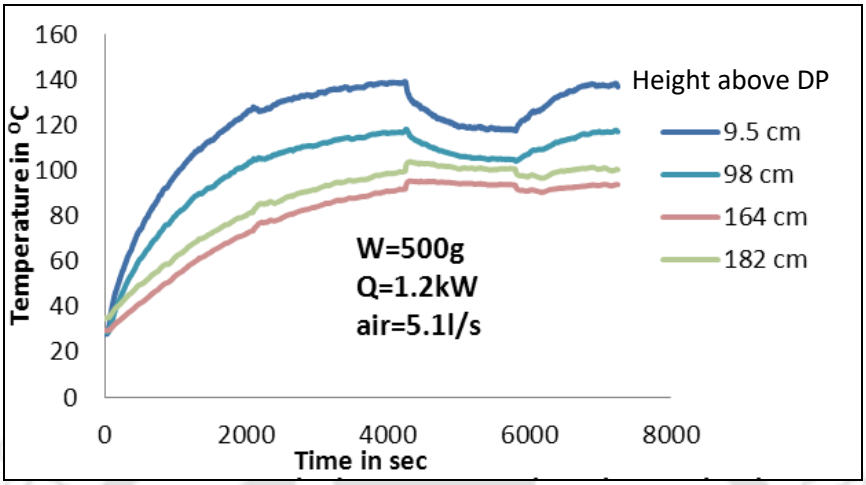

(a)

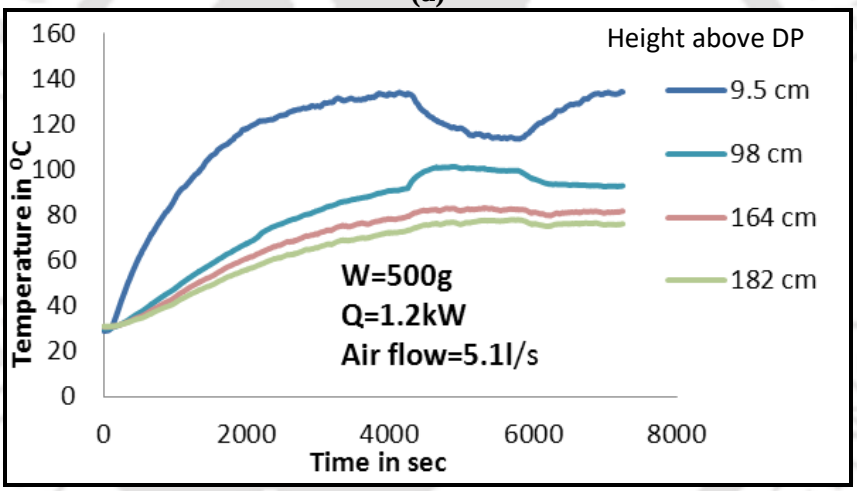

(b)

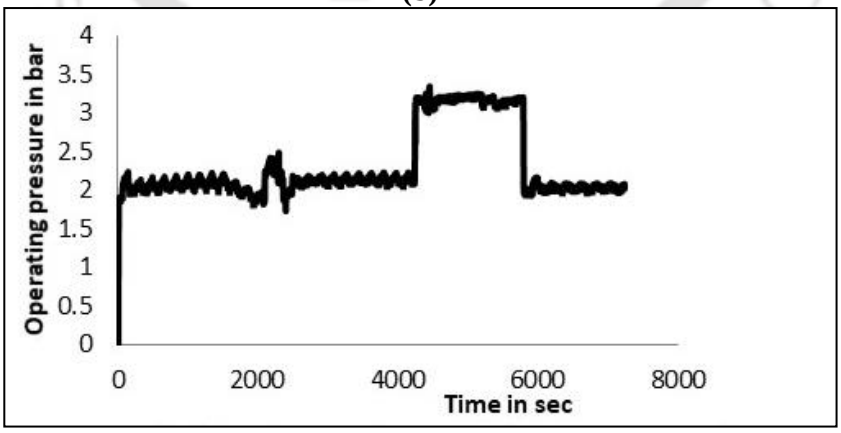

(c)

Fig 5.38 Transient bed temperature (b) surface temperature for (c) sudden changes in operating pressure as the transient input

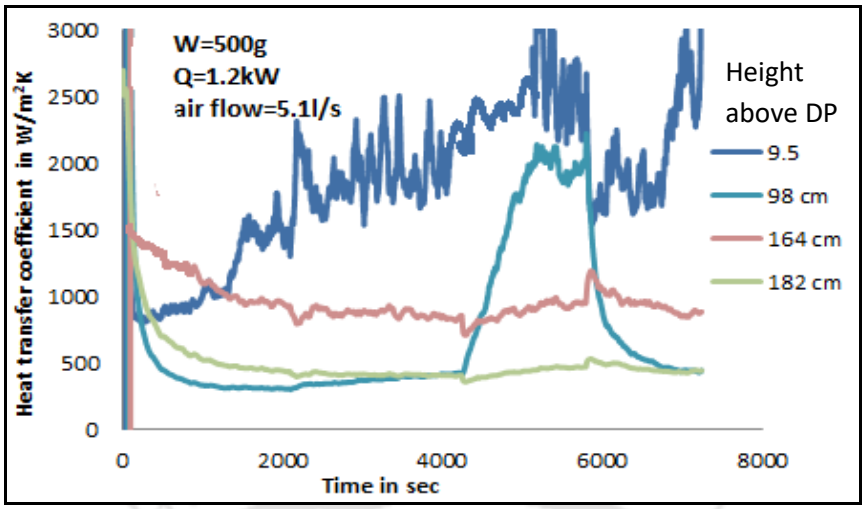

(a)

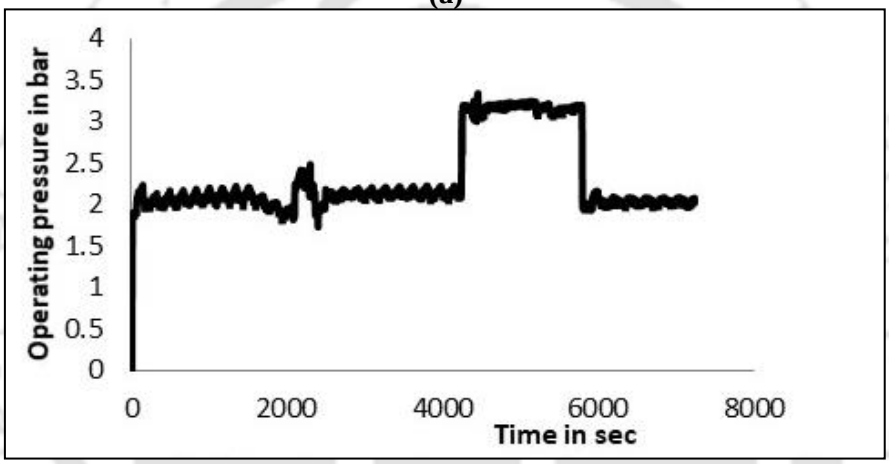

(b)

Fig. 5.39 (a) Transient heat transfer coefficient along the riser height for (b) sudden changes in operating pressure

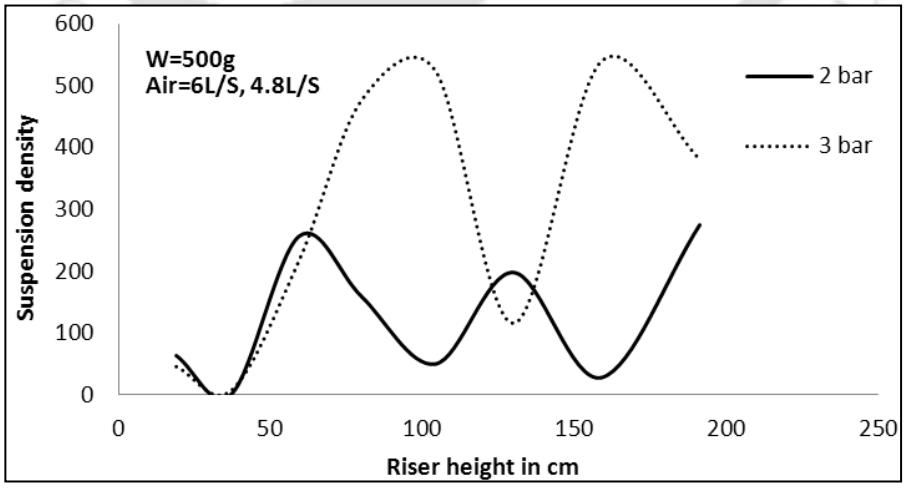

Fig 5.40 Steady state suspension density for various operating pressure

5.4 ANALYSIS OF DATAS THROUGH FAST FOURIER TRANSFORMATION (FFT)

Sample datas from each of the various sets of datas viz transient bed temperature, transient surface temperature, transient heat transfer coefficients and transient bed voidages were taken for signal processing through fast fourier transformation.

5.4.1 FFT OF TRANSIENT SURFACE TEMPERATURE.

Some of the data obtained were analysed through FFT.The FFT graphs are shown below

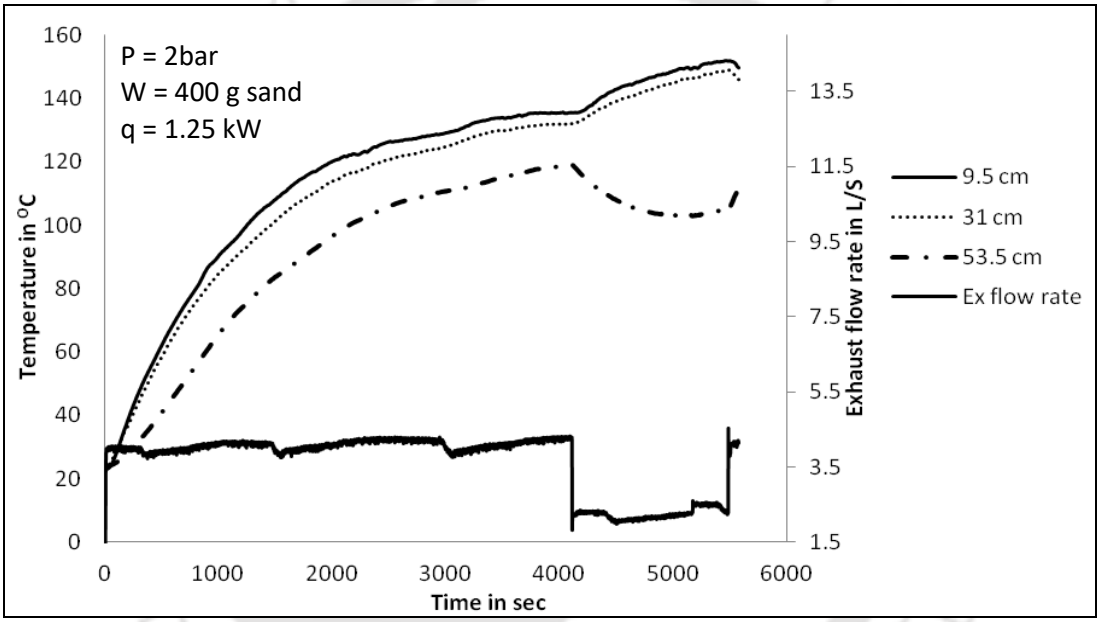

Fig. 5.41 Transient surface temperature at various riser heights for sudden changes in exhaust flow rate (high to low to high) with P=2bar, W=400g, Q=1.25kW

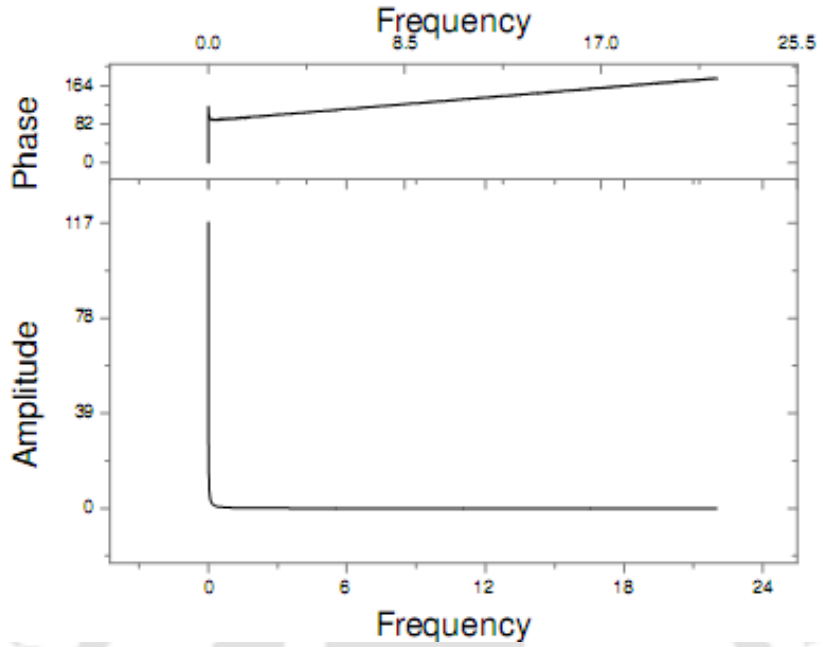

Fig. 5.42 FFT of surface temperature datas at 9.5 cm height showing frequency vs amplitude and phase

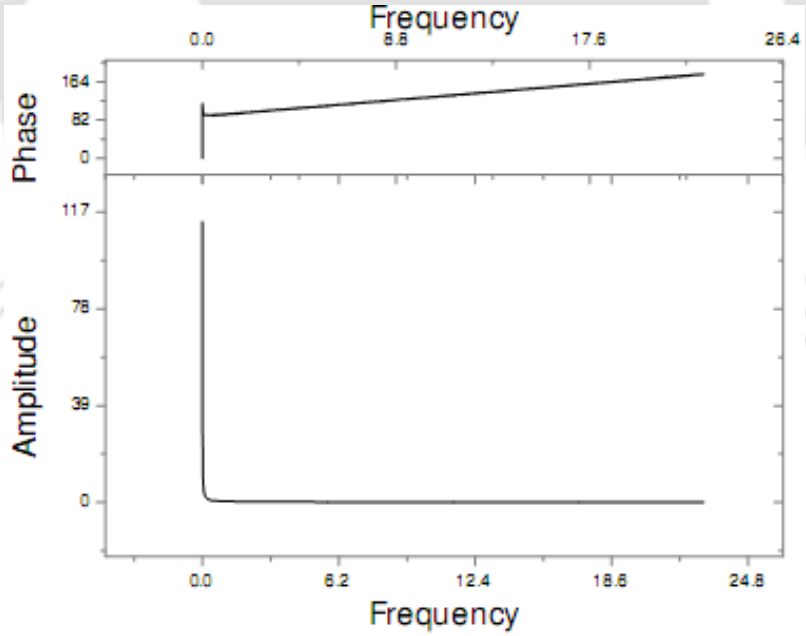

Fig. 5.43 FFT of surface temperature datas at 31 cm height showing frequency vs amplitude and phase

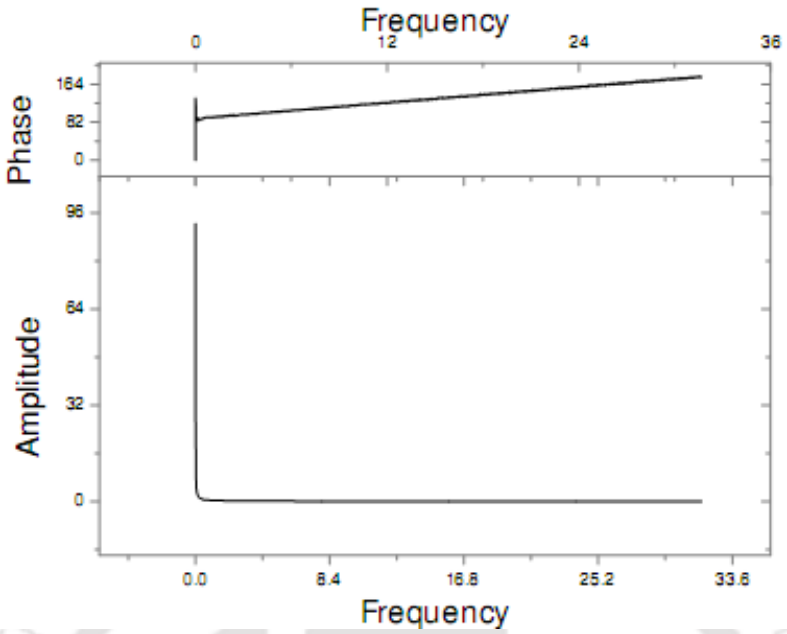

Fig. 5.44 FFT of surface temperature datas at 53.5 cm height showing frequency vs amplitude and phase

From the FFT graphs of the temperature profiles Fig 5.43 and 5.44, it is seen that the signals in all the cases are monotonous and free from external signals.There are various oscillations of negligible magnitude is all the cases. However from the FFT of the exhaust flow rates Fig 5.45 where the frequency vs phase is shown, there are three phases that can be observed, these may be the three different values of exhaust flow rates that were used in the transient input during the experiment.

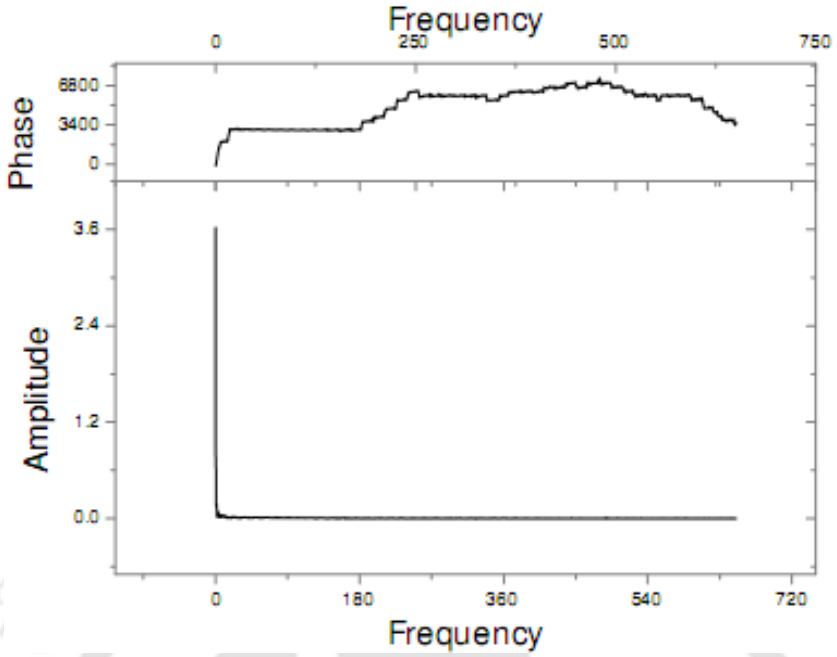

Fig. 5.45 FFT of exhaust flow rate datas showing frequency vs amplitude and phase

5.4.2 FFT OF TRANSIENT HEAT TRANSFER COEFFICIENT.

The FFT graphs are shown below

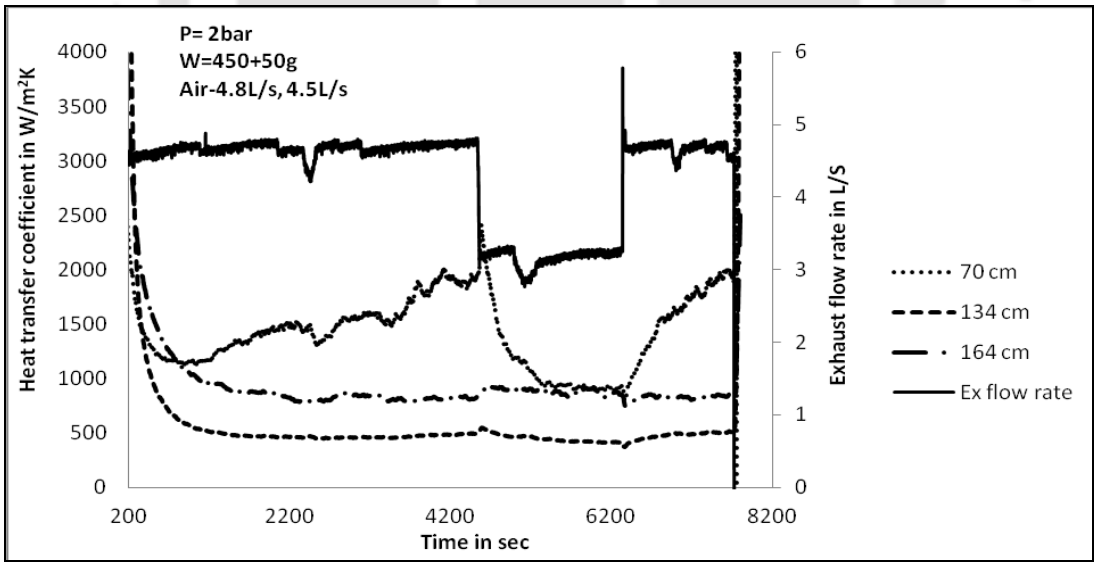

Fig 5.46 Transient heat transfer coefficient various riser heights for sudden changes in exhaust flow rates

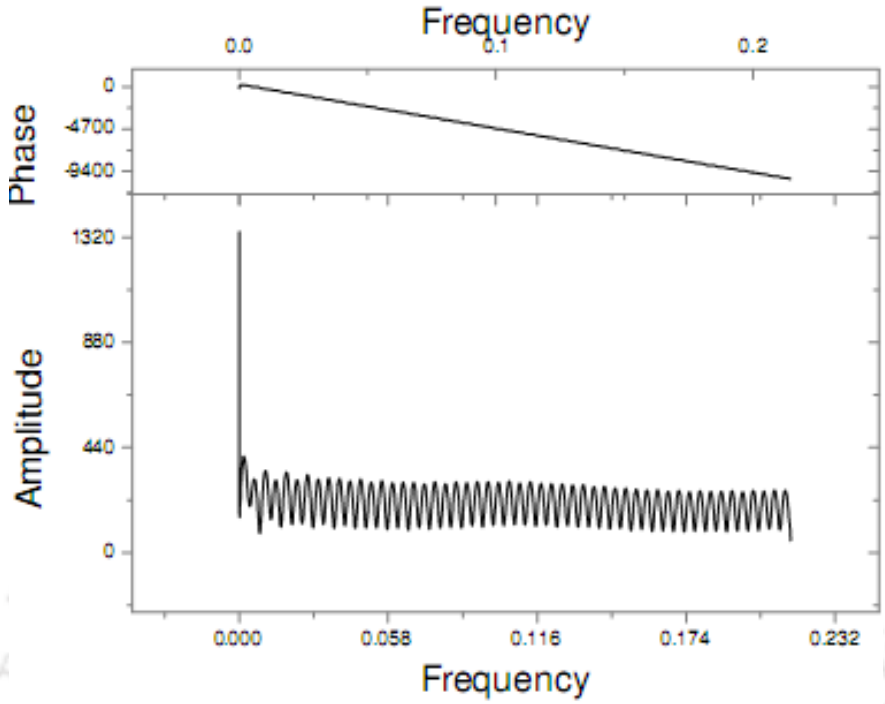

Fig. 5.47 FFT of heat transfer coefficient datas at 70 cm height showing frequency vs amplitude and phase

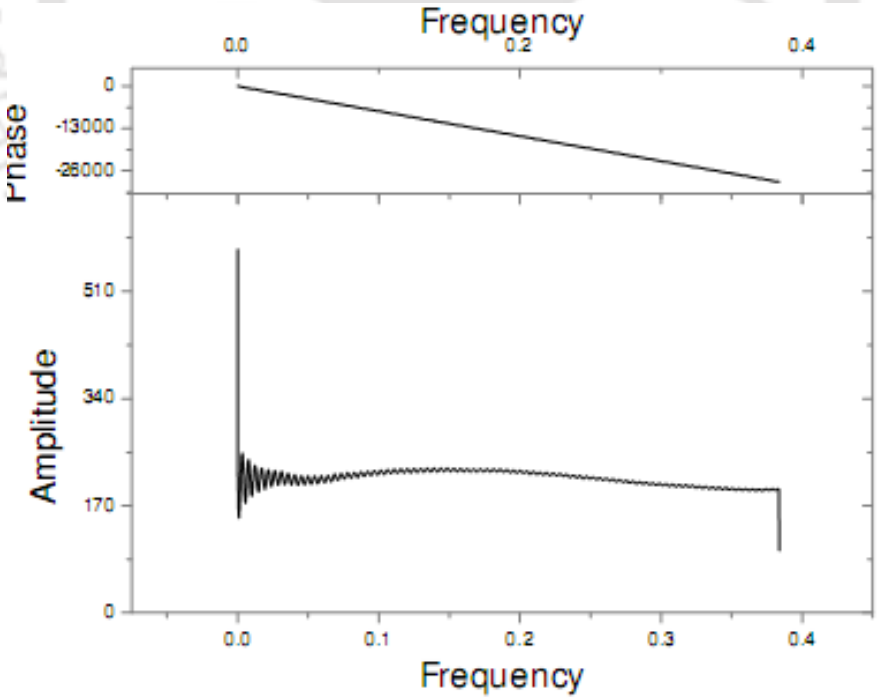

Fig. 5.48 FFT of heat transfer coefficient datas at 134 cm height showing frequency vs amplitude and phase

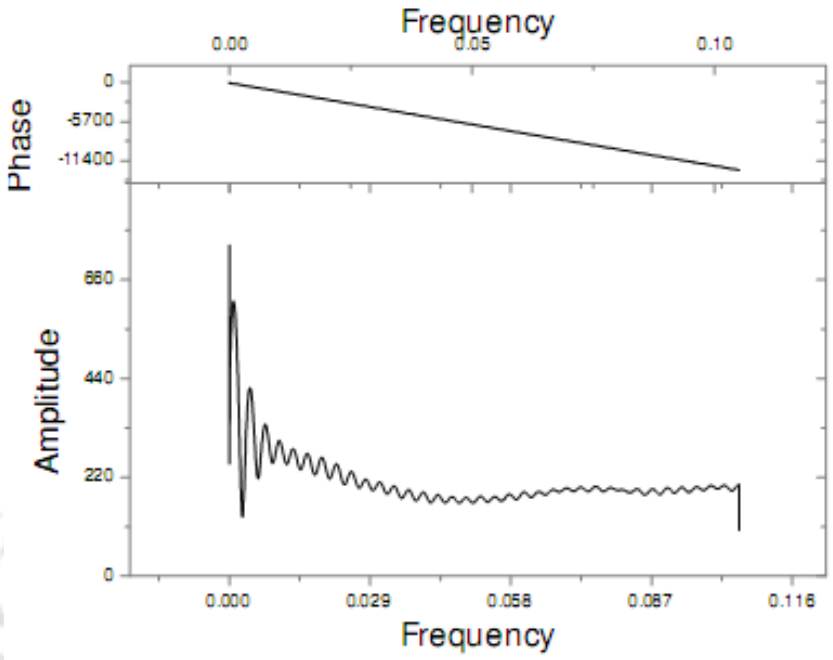

Fig. 5.49 FFT of heat transfer coefficient datas at 164 cm height showing frequency vs amplitude and phase

The FFT graphs for heat transfer coefficient datas as seen from Fig. 5.47 to Fig. 5.49 shows various oscillation of very low magnitude. This is because as the heat transfer coefficient is a function of the difference in bed and surface temperature both of which has fluctuations

5.5. RESPONSE OF THE OUTPUT PARAMETERS TO THE TRANSIENT INPUTS

The response of the temperature profiles and heat transfer coefficients to the input transients were analysed and the results are discussed below

5.5.1 RESPONSE OF BED TEMPERATURE PROFILE TO TRANSIENTS IN EXHAUST FLOW RATES

A typcial change in bed temperature profile with sudden changes in exhaust flow rates as discussed in earlier section is shown below.

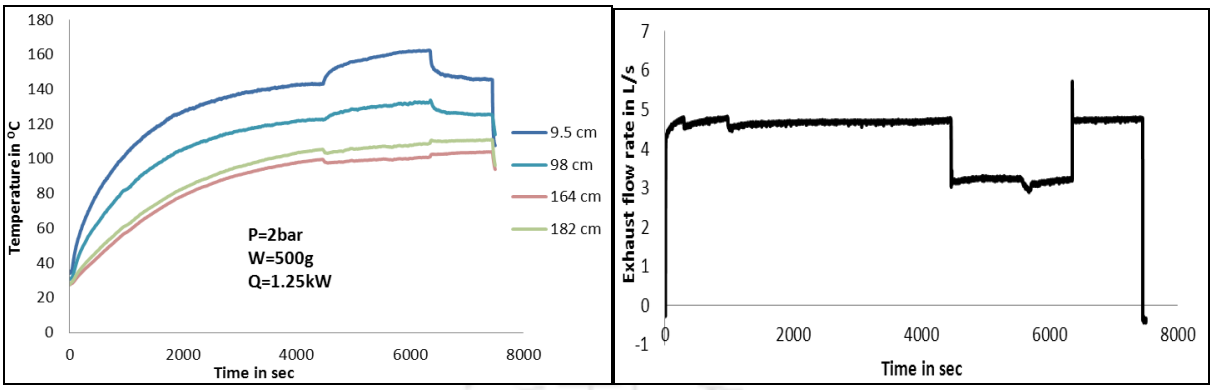

Fig 5.50 Typical changes in bed tempareture profile with sudden changes in exhaust flow rates

The plot of the bed temperature at 9.5 cm height vs the changes in exhaut flow rate is plotted below for the transient part to study the response

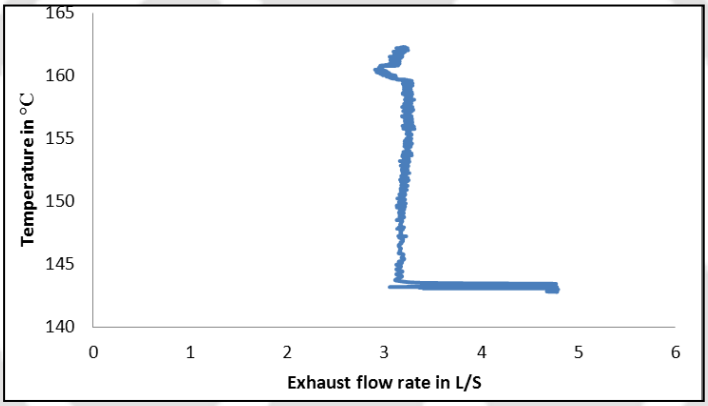

Fig 5.51 Response of bed tempareture profile to sudden changes in exhaust flow rates

5.5.2 RESPONSE OF HEAT TRANSFER COEFICIENT PROFILE TO TRANSIENTS IN EXHAUST FLOW RATES

A typcial change in heat transfer coefficient profile with sudden changes in exhaust flow rates as discussed in earlier section is shown below.

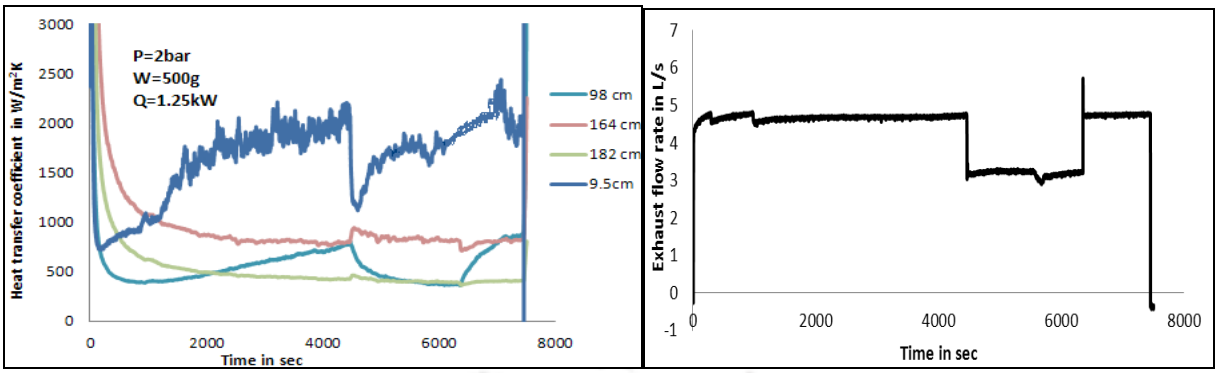

Fig 5.52 Typical changes in heat transfer coefficient profile with sudden changes in exhaust flow rates

The plot of the heat transfer coefficient vs the changes in exhaut flow rate is plotted below for the transient part to study the response

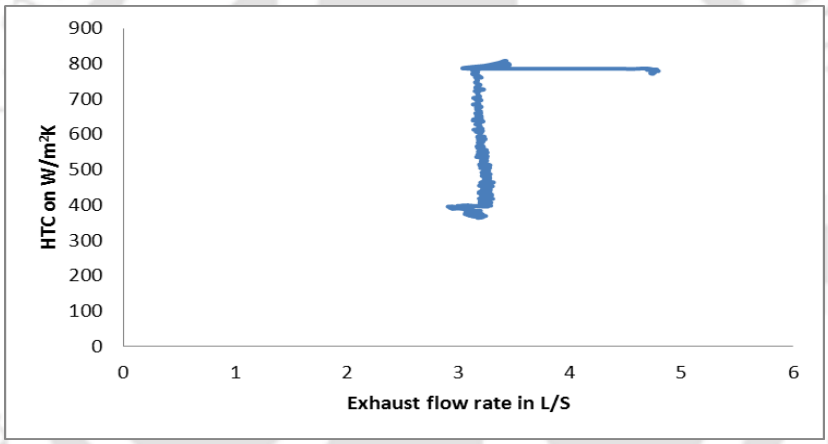

Fig 5.53 Response of heat transfer coefficient profile to sudden changes in exhaust flow rates

From the responses curves it is seen that the step or transient Response comes from the step input. The output response can thus be deduced to be a zero order response.

5.6 SUMMARY OF THE CHAPTER

The transient heat transfer and temperature profiles for both the bed and riser surface were investigated for various input transient conditions like operating pressure, exhaust flow rates, superficial velocity and input heat flux in a PCFB. The investigations were conducted for sand and coal-sand blends of 2.5%. 10%, 12.5% and 20% as bed material. Transient graphs shows steady state reaches within 2000 seconds of operation for airflow rate of 5.1l/s and heat flux of

10.717kW/m^2 and within 3000 seconds for 8.0382kW/m^2. Heat transfer coefficient is observed to have a strong relation to suspension density. Heat transfer coefficient is observed to be highest just near the distributor plate because of its proximity to the heater. In transient conditions it is observed that the heat transfer coefficient increases with sudden decrease in heat input and vice versa. Heat transfer coefficient is observed to show a momentous sharp rise with sudden decrease in the exhaust flow rate which later decreases steadily and vice versa.Also coal-sand blends were found to increase the heat transfer coefficient upto a certain percentage.The experiments related to transients in operating pressure showed that with a sudden drop in operating pressure the heat transfer coefficient is observed to show a momentous increase in value but a steady decrease and the reverse is also true for a sudden increase in operating pressure. The next Chapter presents the results of the experiment carried out to investigate the waste heat recovery from the downcomer of a PCFB during various transient conditions.

Chapter – 6

HEAT RECOVERY

6.1 INTRODUCTION

Based on the experimental procedure described in the Chapter 3, experiments were carried out on the heat exchangers described in the same Chapter. Result of the experimental achievement with significant outcome is presented in this Chapter

6.2 HEAT RECOVERY EXPERIMENTS IN STEADY STATE

Two different types of heat exchangers as described in chapter 3, section 3.41 and 3.42 were used for the initial steady state heat recovery experiment. The experiment was conducted at an operating pressure of 5 bar and superficial velocity of 5.4 l/s or 2.4 m/s in the PCFB. Inventory used was 500g sand of average particle size 355 to 425 micro. The water flow in the heat exchanger was kept constant at 0.00357 kg/s. The steady state was reached after about 3000 seconds. The temperature profiles along with the heat recovered are shown in Figs. 6.1-6.2.

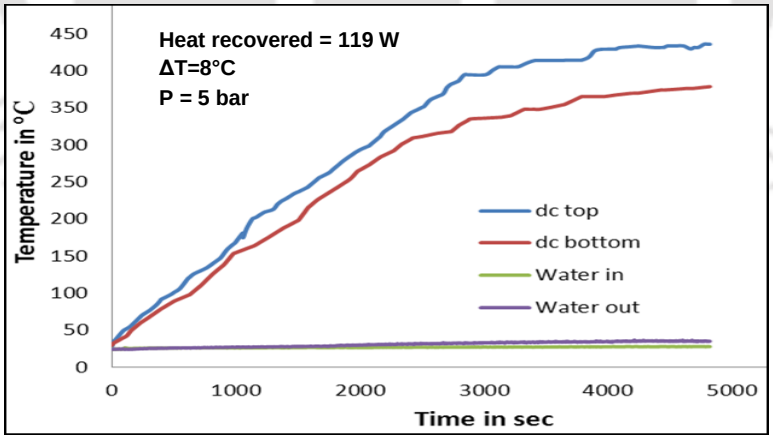

Fig. 6.1 Temperature profile for water jacket type heat exchanger

The amount of heat recovered through this water jacket type heat exchanger was thus found to be 119 W which is on the lower side. Hence further experiments with this heat exchanger are stopped and experiments with the spiral tube type heat exchanger are continued.

The amount of heat recovered through this spiral heat exchanger was thus found to be 284 W. From the results of the experiments on heat recovery during steady state, it is seen that the spiral tube type heat exchanger is more efficient in recovering heat than the water jacket type.

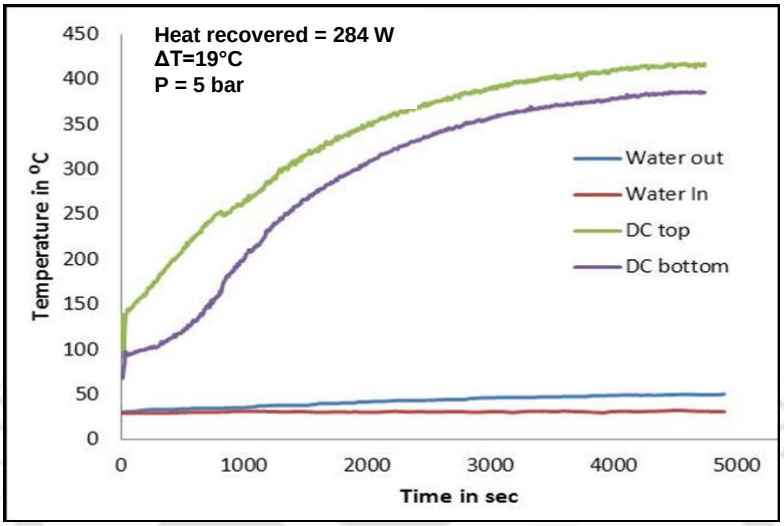

Fig. 6.2 Temperature profile for spiral tube type heat exchanger for operating pressure of 5 bar

Another experiment for heat recovery was also conducted at an operating pressure of 1 bar keeping other input parameters same as the experiments described above. Heat recovered in this experiment is found to be 132 W.

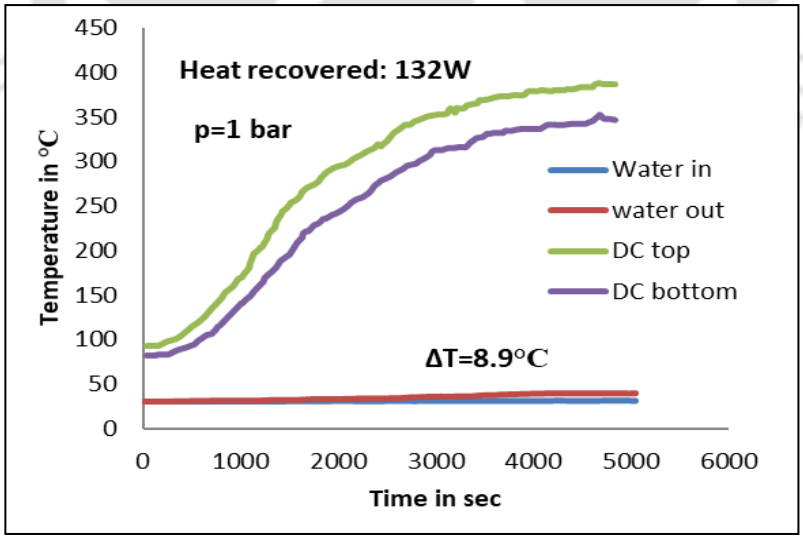

Fig. 6.3 Temperature profile for spiral tube type heat exchanger for operating pressure of 1 bar

From the experiments conducted it was thus found that the heat recovery was more at 5 bar operating pressure with the spiral tube type heat exchanger. Hence further experiments for transient input conditions were conducted at this operating pressure of the PCFB using the spiral tube heat exchanger.

6.3 RESULTS OF THE HEAT RECOVERY EXPERIMENTS DURING TRANSIENT CONDITIONS

The combination of parameters and transients introduced during the experiments on heat recovery are given below in the table 6.1. The transients introduced are shown in bold.

Table 6.1 List of combination of parameters and input transients in heat recovery study.

Sl No	Bed material and weight	Operating Pressure	Power input	Fluidizing air flow rate	Water flow rate in heat exchanger
1	Sand 500 g	5 bar	2.25 kW	**3.6 l/s to 5.1 l/s (Ramp in 300 s)**	0.0035 l/s
2	Sand 500 g	5 bar	2.25 kW	**5.1 l/s to 3.6 l/s (Ramp in 300 s)**	0.0035 l/s
3	Sand 500 g	5 bar	2.25 kW	**3.9 l/s to 5.4 l/s (Step in 1 s)**	0.0035 l/s
4	Sand 500 g	5 bar	2.25 kW	**5.1 l/s to 3.6 l/s (Step in 1 s)**	0.0035 l/s
5	Sand 500 g	5 bar	**1.6 kW to 2.5 kW (Step in 10 s)**	4.5 l/s	0.0035 l/s
6	Sand 500 g	5 bar	**2.5 kW to 1.6 kW (Step in 10 s)**	4.5 l/s	0.0035 l/s
7	Sand 500 g	5 bar	**1.6 kW to 2.5 kW (Ramp in 500 s)**	4.5 l/s	0.0035 l/s
8	Sand 500 g	5 bar	**2.5 kW to 1.6 kW (Ramp in 500 s)**	4.5 l/s	0.0035 l/s

6.3.1 TRANSIENT HEAT RECOVERY DURING SUDDEN CHANGES IN SUPERFICIAL VELOCITY

The heat recovery during the steady state condition of the PCFB for various superficial velocities has been discussed in the previous sections of this chapter. The heat recovery during the sudden changes in superficial velocities is discussed here. Four sets of experiments were performed with step and ramp changes in superficial velocities both for increase and decrease as mentioned in Sl no 1 to 4 in the Table 6.1 above. The superficial velocities are measured with a compressed air flowmeter the outputs of which are fed into the data acquisition system. The changes in superficial velocity are manually regulated with a flow regulating valve attached to the inlet of the compressed air flowmeter. For stepped change the valve is changed from a lower to a higher

value or vice versa instantaneously. For ramped change this is done gradually over a period of approximately 4 minutes or more. The results of these experiments are given in the following figures. From Fig. 6.4 it is seen that with a ramped increase in superficial velocity from 5 Nm^3/hr to 15 Nm^3/hr in about 300 seconds, the heat recovery also increases from a value of around 0.185 kW to around 0.21 kW but after a delay of about 500 seconds. The increase in heat recovery may be due to increase in the temperature in the cyclone in the downcomer section as seen from Fig. 6.5. This may be due to the increased flow rate of the solid particles and its accumulation in the cyclone for a longer time with increased superficial velocity. The delay in the increase as compared to superficial velocity may be due to thermal lag of the wall of the spiral tube inside the heat exchanger and that of the water inside.

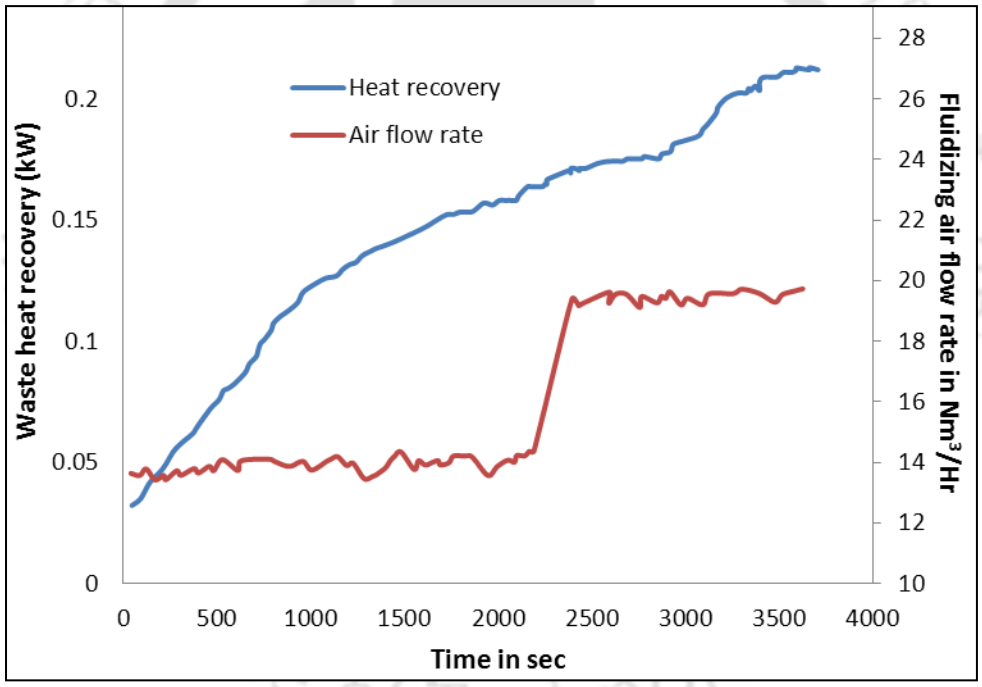

Fig. 6.4 Variation of heat recovery with ramped increase in superficial velocity

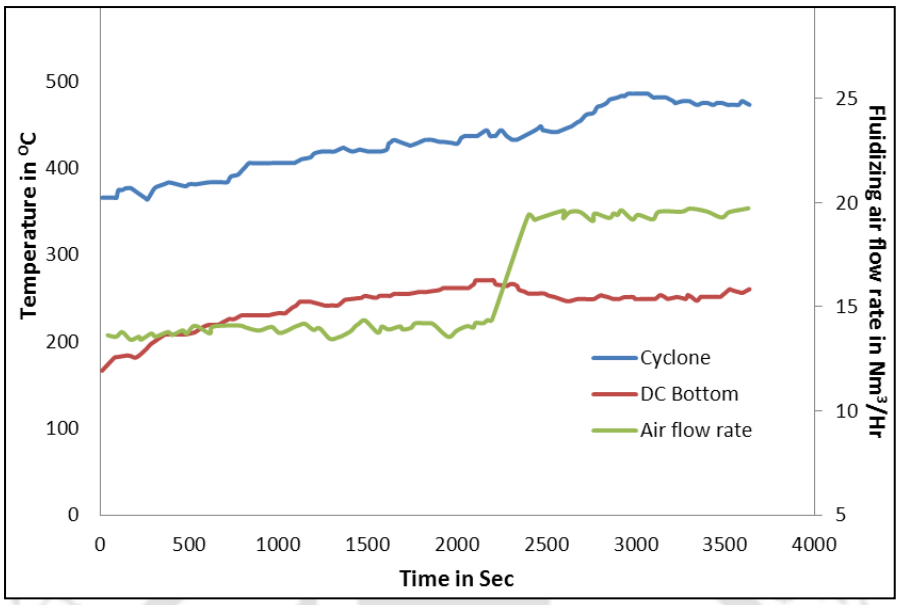

Fig.6.5 Variation of temperatures in the downcomer with ramped increase in superficial velocity

Fig. 6.6 shows the reverse of experiments mentioned above. It shows that with a ramped decrease in superficial velocity, the heat recovery graph also shows a decreasing trend from about 0.275 kw to around 0.225 kw almost at the same rate as that of the decreasing superficial velocity. The decrease in heat recovery may be due to decrease in the temperature in the cyclone in the downcomer section as seen from the Fig. 6.7. This may be due to the decreased flow rate of the solid particles and its accumulation in the cyclone for a shorter time with decreased superficial velocity.

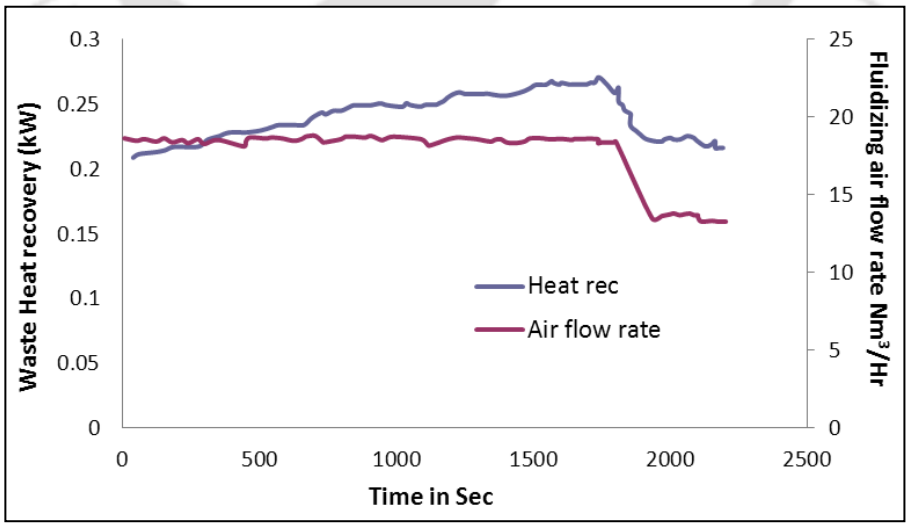

Fig. 6.6 Variation of heat recovery with ramped decrease in superficial velocity

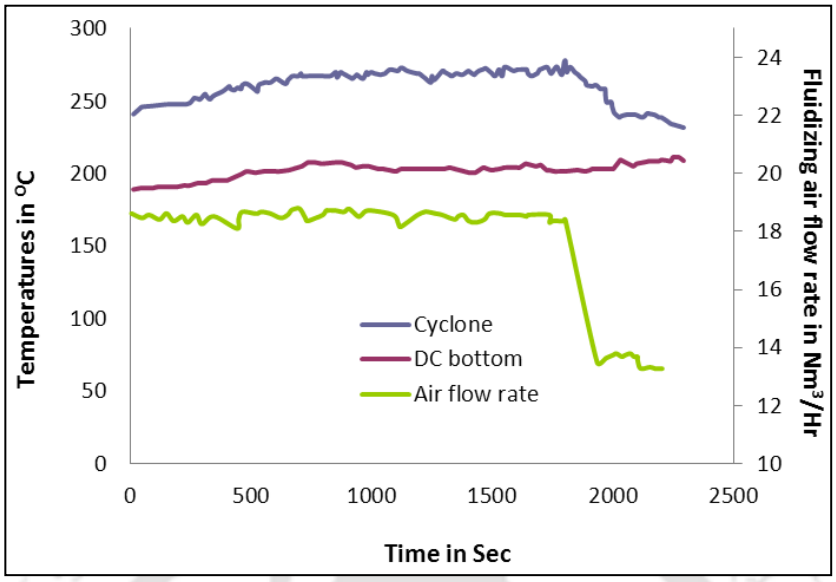

Fig. 6.7 Variation of temperatures in the downcomer with ramped decrease in superficial velocity

The following Figs. 6.8 to 6.11 shows the variations in heat recovery and temperatures in the downcomer section with stepped increase and stepped decrease in superficial velocity.

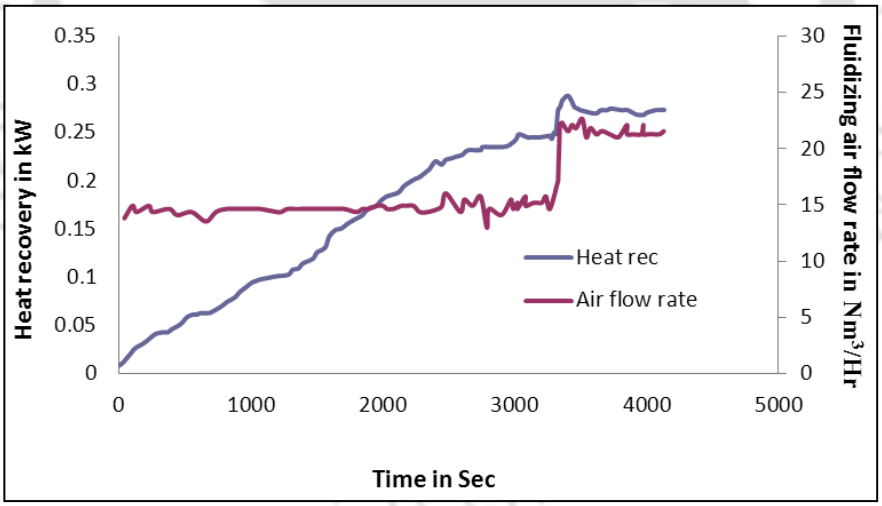

Fig. 6.8 Variation of heat recovery with stepped increase in superficial velocity

From the Fig. 6.8 it is seen that a sudden and instantaneous increase in superficial velocity results in a sudden rise in heat recovery from around 0.25 kw to almost 0.3 kw. The temperature in the cyclone is also seen to rise abruptly with the sudden increase in superficial velocity as seen from the Fig. 6.9. This may be due to the increase in flow rate of solid particles with the increase in superficial velocity. However, the temperature at the bottom of the downcomer shows a slight

decrease. This may be due to the fact that with increase in superficial velocity accumulation of hot solid particles is less at the bottom than at the upper regions and the cyclone.

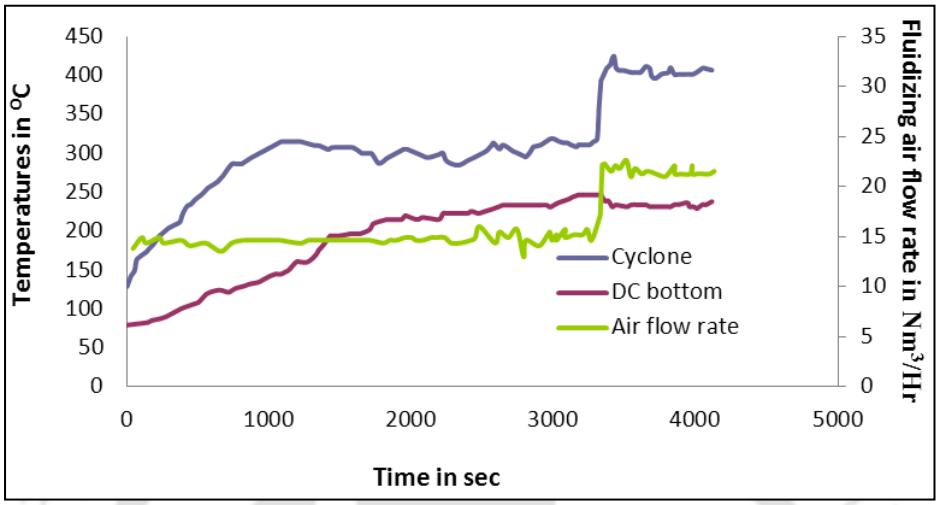

Fig. 6.9 Variation of temperatures in the downcomer with stepped increase in superficial velocity

Figs 6.10 and 6.11 shows the reverse case of the above where the sudden drop in superficial velocity from 20 to 13 Nm3/hr results in sudden drop in heat recovery from 0.3 to 0.215 kW and in cyclone temperature from around 320 to 270 °C. Here too exactly in a reverse phenomenon the temperature at the bottom of the downcomer rises slightly. This may be attributed to the reverse phenomenon as described in the case for sudden increase in superficial velocity.

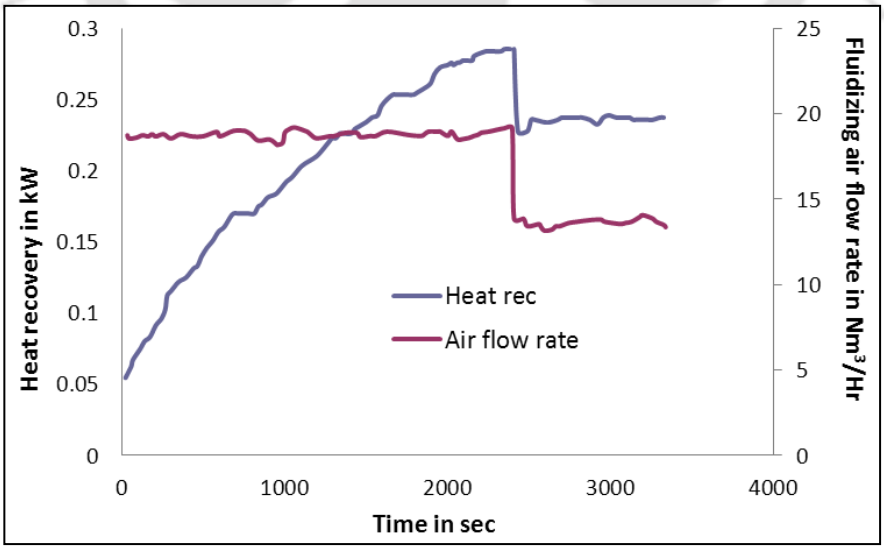

Fig. 6.10 Variation of heat recovery with stepped decrease in superficial velocity

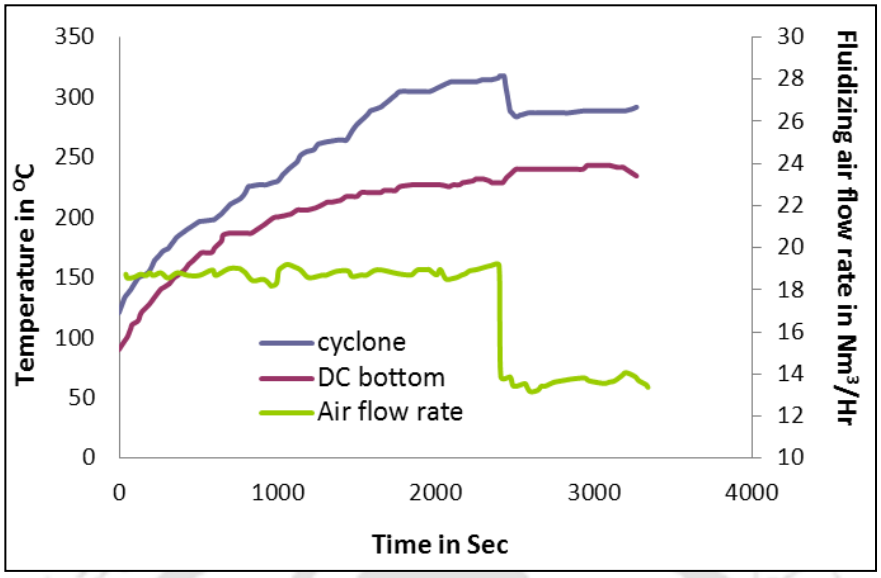

Fig. 6.11 Variation of temperatures in the downcomer section with stepped decrease in superficial velocity

6.3.2 TRANSIENT HEAT RECOVERY DURING SUDDEN CHANGES IN POWER INPUT

Four sets of experiments were performed with step and ramp changes in power input both for increase and decrease as mentioned in Sl no 5 to 8 in the Table 6.1 above. The power input are measured with a multifunction meter the outputs of which are fed into the data acquisition system. The changes in power are manually regulated with a variable autotransformer connected to the heating coil. For stepped change, the adjusting knob of the variable autotransformer is changed from a lower to a higher value or vice versa instantaneously. For ramped change this is done gradually over a period of approximately 4 minutes or more. The results of these experiments are given in the following figures.

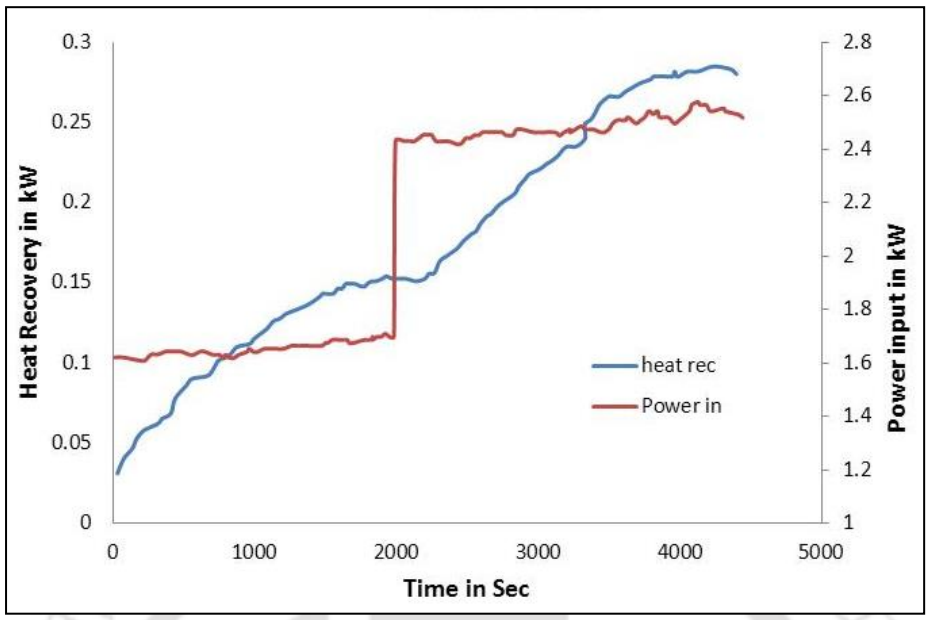

Fig. 6.12 Variation of heat recovery with stepped increase in power input

Figure 6.12 shows the variation of heat recovery with stepped increase in power input from 1.6 kW to 2.5 kW. It is seen that with a sudden abrupt change in input power the heat recovery also changes in an almost constant rate from 0.15 kW to around 0.28 kW. This change takes place in about 800 seconds after a slight delay of 100 seconds. It is obviously due to increase in power input. However, it is observed that the resultant increase in heat recovery is not instantaneous but takes place over a certain interval. This is due to the time taken for the whole system to achieve the steady state. The corresponding changes in the temperatures in the downcomer are shown in Fig. 6.13. The cyclone temperature is observed to change from 300 °C to 400 °C in about 1500 seconds. The temperature of the bottom of the downcomer is also observed to change from 160 °C to 200 °C within this period.

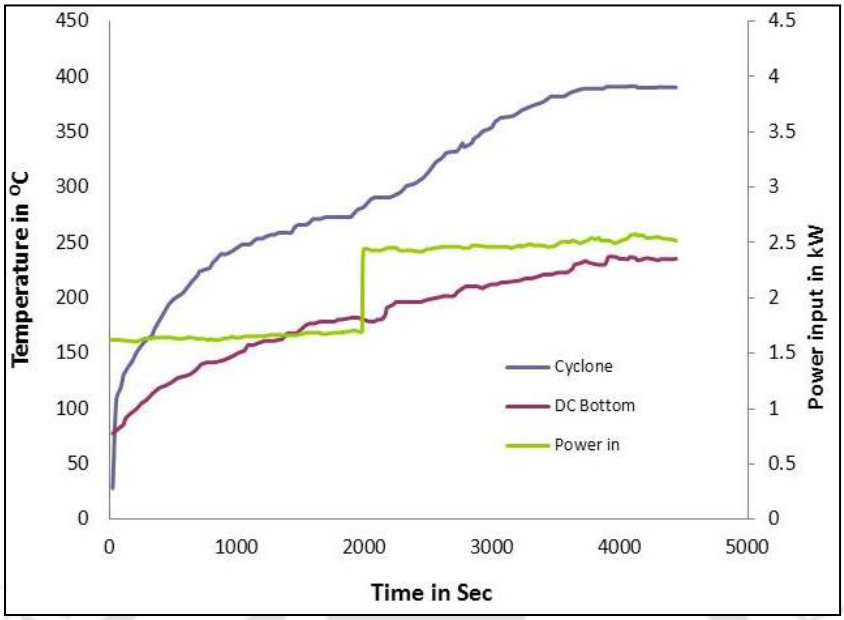

Fig. 6.13 Variation of temperatures in the downcomer with stepped increase in power input

Figure 6.14 shows the variation of heat recovery with stepped decrease in power input from 2.5 kW to 1.6 kW. It is seen that with a sudden abrupt decrease in input power the heat recovery also decreases in an almost constant rate from 0.31 kW to around 0.18 kW. This change takes place in about 1000 seconds which is more than that taken for the change to occur there was a stepped increase in power input. This increased time may be due to the thermal lag associated with the copper tube in the heat exchanger and the water. Here also it is observed that the resultant decrease in heat recovery is not instantaneous but takes place over a certain interval. This is due to the time taken for the whole system to achieve the steady state. The corresponding changes in the temperatures in the downcomer are shown in Fig. 6.17. The cyclone temperature is observed to change from 450°C to 280°C in about 1000 seconds. The temperature of the bottom of the downcomer is also observed to change from 250 °C to 200 °C within this period.

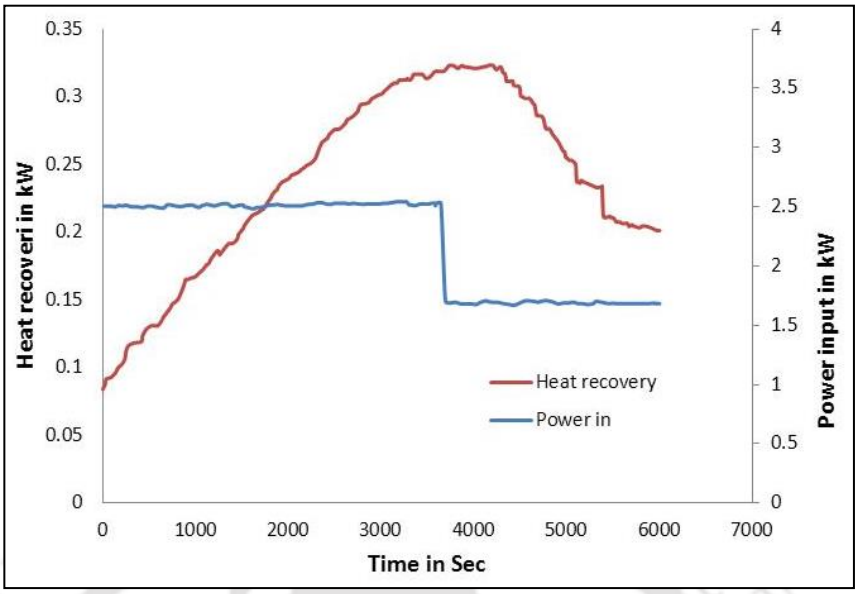

Fig. 6.14 Variation of heat recovery with stepped decrease in power input

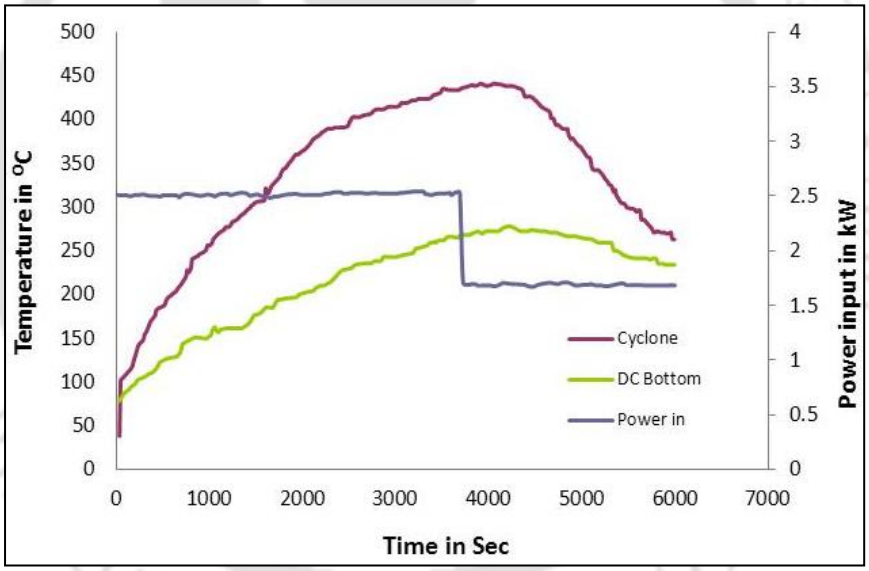

Fig. 6.15 Variation of temperatures in the downcomer with stepped decrease in power input

The variations in heat recovery and temperature of the downcomer with ramped changes in input power are shown in Figs. 6.16 to 6.19. It is observed that trends are similar to those in case of stepped changes in input power. But here the subsequent changes take place over a period of time which is significantly more than that of the experiments with stepped changes.

From Fig. 6.16 it is seen that with the ramped increase in heat input from 1.6 kW to 2.5 kW the heat recovery increases from 0.16 kW to 0.35 kw in almost 4000 seconds compared to 800 seconds as seen in Fig 6.14 when there was a stepped increase in power input. Moreover, there is also a delay of 200 seconds here

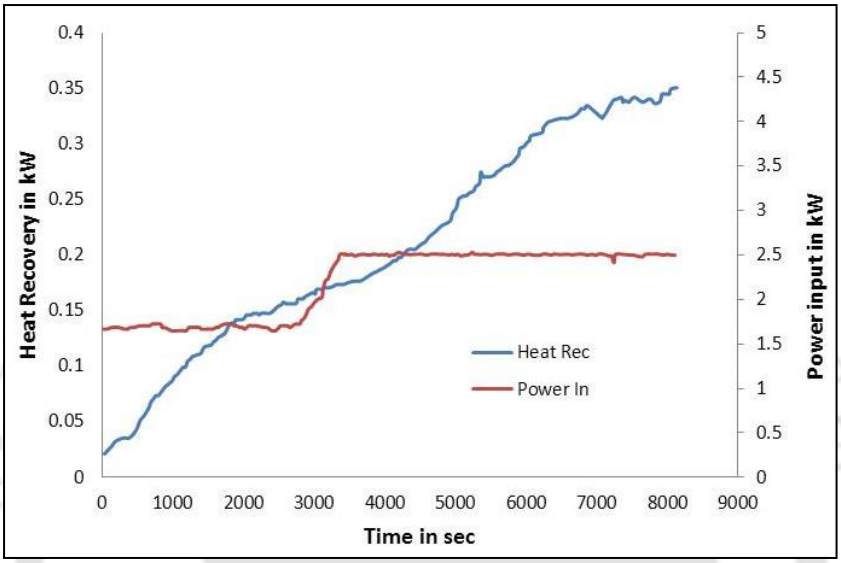

Fig. 6.16 Variation of heat recovery with ramped increase in power input

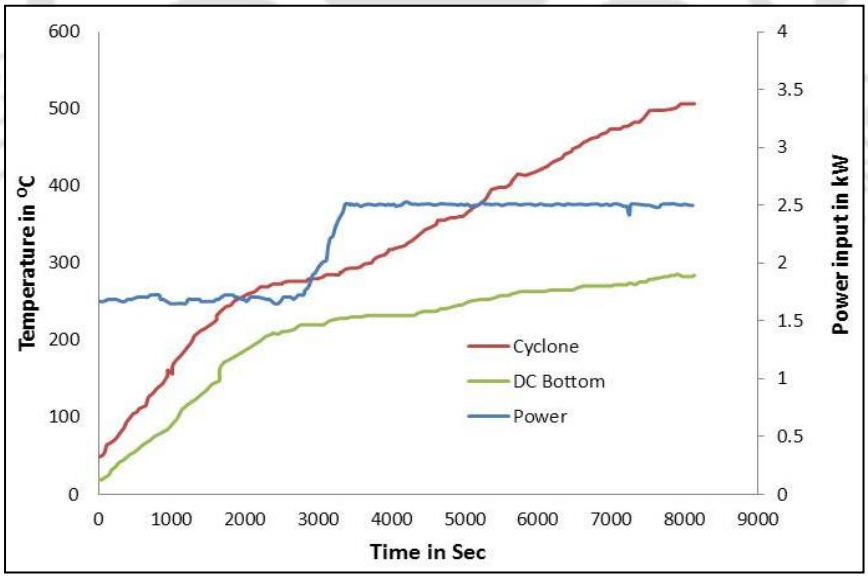

Fig. 6.17 Variation of temperatures in downcomer with ramped increase in power input

The variations in temperatures of the downcomer section with a ramped increase in power input are shown in Fig 6.17. Here also it is observed that the cyclone temperature rises from around 250 °C to 500 °C in about 2000 seconds where this time was 1000 second in case of stepped change in power input.

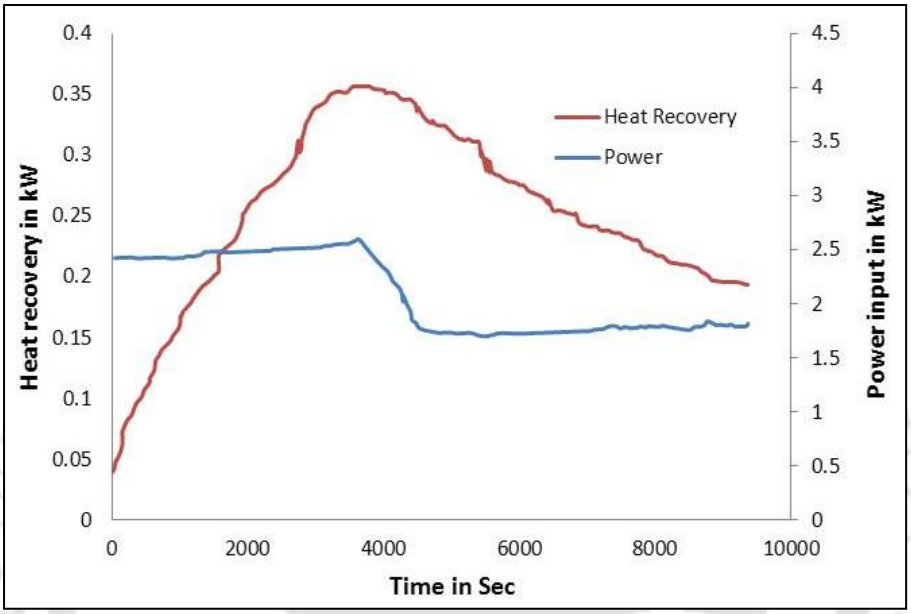

Fig. 6.18 Variation of heat recovery with ramped decrease in power input

The variations in heat recovery and temperatures of the downcomer section with the ramped decrease in power input are shown in Figs 6.18 and 6.19. From these figures it is observed that the variations are a reverse of those that occurred when the change was a ramped increase. It is observed that for a ramped decrease in power from 2.5 kW to 1.9 kW in about 500 seconds results in decrease in heat recovery from 0.35 kW to 0.2 kW in about 6500 seconds. The change in cyclone temperature takes place in about 4000 seconds from 430 to 270 °C ie 0.05 °C per second while the temperature at the bottom of the downcomer takes place at the rate of 0.0125 °C per second from 250 to 200 °C.

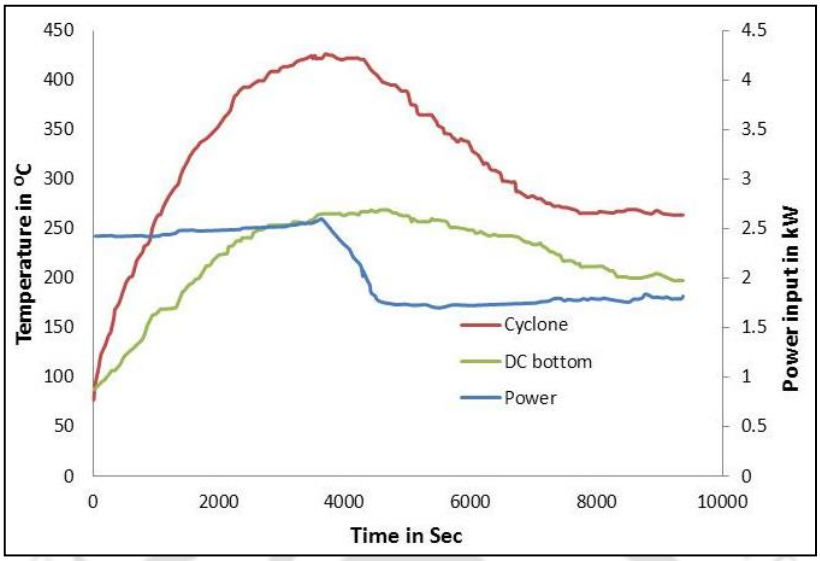

Fig. 6.19 Variation of temperatures in the downcomer with ramped decrease in power input

The response in output that takes place during the transients in input parameters are summarized in the Table 6.2 (a) Transient in airflow rates and (b) transient heat input

Table 6.2 (a) Summary of the results of transient heat recovery during transients in fluidizing air flow rates

Rate of change in Airflow rate as the transient input	**Resultant rate of change in heat recovery**	**Time for change in output to take effect**
0.005 per second increase	0.00005 kW/s	Delay of ~500 seconds
0.005 per second decrease	0.0000625 kW/s	Instantaneous
Instantaneous Increase	Instantaneous Increase	Instantaneous
Instantaneous decrease	Instantaneous decrease	Instantaneous

Table 6.2 (b) Summary of the results of transient heat recovery during transients in heat input

Rate of change in Heat input as the transient input	**Resultant rate of change in heat recovery**	**Time for change in output to take effect**
Instantaneous Increase	0.0001625 kW/s increase	Delay of ~100 seconds
Instantaneous decrease	0.00013 kW/s decrease	Delay of ~100 seconds
0.0018 kW/s increase	0.0000475 kW/s increase	Delay of ~200 seconds
0.0018 kW/s decrease	0.000023 kW/s decrease	Delay of ~200 seconds

6.4 SUMMARY OF THE CHAPTER

Heat recovery from the downcomer of a PCFB under steady state and transient conditions were investigated using two different types of heat exchanger viz water jacket type heat exchanger and spiral tube type heat exchanger where the later was observed to be more efficient.

Steady state heat recovered from the downcomer section with a water jacked type heat exchanger fitted with fins was found to be 119 W for a superficial velocity of 2.4 m/s and inventory of 500g sand. Power input was 2.25 kW and the amount of heat recovered from the downcomer section with a spiral tube type heat exchanger was found to be of the order of 284 W for the same operating parameters. The transient experiments showed that sudden (stepped) and slow (ramped) changes in superficial velocity and power input results in corresponding changes in the heat recovery subsequent to changes in temperatures at the top and bottom of the downcomer section. The following chapter gives a detailed conclusion of the transients studies carried on a PCFB and along with heat recovery from the downcomer

Chapter – 7

CONCLUSIONS AND SCOPE FOR FUTURE WORK

7.1 CONCLUSION

The transient bed hydrodynamic behaviour along with the transient heat transfer and temperature profiles for both the bed and riser surface were investigated for various input transient conditions like operating pressure, exhaust flow rates, superficial velocity and input heat flux in a pressurized circulating bed. Experiments were also conducted to investigate the heat recovery from the downcomer section. A PCFB unit with height of 2.0 m and inner diameter of 54 mm was fabricated for the purpose. The investigations were conducted for coal blended with sand with 0%, 2.5%. 10%, 12.5% and 20% (W/W) as bed material. Compressed air supplied from a compressor was used for generating the fluidizing air. The heat recovery was done using two different types of heat exchangers viz water jacket type heat exchanger and spiral tube type heat exchanger. These heat exchangers were attached to the downcomer and water was used as the heat recovering fluid from the core of the downcomer. For first sets of experiments involving the upper splash region of the bed, the heating was done by wrapping kanthal heating coils over the upper splash region of the riser covering a length of 600 mm of the riser surface at a height of 1400 mm from the distributor plate. The heating for the second set of experiments involving the riser was achieved by using a tubular furnace of length 810 mm connected to the inlet of the PCFB just after the compressor. The air was heated before entering the PCFB. The transient in input heat flux was introduced by using an auto-transformer attached to the heater circuit which was used to regulate the input voltage. The transients in the superficial velocities were introduced by using a flow control valve attached to the inlet of fluidizing air at the bottom of the distributor plate whereas the transients in the operating pressure were introduced with the aid of a pressure regulator attached to the compressor. Moreover, another flow regulating valve was attached to the outlet of the exhaust gas at the top of the cyclone separator to achieve the transients in the exhaust flow rates. Finally, the FFT analysis of all the data were carried out. The response of the output parameters like temperature and heat transfer coefficient to the input transients was also analyzed.

7.1.1 CONCLUSIONS OF TRANSIENT HYDRODYNAMIC STUDIES

- Drastic output changes in voidages values at the upper regions of 104.25 cm and 159 cm are seen where the voidages change by about 48% from an average value of around 0.64 to an average value of about 0.95 as a result of input transients in the form of decrease in exhaust flow rate
- The output changes in voidage resulting from an input transient in the form of decrease in exhaust flow rate was observed to be insignificant in the lower portion of the bed as the transient introduced is far away from the lower region at the exhaust of the cyclone.
- The change in output pattern follows the same pattern as the input transient which can be thus interpreted as a first order response in the upper region of the riser.
- Reverse trend in the output changes in voidages is observed for an input transient in the form of a sudden increase in exhaust flow rate.
- Drastic output changes in voidages values at the upper regions of 191, 159, 104.25 and 80 cm are observed where the output voidage changes by about 5%, 30%, 28% and 16% respectively from values of 0.85, 0.98, 0.98 and 0.9 respectively to values of 0.8, 0.68, 0.7 and 0.75 respectively as a result of input transients in the form of decrease in operating pressure.
- The output changes in voidage resulting from an input transient in the form of decrease in operating pressure was observed to be insignificant in the lower portion of the bed may be due to the fact that the reduction in pressure results in a decrease in pressure drop along the riser which is enough to carry the solid particles to the upper region and less solid beyond that to the cyclone and downcomer resulting in increased solid concentration at the upper regions and decrease in voidage.
- The output changes in voidages follow the similar pattern as the input transient in operating pressure.
- It is observed that the voidage for all the percentage blends are lower near the bottom of the riser. The voidage values at this particular location decreases with increasing percentage blend of coal. This may be due to the increase in weight of inventory with increasing percentage of coal which require higher force to overcome the weight of the bed.

- The phase vs frequency graph obtained from FFT analysis of the voidage profiles shows a variation in phases which may be a result of the continous fluctuations in the voidage values. A sharp spike observed in the phase variation with frequency for the voidage a higher region may be a representation of the sudden change in the voidage with the sudden change in exhaust flow rate value

7.1.2. CONCLUSION OF THE TRANSIENT HEAT TRANSFER EXPERIMENTS ON THE UPPER SPLASH REGION

- Transient graphs shows steady state to be reached within 5000 seconds from startup for airflow of 5.1l/s and heat flux of 1.5kw/m^2 and 2kw/m^2 for all the percentage blends
- Heat transfer coefficient increases along the height of the heat transfer probe. Similar trends have been observed by Kalita *et al*. (2013). The maximum value being 22 W/m^2K at a height of 1.8 m and 19 W/m^2K at a height of 1.4 m for airflow of 5.1l/s, 500g sand and heat flux of 1.5kw/m^2. It is thus observed that the HTC is 15% higher at the topmost region than at the bottom region of the heat transfer probe.
- The higher heat transfer near the riser exit may be due to an increase in solid concentration near the exit as the drag force acting on the bed material lifts the particles to the top zone.
- Bed temperature is more near the riser wall than at the core by about 142% .Similar observations were made by P. Kalita *et al*. (2013). This is probably due to the presence of higher concentration of larger particle clusters near the wall of the riser
- Sand with coal blends of 12.5% blend and 2.5% blend has a 9% better heat transfer coefficient than the pure sand and 20% sand.
- Heat transfer coefficient increases by about 11% with increased heat flux from 1.5 kW/m^2 to 2 kW/m^2.
- The average range or temperature drop is around 10°C when the air flow rate is increased from 5.1 l/s to 6.6 l/s with a heat flux of 1.5 kW/m.
- Heat transfer coefficient suddenly decrease and then increase steadily to a higher value when airflow rate is suddenly increased and vice versa

- Sudden increase in flowrate of the fluidizing air from 5.1 l/s to 6.6 l/s with a heat flux of 1.5 kW/m results in a sudden decrease in the heat transfer coefficient for a few seconds from a value of around 35 to 30 W/m^2K to and than a steady increase to a higher value of around 40 W/m^2K at the height of 1.8 m from DP. Similar changes occur at other eegions also.
- The same trend as above is observed in a reversed order for sudden decrease in flow rate of fluidizing air from 5.1 to 3.0 l/s.

7.1.3 CONCLUSION OF TRANSIENT HEAT TRANSFER EXPERIMENTS ON THE RISER COLUMN

- Transient graphs shows steady state to be reached within 2000 seconds from startup for airflow of 5.1 l/s and heat flux of 10.717 kw/m^2 and within 3000 seconds for 8.0382 kw/m^2.
- Heat transfer coefficient is observed to be highest with an average value of around 3 kW/m^2K just near the distributor plate because of its proximity to the heater at an operatin pressure of 2 bar, superficial air flow rate of 5.1 l/s and input heat of 0.9 to 1.2 kW.
- It is observed that both the bed and surface temperature show an increase with sudden increase in power as a transient input from 0.9 to 1 kW until they reach a subsequent steady state with an increased temperature varying from 50 to 20% higher at different heights from DP.
- HTC was found to be 1.5 kW/m^2K at a height of 70 cm and around 0.6 kW/m^2K at 98 and 182 cm heights. For a input transien of sudden power increase from 0.9 to 1 kW, it is observed that the heat transfer coefficient instantaneously increases by about 20 to 50% at different heights from DP but again reduces to the earlier value.Subsequently it again shows a rise by about 20%.
- The trend is just a reverse for an input transient of sudden decrease in power.
- HTC is observed to show a momentous sharp rise varying from 10 to 20% at different heights from DP with sudden decrease in the exhaust flow rate as the transient input

which later decreases steadily and vice versa.This instaneous sharp increase of decrease is of the order of around 15 w/m^2K.

- Experiments with increased bed inventory weight showed that the HTC slightly increases with 100g increase in bed material.
- With a sudden drop in operating pressureas the transient input, the HTC is observed to show a momentous increase in value varying from 50 to 20% and subsequently a steady decrease to the earlier value. The reverse trend is observed for a sudden increase in operating pressure as the transient input.
- Analysis of data through FFT was done. It was found that the signals were monotonic signals and no phase shift was observed. The response of the output parameters like temperature and heat transfer coefficient to the input transients was also analysed and it was found that the response follows that of a zero order instrument.

7.1.4 CONCLUSION OF HEAT RECOVERY EXPERIMENTS

- Amount of heat recovered during steady state from the downcomer section with a (a) water jacked type heat exchanger fitted with fins and (b) spiral tube type heat exchanger was found to be 119 W and 284 respectively for a superficial velocity of 2.4 m/s and inventory of 500 g sand. Power input was 2.25 kW. The temperatures at the top and bottom of the downcomer section was found to be approximately 420 °C and 350 °C respectively
- Sudden (stepped) and slow (ramped) changes in superficial velocity and power input results in corresponding changes in the heat recovery subsequent to changes in temperatures at the top and bottom of the downcomer section.
- With a ramped increase in superficial velocity from 5 Nm^3/hr to 15 Nm^3/hr in about 300 seconds, the heat recovery also increases from a value of around 0.185 kW to around 0.21 kW but after a delay of about 500 seconds.
- with a ramped decrease in superficial velocity, the heat recovery graph also shows a decreasing trend from about 0.275 kW to around 2.25 kW almost at the same rate as that of the decreasing superficial velocity.

- In case of stepped changes it was observed that a sudden and instantaneous increase in superficial velocity results in a sudden rise in heat recovery from around 0.25 kW to almost 0.3 kW.
- Variation of heat recovery with stepped decrease in power input from 2.5 kW to 1.6kW showed that with a sudden abrupt decrease in input power the heat recovery also decreases in an almost constant rate from 0.31 kW to around 0.18 kW. This change takes place in about 1000 seconds.
- The variation of heat recovery with stepped increase in power input from 1.6kW to 2.5 kW showed that with a sudden abrupt change in input power the heat recovery also changes in an almost constant rate from 0.15 kW to around 2.8 kW. This change takes place in about 800 seconds.

7.2 SCOPE FOR FUTURE WORK

The present work was a pure experimental one performed on a laboratory scale set up. The transient hydrodynamic and heat transfer behaviour of the PCFB were investigated experimentally. The important findings have been highlighted in chapters 4 and 5. However there are lots of scopes for further research which are discussed below

- **Transient Studies in a Scaled up Set Up**. The transient studies can be repeated in a bigger and a realistic set up with higher heat flux and bed inventories. Moreover, this study can be extended by applying various biomass as bed inventories.
- **Simulation of Transient PCFB experiments.** Modelling and simulation works can be taken up using the datas available in the present studies.
- **Transient studies for higher temperatures**. The present study was limited to heat transfer studies only at a comparatively low temperature range. As such there is much scope for extensive transient studies at higher temperature for combustion and gasification processes.
- **Improvement of the device for measurement of solid mass flux.** The measurement of solid mass flux during the continuous run of the experiments is a challenge speacially at higher temperatures. There is thus a very good scope for designing a device for measuring the solid mass flux by using some type of photo sensitive device or infra red device.

REFERENCES

Abdelmotalib, H. M., Ko, D. G., and Im, I. T., 2016. A study on wall-to-bed heat transfer in a conical fluidized bed combustor. *Applied Thermal Engineering*, 99, pp. 928–937.

Abdullah, M. Z., Husain, Z. and Ying Pong, S. L., 2003. Analysis of cold flow fluidization test result for various biomass fuels. ***Biomass and Bioenergy*, 24(6), pp. 487-494.**

Anderson, B. A. and Leckner, B., 1993**.** Local lateral distribution of heat transfer on tube surface of membrane wall in CFB boilers. *Proceedings of the fourth International conference on circulating fluidized beds, Hidden Valley, Pennsylvania, USA*, pp. 368-373.

Anthony, E.J., (1995). *Pressurized Fluidized Bed Combustion*, Blackie Academic & Professional, Glasgow.

Barletta M., 2009. Progress in abrasive fluidized bed machining. *Journal of Materials Processing Technology*, 209, pp.6087–6102

Baskakov, A. P., Munts, V. A. and Pavlyuk, E. Y., 2013. Transients in a Circulating Fluidized Bed Boiler. *Thermal Engineering*, 60 (11), pp.775–782.

Basu, P. and Nag, P. K., 1987. An investigation into heat transfer in circulating fluidized beds. *International Journal of Heat and Mass Transfer*, 30 (11), pp. 2399-409.

Basu, P., 1990**.** Heat transfer in high temperature fast fluidized beds. *Chemical. Engineering Science*, 45 (10), pp.3123-3136

Basu, P., Lawrence, D., Ali, M. N. and Nag, P. K., 1991. An experimental investigation into the effect of fins on heat transfer in circulating fluidized beds. *International Journal of Heat Mass Transfer,* 34 (9), pp. 2317-2326

Basu, P. and Leming, C., 1996. Heat transfer in a pressurized circulating fluidized bed. *International Journal of Heat and Mass Transfer*, 39 (13), pp.2711-2722.

Basu, P. (2006). *Combustion and Gasification in Fluidized beds*. Taylor and Francis (CRC Press). UK,

Bodelin, P., Molodtsof, Y. and Delebarre, A., 1993. Flow structure investigations in a CFB, *Proceedings of the fourth International conference on circulating fluidized beds, Hidden Valley, Pennsylvania*, pp. 151-156.

Brerton, C., and Grace, J., 1992. The transition to turbulent fluidization. *Chemical engineering research and design*, 70 (92), pp.246-251

Bricout, V. and Louge, M. Y., 2004. Measurements of cyclone performance under conditions analogous to pressurized circulating & fluidization. *Chemical Engineering Science*, 59, pp.3059 – 3070

Brown, S. L. and Lattimer, B. Y., 2013. Transient gas-to-particle heat transfer measurements in a spouted bed. *Experimental Thermal and Fluid Science*, 44, pp.883–892.

Bruce, J., Milne, Berruti, F., Leo, A., Theo, J. W., 1993. The hydrodynamics of the internally circulating fluidized bed at high temperature. *Proceedings of the fourth International conference on circulating fluidized beds, Hidden Valley, Pennsylvania, USA*, pp.29-34.

Chen, H. and Li, H., 2004**.** Characterization of a high-density downer reactor. *Powder Technology*, 146, pp.84–92

Cheng, L. and Basu, P., 1999. Effect of pressure on loop seal operation for a pressurized circulating fluidized bed. *Powder Technology*, 103, pp.203–211.

Crane, R., Barbaris, L. N. and Behrouzi, P., 1992. Particulate behaviour in cyclone separators with secondary gas extraction. *Journal of Aerosol Sci.* 23 (1), pp.765-S768

Dai, d., Zhou, Y. and Liu, J., 2011. Liquid metal based thermoelectric generation system for waste heat recovery. *Renewable Energy*, 36, pp.3530-3536

Demir, M. E. and Dincer, I., 2017. Performance assessment of a thermoelectric generator applied to waste heat recovery. *Applied Thermal Engineering*, 120, pp.694-707.

Dewil, R., Baeyens, J., and Caerts, B., 2008. CFB cyclones at high temperature: Operational results and design assessment. *Particuology*, 6, pp.149–156.

Dolz, V., Novella, R., García, A. and Sánchez J., 2012. HD Diesel engine equipped with a bottoming Rankine cycle as a waste heat recovery system. Part 1: Study and analysis of the waste heat energy. *Applied Thermal Engineering*, 36, pp.269-278.

Ebert, T. A., Glicksman, L. R. and Lints, M., 1993**.** Determination of particle and gas convective heat transfer component in circulating fluidized bed. *Chemical*. *Engineering Science*. 48, pp.2179-2188

Ehsani, M., Movahedirad, S. and Shahhosseini S., 2016. The effect of particle properties on the heat transfer characteristics of a liquid-solid fluidized bed heat exchanger. *International Journal of Thermal Sciences*, 102, pp.111–121.

Elsayed, K. and Lacor, C., 2012**.** The effect of the dust outlet geometry on the performance and hydrodynamics of gas cyclones. *Computers & Fluids*, 68, pp.134–147

Eriksson, M. and Golriz, M. R., 2005. Radiation heat transfer in circulating fluidized bed combustors. *International journal of Thermal Sciences,* 44, pp.399-409.

Fattahi, M., Hosseini, S. H., and Ahmadi, G., 2015. CFD simulation of transient gas to particle heat transfer for fluidized and spouted regimes. *Applied Thermal Engineering*, 105, pp.1–12.

Fu, J., Liu, J., Ren, C., Wang, L., Deng, B. and Xu, Z., 2012. An open steam power cycle used for IC engine exhaust gas energy recovery. *Energy,* 44, pp.544-554

Geldart D., 1973.Types of gas fluidization**.** *Powder technology*, 7 (5), pp.285=292.

Gnanapragasam, N. V. and Reddy, B. V., 2008**.** Numerical modeling of bed-to-wall heat transfer in a circulating fluidized bed combustor based on cluster energy balance. *Int. J. Heat Mass Transfer*, 51, pp.5260-5268

Grace, J.R. (1986). Heat transfer in circulating fluidized beds, Basu, P. (Ed.), *Circulating Fluidized Bed Technology*. Pergamon, Canada. pp. 63-81.

Grace, J.R., 1986**.** Contacting modes and behavior classification ofgas-solid and other two-phase suspensions. *The Canadian journal of chemical engineering*, 64(3), pp. 353-363.

Grace J R., 2000. Reflections on turbulent fuidization and dense suspension upflow, *Powder technology*, 113 (3), pp. 242-248.

Gupta, A.V.S.S.K.S., and Nag, P.K., 2002. Bed-to-wall heat transfer behavior in a pressurized circulating fluidized bed. *International Journal of Heat and Mass Transfer*, 45, pp.3429–3436.

Hamada, M., Abdelmotalib, A., Mahmoud, A.M., Youssef, B., Ali, A., Hassan, B., Suk Bum Youn, C. and Ik-Tae, Im., 2015**.** Heat transfer process in gas–solid fluidized bed combustors: A review. *International Journal of Heat and Mass Transfer*, 89, pp. 567–575.

He, M., Zhang, X., Zeng, K. and Gao, K., 2011. A combined thermodynamic cycle used for waste heat recovery of internal combustion engine. *Energy,* 36, pp.6821-6829.

Huang, Y., Turton, R, Park, J., Famouri P. and Boyle, E. J., Dynamic model of the riser in circulating fluidized bed. *Powder Technology*. 163 pp. 23–31.

Izquierdo-Barrientos, M. A., Sobrino, C. and Almendros-Ibáñez, J. A., 2015. Experimental heat transfer coefficients between a surface and fixed and fluidized beds with PCM. *Applied Thermal Engineering*, 78, pp.373–379.

Jain, R., Dandotiya, D. and Jain, A., 2013. Performance Improvement of a Boiler through Waste Heat Recovery from an Air Conditioning Unit. *International Journal of Innovative Research in Science, Engineering and Technology*, 2, pp. 43-49

Jiang, P., Cai, P. and Fan, L., 1993. Transient behavior in fast fluidization. *Proceedings of the fourth International conference on circulating fluidized beds, Hidden Valley, Pennsylvania, USA*, pp. 143-150.

Jiang, Y., Chen, Z., Shao, H., Zhao, Y., Luo, Z., Tan, M. and Hong, P., 2016. The Effect of a Porous Medium on Fluidization Characteristics in Air Dense Medium Fluidized Bed. *Powder Technology*, 301, pp.1227–1234.

Kalita, P., Saha, U. K. and Mahanta, P., 2013a. Effect of biomass blending on hydrodynamics and heat transfer behavoiur in a pressurized circulating fluidized bed unit, *International Journal of Heat and Mass Transfer*, 60,pp.531–541

Kalita, P., Mahanta, P. and Saha U. K., 2013b. Some studies on wall-to-bed heat transfer in a pressurized circulating fluidized bed unit. *Procedia Engineering, 56*,pp. 163–172.

Kalita, P., Saha, U. K. and Mahanta, P., 2013c. Parametric study on the hydrodynamics and heat transfer along the riser of a pressurized circulating fluidized bed unit. *Experimental Thermal and Fluid Science*, 44, pp.620–630.

Kalita, P., Mahanta, P. and Saha, U. K., 2014. Study of bed-to-wall heat transfer with twisted tape at the upper splash region of a pressurized circulating fluidized bed unit. *International Journal of Heat and Mass Transfer*,78, pp.260–266.

Klimanek, A., and Bigda, J., 2018. CFD modelling of CO_2 enhanced gasification of coal in a pressurized circulating bed reactor. *Energy*, 160, pp. 710-719

Kolar, A. K. and Sundaresan, R., 2002. Heat transfer characteristics at an axial tube in a circulating fluidized bed riser. *Int. J. Therm. Sci*, 41, pp. 673–681.

Koornneef, J., Junginger, M. and Faaij, A., 2007**.** Development of fluidized bed combustion—An overview of trends, performance and cost. *Progress in Energy and Combustion Science*, 33, pp.19–55

Kunii, D., and Levenspiel, O., (2005). *Fluidization Engineering*. Elsevier, 2nd Edition, New Delhi, India.

Langan, M. and O'Toole, K., 2017. A new technology for cost effective low grade waste heat recovery. *Proceedings of the 1st International Conference on Sustainable Energy and Resource use in Food Chains, ICSEF, Berkshire, UK*. PP. 19-20

Lewnard, J. J., Herb, B. E. and Tsao T. R., 1993. Effect of design and operating parameters on cyclone performance for circulating fluidized bed boilers. *Proceedings of the fourth International conference on circulating fluidized beds, Hidden Valley, Pennsylvania, USA,* pp.*636-641.*

Li, Z., Van Sint Annaland, M., Kuipers, J. A M. and Deen N. G., 2016. Effect of superficial gas velocity on the particle temperature distribution in a fluidized bed with heat production. *Chemical Engineering Science*, 140, pp.279–290.

Liang-Chen W., 2014. Analysis of the reusability of the energy of the exhaust gas from the calciner for the production of carbon. *Int.J. Energy Science Direct Energy*, 78, pp. 439-450

Li, Y. and Kwuak, M. (1980). *Fluidization III,* Grace J. R. and Masten J. M., (eds), Plenum, New york

Li, Y., Lu, Y., Wang, F., Han, K., Mi, W., Chen, X. and Wang P., 1997. Behavior of gas-solid flow in the downcomer of a circulating fluidized bed reactor with a V-valve. *Powder Technology*, 91, pp.I 1-16

Liu, M. Y., Leng, W. and Qiang, A., 2008**.** Transient aspects of inner wall temperatures at different spatial positions in fluidized bed evaporators. *Chemical Engineering and Processing*,47, pp.2066–2075.

Loganathan, L. and Sivakumar, P., 2013**.** Waste heat recovery steam generator in sponge iron plant, T*he SIJ Transactions on Industrial, Financial & Business Management*,1, pp.23-28.

Mahalingam, M. and Kolar A. K., 1993. Experimental correlation for average heat transfer coefficient at the wall of a circulating fluidized bed. *Proceedings of the fourth International conference on circulating fluidized beds, Hidden Valley, Pennsylvania, USA,* pp. 390-395

Matsuda, S., 2008. Measurement of solid circulation rate in a circulating fluidized bed. *Powder Technology*, 187, pp.200–204.

Maurya, S. K., Awasthi, S., 2014. Waste Heat Recovery: An Analytical Study Of Combined Ejector And Vapour Compression Refrigeration System. *International Journal of Engineering Sciences & Research Technology,* 3, pp.1422-1425.

Molems, O. and Gliuckler, M., 1996**.** Development of a cyclone separator with new design. *Powder Technology*, 86, pp.37-40.

Molerus, O., 1993**.** Arguments on heat transfer in gas fluidized beds. *Chemical Engineering Science,* 48, pp.761-770.

Nag, P. K. and Ali, M. S., 1993. An experimental study of the effect of fins on heat transfer in a high temperature circulating fluidized bed. *Proceedings of the fourth International conference on circulating fluidized beds. Hidden Valley, Pennsylvania, USA*, pp.362-367.

Nag, P. K. (2001). *Power Plant Engineering*. 2nd Edition, McGrow Hill Publication Company Pvt. Ltd., New Delhi, India,

Naik, D. and **Neeharika**., 2012. Waste heat to power systems. *US Environmental Protection Agency*.

Narayanana, K. V. and Natarajan, E., 2007**.** Experimental studies on co-firing of coal and biomass blends in India. *Renewable Energy,* 32, pp.2548–2558.

Negash, A., Kim, Y. M., Shin, D. G. and Cho, G. B., 2018. Optimization of Organic Rankine cycle used for waste heat recovery of construction equipment engine with additional waste heat of hydraulic cooler. *Energy*, 143, pp.797-811.

Ouyang, S., Li, X. G., Davies, G. and Potter, O. E., 1996. Heat transfer between a vertical tube bundle and fine particles in a CFB downcomer with and without circulation of solids. *Chemical Engineering and processing*. 35, pp. 21-27.

Pandiyarajan, V., Pandian, M. C., Malan, E., Velraj, R. and Seeniraj R. V., 2011. Experimental investigation on heat recovery from diesel engine exhaust using finned shell and tube heat exchanger and thermal storage system. *Applied Energy*, 88, pp.77–87

Park, C. K. and Basu, P., 1997. A model for transient response to the change of fuel feed rate to a circulating fluidized bed furnace. *Chemical Engineering Science,* 52 (20), pp.3499- 3509.

Perales, J. F., Coll, T., Llop, M. and Puigjaner, L.,(1991). **'**On transition from bubbling to fast fluidization regimes', in Basu, P., Hasatani, M. and Hario, M.(Eds.), *Circulating Fluidized Bed Technology, vol. III*, Pergamon, New York, pp. 73-78.

Pitié, F., Zhao, C.Y., Baeyens, J., Degrève, J. and Zhang, H.L., 2013**.** Circulating fluidized bed heat recovery/storage and its potential to use coated phase-change-material (PCM) particles, *Applied Energy*, 109, pp.505-513

Plasynski, S., Klinzing, G. and Mathur M., 1994. High pressure vertical pneumatic transport investigation. *Powder Technol*. 79, pp. 95–109.

Qi, X. B., Zhang, H. and Zhu, J., 2008**.** Friction between gas–solid flow and circulating fluidized bed downer wall. *Chemical Engineering Journal*, 142, pp.318–326.

Reddy, B.V. and Basu, P., 2001. A model for heat transfer in a pressurized circulating fluidized bed furnace. *International Journal of Heat and Mass Transfer*, 44, pp. 2877-2887

Reddy, B.V. and Basu, P., 2002**.** Estimation of the Effect of System Pressure and CO_2 Concentration on Radiation Heat Transfer in a Pressurized Circulating Fluidized Bed Combustor. *Institution Of Chemical Engineers*, 80(A), pp.178-182.

Reddy, C. C. S., Naidu, S. V. and Rangaiah, G. P., 2013. Waste heat recovery methods and technologies. *Chemical Engineering*, 120, pp.28-38.

Reddy, S.B.K. and Knowlton, T.M., 1996. The effect of pressure on CFB riser hydrodynamics. *Proceedings of the 5th International Conference on CFB, Beijing, DB15 CFB V preprints*.

Richtberg, M., Richter, R. and Wirth, K.E., 2005. Characterization of the flow patterns in a pressurized circulating fluidized bed. *Powder Technology*, 155, pp.145-152.

Rietema, K. and Hoebink, J., 1977. Transient phenomenon in fluidized beds when switching the fluidizing agent from one gas to another. *Powder Technology*. 18(5), pp.257 – 265.

Riyadh, S. and Turaihi, A., 2012. Transient thermal behavior of a fluidized column. *The Iraqi journal for mechanical and materials engineering*, 12 (1), pp.814-828.

Rodriguez, O. H. M., Pecora, A. A. B., and Bizzo, W. A., 2002. Heat recovery from hot solid particles in a shallow fluidized bed. *Applied thermal Engineering*, 22, pp.145-160.

Roy, J. P., Mishra, M. K. and Misra, A., 2010. Parametric optimization and performance analysis of a waste heat recovery system using Organic Rankine heat Cycle. Energy, 35, pp.5049-5062

Rusheljuk., 2006. Heat transfer in circulating fluidized bed. *Doctoral school of energy and geotechnology*, Tallinn University of technology, Kuressaare, pp. 16–21.

Saidawat, Y., 2015. Power Generation from Waste Heat Extracted Through Clinker Production in Cement Industry. *International Journal in IT and Engineering*, 03, pp.23-33.

Salam, T. F. and Grabs, B. M., 1987. Multiple fluidized-bed heat recovery: an investigation. *Heat Recovery System & CHP*, 7 (4), pp.311—318.

Schnitzlein, M. G. and Weinstein, H., 1988**.** Flow characterization in high velocity fluidized beds using pressure fluctuations. *Chemical engineering science*, 43 (10), pp.2605-2614.

Seo, M. W., Goo, J. H., Kim, S. D., Lee, J. G., Guahk, Y. T., Rho, N. S. and Song B. H., 2014. The transition velocities in a dual circulating fluidized bed reactor with variation of temperatures. *Powder Technology*, 264, pp.583–591.

Shen, X., Zhou, N., and Xu, Y., (1991). 'Experimental study on heat transfer in a pressurized circulating fluidized bed'. in Basu, P., Hasatani, M. and Hario, M.(Eds.). *Circulating Fluidized Bed Technology, vol. III*, Pergamon, New York, pp. 451–456.

Shi, Y., Zhong, W., Shao, Y, and Liu, X., 2019. Energy efficiency analysis of pressurized oxy coal combustion system utilizing circulating fluidized bed. *Applied Thermal Engineering*, 150, pp.1104-1115.

Sobrino, C., Ellis, N. and Vega, M., 2009. Distributor effects near the bottom region of turbulent fluidized beds. *Powder Technology*, 189, pp.25–33.

Soylemez, M. S., 2008. Optimum length of finned pipe for waste heat recovery. *Energy Conversion and Management*, 49, pp.96–100.

Srinivas, G., 2012. Low-grade waste heat recovery for simultaneous chilled and hot water generation. *Applied Thermal Engineering*, 42, pp.191-198

Stefanova, A., Bi, H. T., Lim, J. C. and Grace, J. R., 2011.Local hydrodynamics and heat transfer in fluidized beds of different diameter. *Powder Technology*, 212, pp.57–63.

Stijepovic, M. Z. and Linke, P., 2011. Optimal waste heat recovery and reuse in industrial zones, Energy, 36, pp.4019-4031.

Sua Y. and Maob Y., 2006**.** Experimental study on the gas–solid suspension flow in a square cyclone separator. *Chemical Engineering Journal*, 121, pp. 51–58.

Sundaresan, R. and Kolar, A. K., 2013. Axial heat transfer correlations in a circulating fluidized bed riser. *Applied Thermal Engineering*, 50, pp.985–996.

Tata engineering service (2014) *An insight into advanced technology in circulating fluidized bed combustion steam generators*, online at http:// www.tce.co.in/cfbs sg_tce_paper,accessed 30/04/19

Tuzla, K., Sharma, A. K., Chen, J. C., Schiewe, T., Wirth, K. E., and Molerus O., 1998. Transient dynamics of solid concentration in downer fluidized bed. *Powder Technology*, 100, pp.166 – 72.

Umamaheswari, S., Suganthi, M., Suresh, P. and Kannan, K., 2013. Growing Trend of Process off Gas and Waste Heat Recovery in Captive Power Generation. *International Journal of Scientific Research*, 2,pp.175-181.

Varga, Z. and Palotai, B., 2017. Comparision of low temperature waste heat recovery methods. *Energy*, 137, pp.1286-1292.

Viklund, S. B. and Johansson, M., 2014. Technologies for utilization of industrial excess heat: Potentials for energy recovery and CO_2 emission reduction. *Energy Conversion and Management*, 77, pp.369-379.

Viswanathan, M. (2017). *Digital modulation using matlab: Build simulation models from scratch.* Independent publisher

Winaya, Nyoman, S. and Basu, P., 2001. Effect of pressure and carbon dioxide concentration on heat transfer at high temperature in a pressurized circulating fluidized bed (PCFB) combustor. *International Journal of Heat and Mass Transfer*, 44, pp. 2965-2971

Weinstein, W., Graff R.A., Meller M., and Shao, M.J. (1983). The effect of imposed drop across a fast fluidized bed, fluidization , Kunii, D. and Toei, R. (eds), *Engineering foundation*. United engineering trustees Inc, New York. pp. 209-306.

Werther, J., 2009**.** Potentials of biomass co-combustion in coal-fired boilers, *Proceedings of the 20th International Conference on fluidized bed combustion, Springer Dordrecht Heidelberg, London (Tsinger University Press, Beijing), China*,pp. 27-42**.**

Wiman, J. and Almstedt, A. E., 1997. Hydrodynamics, erosion and heat transfer in a pressurized fluidized bed: influence of pressure, fluidization velocity, particle size and tube bank geometry. *Chemical Engineering Science*, 52 (16), pp.2677-2695.

Wirth, K.E., 1995. Heat transfer in circulating fluidized beds. *Chemical Engineering Science*, 50, pp. 2137-2151.

Yates, J. G., 1996. Effects of Temperature and Pressure on Gas-Solid Fluidization. *Chemical Engineering Science*, 51(2), pp.167- 205.

Zeng, B., Lu, X., Liu, H., 2010. Influence of CFB (circulating fluidized bed) boiler bottom ash heat recovery mode on thermal economy of units. *Energy*, 35, pp. 3863-3869.

Zenz, F. A. and Othmer, D. F., (1960). *Fluidization and fluid particle system*. Van nostrand reinhold, New york

Zhang, H. and Zhu, J. X., 2000. Hydrodynamics in downflow fluidized beds (2): Particle velocity and solids flux Profiles, *Chemical Engineering Science*, 55, pp.4367-4377

Zhang, H. L., Baeyens, J., Degrève, J. , Cáceres, G., Segal, R. and Pitié, F., 2014. Latent heat storage with tubular-encapsulated phase change materials (PCMs). *Energy*, 76, pp.66-72.

Zhang., Huili & Degrève., Jan & Dewil., Raf & Baeyens., 2015. Wall-to-Suspension Heat Transfer in a CFB Downcomer. *Journal of Powder Technology*, 1, pp 1-12

Zheng, Q. and Zhang, H., 1993. Experimental study of the effect of bed exits with different geometric structure on internal recycling of bed materials in CFB boilers, *Proceedings of the fourth International conference on circulating fluidized beds, Hidden Valley, Pennsylvania, USA*, pp. 175-180

Zhongyi, S., Yaodong, W., Tony, R. and Ye, H., 2015**.** Analysis of energy utilization and waste in China's processing industry based on a case study. *The 7th International Conference on Applied Energy – ICAE2015, Energy Procedia*, 75, pp. 572 – 577.

Zhou, X., Cheng, L., Wang, Q., Luo, Z. and Cen, K., 2012. Non-uniform distribution of gas–solid flow through six parallel cyclones in a CFB system: An experimental study. Particuology, 10, pp.170– 175

Zhu, J.-X., Yu, Z.-Q., Jin, Y., Grace, J. R. and Issangya, A., 1995. Co-current downflow circulating fluidized bed (downer) reactors — A state of the art review. *The Canadian journal of chemical engineering*, 73(5), pp. 662 - 677

Zhu, J.-X. and Wei, F., (1996). **'**Recent developments of downer reactors and other types of short contact reactors'. in Large, J. F. and Laguerie, C (eds), *Fluidization VIII*, Engineering Foundation, **New** York, pp. 501-510.

Appendices

Appendix – I
Calibration of Thermocouple and Data Acquisition System

The data acquisition system used in the experiments has provision for displaying and recording temperature reading from connected thermocouples types. To minimize any error in the temperature readings the thermocouples and the data acquisition system is calibrated with reference to standard temperature readings obtained in a variable temperature water bath. One junction of the thermocouple is immersed in the water bath and its temperature varied in regular intervals of 5 °C while the other junction is fitted to the data acquisition system. The readings from the water bath and the data acquisition are recorded and plotted for calibration. The calibration curve so obtained is presented in Fig I.1 below.

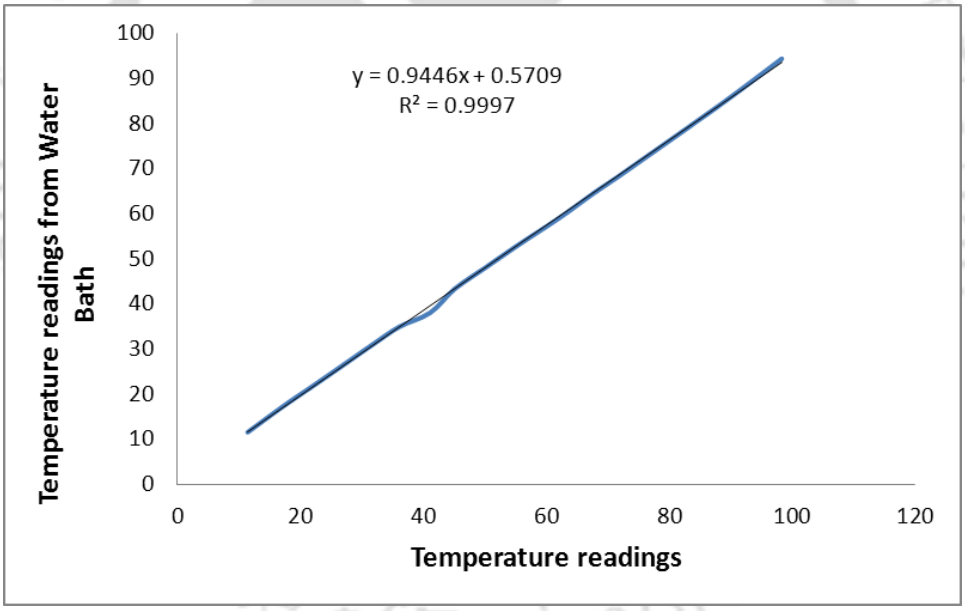

Fig. 1.1 Calibration curve for Temperature Readings

Appendix – II
Calibration of Pressure Sensors

The calibration of pressure sensor is done using a hydraulic dead weight tester. This equipment consists of a loading plate where standard dead weights can be placed to apply pressure to a hydraulic oil circuit. This pressure can be transmitted through the circuit to a test port where the pressure sensor that require calibration is fitted. The piezo resistive pressure sensor which is used in the experiments is fitted to this test port. The required excitation voltage is supplied to the sensor and the output voltage is read on a data acquisition system which can display a minimum of 0.01V. Starting from 0, the pressure on the load plate is increased in steps of 0.5 bar to a maximum of 10 bar. For each the pressure applied the output voltage is noted both for upscaling and down scaling. Typical calibration curves for one such pressure sensor is given below in Fig. II.1

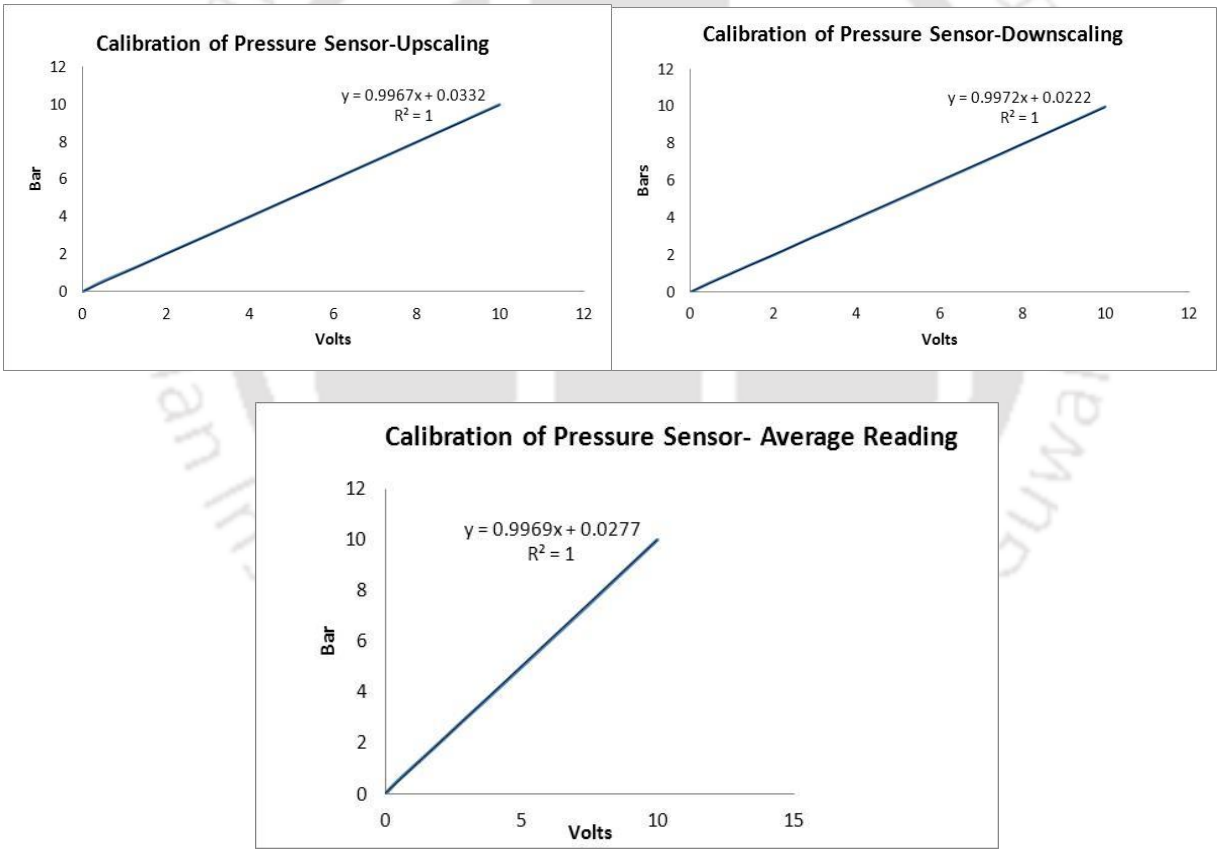

Fig. II.1 Calibration curves for Pressure Sensor

Appendix – III
Measurement of exhaust airflow rate and calibration of orifice meter

By assuming steady-state, incompressible flow in a horizontal pipe with negligible frictional losses, Bernoulli's equation reduces to the following equation relating the conservation of energy between two points on the same streamline:

$$p_1 + \frac{1}{2} * \rho * V_1^2 = P_2 + \frac{1}{2} * \rho * V_2^2$$

Or $p_1 - P_2 = \frac{1}{2} * \rho * V_2^2 - \frac{1}{2} * \rho * V_1^2$

By continuity equation

$$q_v = A_1 * V_1 = A_2 * V_2 \; or \; V_1 = \frac{q_v}{A_1} \quad and \quad V_2 = \frac{q_v}{A_2}$$

$$P_1 - P_2 = \frac{1}{2} * \rho * \left(\frac{q_v}{A_2}\right)^2 - \frac{1}{2} * \rho * \left(\frac{q_v}{A_1}\right)^2$$

$$\therefore q_v = A_2 \sqrt{\frac{1}{1 - \left(\frac{d}{D}\right)^4}} \sqrt{2(p_1 - p_2)/\rho} \qquad \text{(III.1)}$$

This equation gives the flow theoretical rate where

q_v = Volumetric flow rate in m^3/s

A_2 = Cross sectional area of the orifice

D = Diameter of the pipe

D = diameter of the orifice hole

P_1 and P_2 are the upstream and downstream pressure respectively.

ρ is the fluid density

The calibration of the orifice meter was done by plotting the values of exhaust flow rate calculated from the equation (III.1) above based on the pressure difference across the orifice

plate against the values shown on a Carioles mass flow meter attached to the outlet of the orifice meter. The calibration curve is presented below in the figure III.1

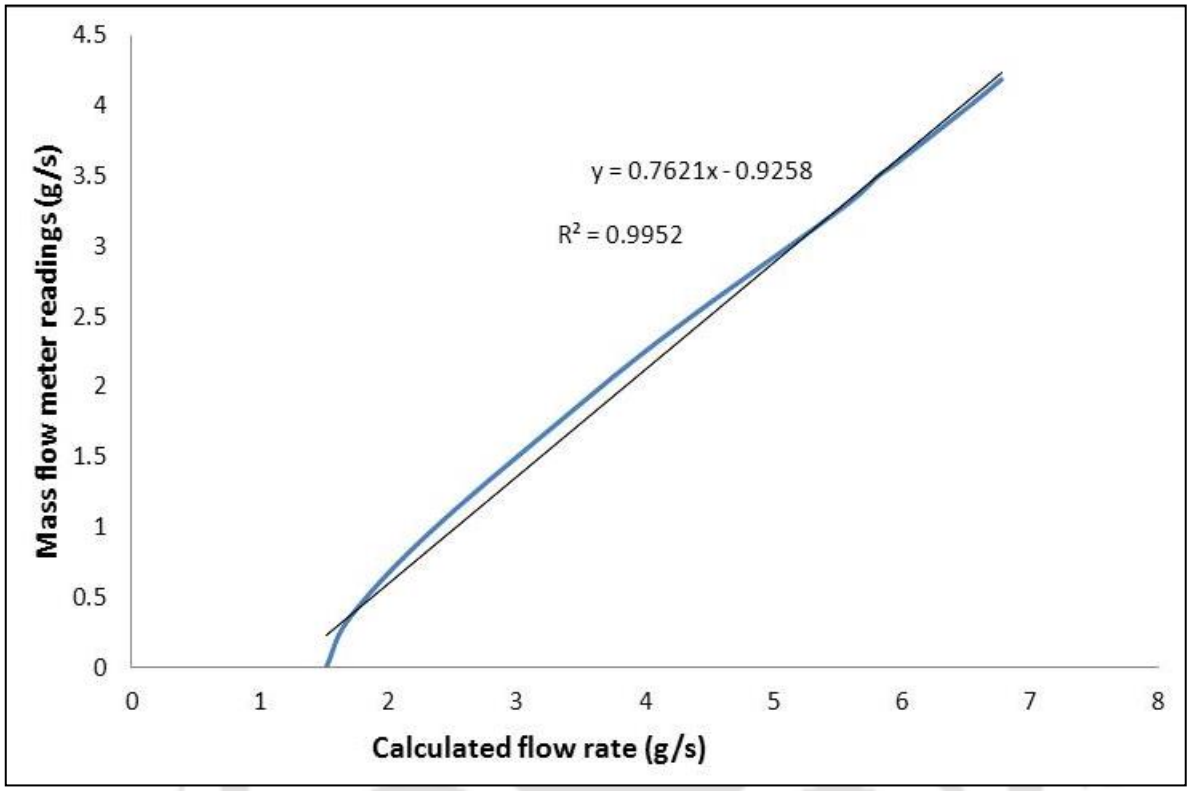

Fig. III.1 Calibration curve for orifice meter

Appendix – IV
Calibration of Compressed air flow meter

The compressed air flow meter used in the experiments digitally displays the flow rate in Nm^3/h. A provision for analog output in mAmp is also available in the equipment which is connected to the data acquisition system for recording the flowrates. The output from this equipment in mAmp is calibrated with the displayed values and the calibration curve obtained is presented below in the figure (IV.1)

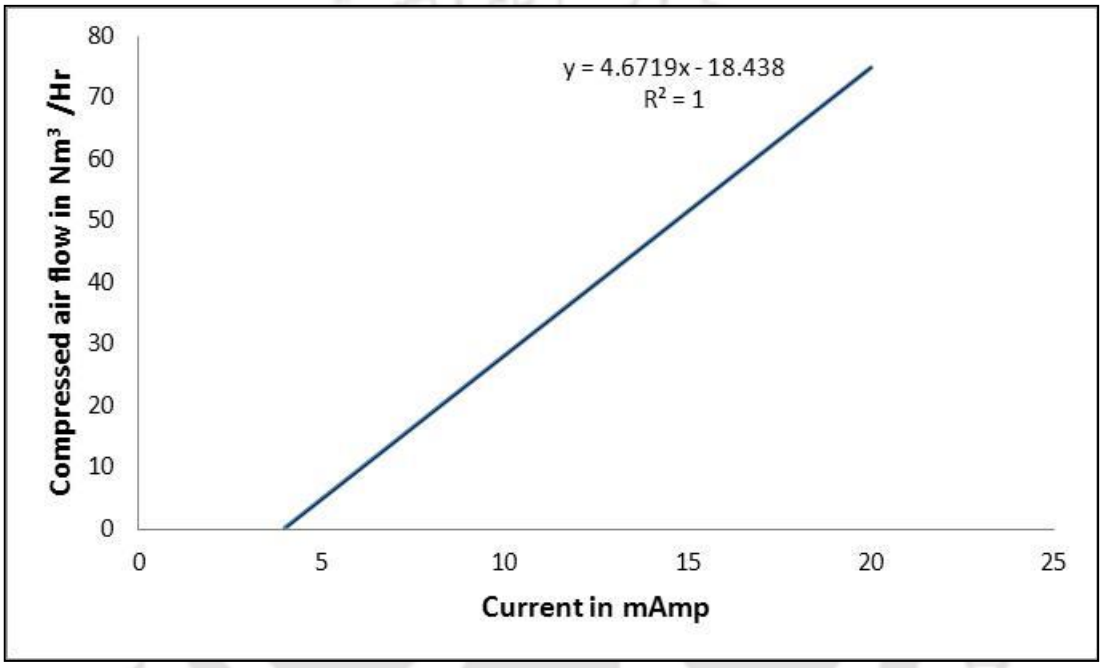

Fig. IV.1 Calibration curve for compressed air flowmeter

Appendix –V
List of Equipment/Instruments used

- Data acquisition system: Agilent 34970A with 20 channel multiplexure 34901A, accuracy 0.004% (DCV), 0.1 °C (thermocouple)
- Compressor: capacity 225 litres, Maximum working pressure 12.30 kg/cm^2 , motor: 3 hp, manufacturer: Ingersoll Rand, Model: 01481
- Weighing balance: Range 0.04 to 15 kg. error-2 gm, Model: SP/pls-15FLP, Manufacturer: Shyam switchgears Pvt Ltd.
- Auto transformer: Make: VARIVOLT. Range 0 t0 270V, 10 and 15 Amp
- Pressure gauge: Make Swagelok, Model: EN837-1
- Pressure regulator: Make Swagelok
- Sieves: Standard ASTM and BIS sieves
- Stop watch, ball valve, gate valve, Butterfly valve, Flow control valve,
- Pressure transducers: Make Abustek and GEMS, range 0 to 5 bars and 0 to 10 bar, Accuracy ± 0.25% of full scale
- Thermocouple : K type, accuracy ± 0.4 %, response time 0.003 sec.
- Dead weight tester for calibration of pressure transducers
- Constant temperature bath: Julabo heating circulator [Model: SE-12 Make - Julabo labortechnik Gmbh]
- Compressed air flowmeter: Make Testo. (Model: TESTO 6441) range 0.25 to 75 Nm^3/h, Accuracy ± 3% of measured value, ± 0.3 % of final value.
- DC voltage supply: Model: Beetek-3005, Output voltage Range: 0 to 30V, 5A

For overall uncertainity analysis, the following quantities were considered

1. Temperature : ± 0.5°C
2. Pressure: 0.05 bar
3. Distance between pressure tappings: 1mm
4. Loss of inventory: ±1 gm
5. Visual error: ±0.5
6. Bulk temperature calculation: ±1°C

1. Uncertainity in calculating wall to bed heat transfer coefficient, h (W/m^2K)

The uncertainties of the required parameters are:

q = 1.9017 ± 0.1W

D = 0.054 ± 0.005m

L = 0.50 ± 0.001m

T_s = 120 ± 0.5 °C

T_b = 35 ± 0.5 °C

Heat transfer coefficient is calculated using the formula

$$h = \frac{q}{A_s(T_s - T_b)} = \frac{q}{\pi \times D \times L \times (T_s - T_b)}$$

$$\therefore \frac{\partial h}{\partial q} = \frac{1}{\pi \times D \times L \times (T_s - T_b)}$$

$$\frac{\partial h}{\partial D} = -\frac{q}{\pi \times D^2 \times L \times (T_s - T_b)}$$

$$\frac{\partial h}{\partial L} = -\frac{1}{\pi \times D \times L^2 \times (T_s - T_b)}$$

$$\frac{\partial h}{\partial T_s} = \frac{q}{\pi \times D \times L}\left[\frac{-1}{(T_s - T_b)^2}\right] = -\frac{q}{\pi \times D \times L \times (T_s - T_b)^2}$$

$$\frac{\partial h}{\partial T_b} = \frac{q}{\pi \times D \times L \times (T_s - T_b)^2}$$

The overall uncertainity

$$U_h = \sqrt{\left(\frac{\partial h}{\partial q}\right)^2 \times (\Delta q)^2 + \left(\frac{\partial h}{\partial D}\right)^2 \times (\Delta D)^2 + \left(\frac{\partial h}{\partial L}\right)^2 \times (\Delta L)^2 + \left(\frac{\partial h}{\partial T_s}\right)^2 \times (\Delta T)^2 + \left(\frac{\partial h}{\partial T_b}\right)^2 \times (\Delta T_b)^2}$$

= 0.039085

Uncertainity = 3.9085%

2. Uncertainity in calculating bed voidage

Bed voidage is calculated using the formula

$$\varepsilon = 1 - \frac{10 \times \Delta P}{\rho_s \times L_m} \times 1019.44$$

$$\frac{\partial \varepsilon}{\partial \Delta P} = -\frac{10}{\rho_s \times L_m}$$

$$\frac{\partial \varepsilon}{\partial L_m} = \frac{10 \times \Delta h}{\rho_s \times L_m^2}$$

$$\frac{\partial \varepsilon}{\partial \rho_s} = \frac{10 \times \Delta h}{\rho_s^2 \times L_m}$$

Overall uncertainity may be calculated as

$$\mathbf{U=}\sqrt{\left(\frac{\partial \varepsilon}{\partial \Delta P}\right)^2 \times (\Delta h)^2 + \left(\frac{\partial \varepsilon}{\partial L_m}\right)^2 \times (\Delta L_m)^2 + \left(\frac{\partial \varepsilon}{\partial \rho_s}\right)^2 \times (\Delta P)^2} \mathbf{= \pm 0.005 \text{ to } \pm 0.659\%}$$

3. Uncertainity in solid circulation rate

The uncertainties of the required parameters are:

$\rho_s = 1690 \pm 5kg$

$L_a = 0.135 \pm 0.002m$

$d_D = 0.0254 \pm 0.005m$

$t = 30 \pm 0.2s$

The formula for soild circulation rate is:

$$G_s = \frac{\rho_s \times L_a \times A_D \times (1-\varepsilon_{mf})}{A_B \times t}$$

$$= \frac{\rho_s \times L_a \times d_D^2 \times (1-\varepsilon_{mf})}{d_B^2 \times t}$$

$$\frac{\partial G_s}{\partial \rho_s} = \frac{L_a \times d_D^2 \times (1-\varepsilon_{mf})}{d_B^2 \times t}$$

$$\frac{\partial G_s}{\partial L_a} = \frac{\rho_s \times d_D^2 \times (1-\varepsilon_{mf})}{d_B^2 \times t}$$

$$\frac{\partial G_s}{\partial d_D} = \frac{2 \times \rho_s \times L_a \times d_D \times (1-\varepsilon_{mf})}{d_B^2 \times t}$$

$$\frac{\partial G_s}{\partial d_b} = \frac{2 \times \rho_s \times L_a \times d_D^2 \times (1-\varepsilon_{mf})}{d_B^2 \times t}$$

$$\frac{\partial G_s}{\partial t} = \frac{\rho_s \times L_a \times d_D^2 \times (1-\varepsilon_{mf})}{d_B^2 \times t^2}$$

The overall uncertainity in measuring soild circulation rate is

$$U_{G_s} = \sqrt{\left(\frac{\partial G_s}{\partial \rho_s}\right)^2 \times (\Delta\rho_s)^2 + \left(\frac{\partial G_s}{\partial L_a}\right)^2 \times (\Delta L_a)^2 + \left(\frac{\partial G_s}{\partial d_D}\right)^2 \times (\Delta d_D)^2 + \left(\frac{\partial G_s}{\partial d_B}\right)^2 \times (\Delta d_B)^2 + \left(\frac{\partial G_s}{\partial t}\right)^2 \times (\Delta t)^2}$$

= 0.0532

So, uncertainty is ± 5.32%

List of Publications

International / National Conferences

- **R. Saikia**, P. Mahanta, Transient Hydrodynamics and heat transfer behaviour in a pressurised circulating fluidized bed, *Proceedings of the 24th National and 2nd International ISHMT-ASTFE Heat and Mass Transfer Conference (IHMTC-2017*), December 27-30, 2017, BITS Pilani, Hyderabad, India.
- Hirakh Jyoti Das, **Rituraj Saikia** and Pinakeswar Mahanta, 2019, A comparative study on the hydrodynamic and heat transfer behaviour of conical fluidized bed with that of a columnar pressurized circulating fluidized bed, *National Conference on Waste to Energy Conversion (NCWEC-2018)*, 28th -29th December 2018, NIT Mizoram
- Hirakh Jyoti Das**, Rituraj Saikia**, Md Shoaib Aamir and Pinakeswar Mahanta, Effect of Spiral on Drying Characteristics in Conical Bubbling Fluidized Bed Paddy Dryer, *17th International Conference on Sustainable Energy Technologies (SET 2019)*, 20th – 22th of August 2019, Kuala Lumpur, Malaysia.
- P. Kalita, R. Gogoi, **R. Saikia** and P. Mahanta, Effect of distributor plate on bed hydrodynamics and heat transfer in a pressurized cold circulating fluidized bed unit, in the International *Symposium on Aspects of Mechanical Engineering and technology for Industry*, NERIST, Itanagar, Arunachal Pradesh, December 6-8, 2014, pp.52-61

International Journals

- **R. Saikia**, P. Mahanta, Transient Hydrodynamics and Heat Transfer Behaviour in a Pressurized Circulating Fluidized Bed During Abrupt Changes in Operating Pressure, *Journal of Heat Transfer*. (under review)
- Hirakh Jyoti Das**,** Md Shoaib Aamir, **Rituraj Saikia** and Pinakeswar Mahanta, 2019, Performance evaluation of drying characteristics in conical bubbling fluidized bed dryer, *Powder Technology*, May, 2019 (under review).